國　立　交　通　大　學

奈 米 科 技 研究所碩士班

碩 士 論 文

新穎側向閘極奈米線場效電晶體應用於即時偵測生物感測器

Real-Time and Label-Free Detection of the Biomolecules with a Novel Side-Gated SiNW-FET Biosensor

研 究 生: 夏德玲

指導教授: 柯富祥 博士

中華民國九十七年六月

Acknowledgment

致謝的開頭當然要把位置留給柯博，感謝柯博這兩年來在學術以及態度上給我的教誨，讓我在專業領域以及待人處事上能更進一步，再加上班長這個職務給我的歷練讓我更能懂得”掌握大局；洞悉人心”。

感謝其昌、俊淇學長在實驗上的帶領以及幫忙，這兩年下來多謝你們的包容讓我能夠順利的交出論文順利的畢業; 感謝坤霖、老鼠學長在我剛進實驗室帶我認識二餐的環境; 志威學長的跳舞天份也是讓我印象深刻; 謝謝群芳、志杰、敬雅在實驗上的協助; 最要感謝就是奕儂，從一起實驗一起玩樂一起熬夜，謝謝你帶給我碩士生涯一段難忘的回憶~

佳典!曾經一段不愉快讓我長大也讓我了解社會的現實面，謝謝你讓我們還能回到最初簡單的相處，這兩年來你教會我很多謝謝你。

吳中書!我們真是不打不相識~對吧?最想讓我說謝謝的~就是你，在我人生懵懂時人生低潮時，都有你的參與。謝謝你總是用簡單的字句影響我，謝謝你願意接納這樣壞脾氣的我，對你~我心裡真的有太多的感謝跟不捨。但你說好朋友不講這種客套話，所以老話一句: 謝謝這裡有小胖；謝謝這裡有香皮。

魏大爺!你是我一進來這裡第一個交心的好朋友，到現在也都還是在我的心裡重要的位置，第一次喝醉你就幫了我一個大忙→幫我遛狗。打從那時候起，我就決定要跟你當好朋友，常常覬覦你的密閉小空間，我可是受到它不少恩惠唷。哈!!你這個行動土地公真是讓我又羨慕又忌妒阿!

菲菲!在這裡的我會不會讓你失望了呢?我好像沒什麼資格可以當你學姐了，不像從前可以給你很多專業上的幫助，倒是不成熟的我還需要你的幫忙跟陪伴!很開心能跟你再續前緣，簡簡單單的欣賞你!

嗯牆!知道我在說你~不要轉頭!!第一眼看到妳就想把你折斷。哈哈!誰叫你那麼瘦，謝謝你的到來讓我在這個實驗室增添許多笑料，聊的來是一種奇妙的緣分不在乎時間的長短。期許你在實驗上的專業領域能有所成長跟突破!

正姐!你真是個讓我歎為觀止的一號人物阿!除了萬事通之外，你的好歌聲更是讓我難忘，再加上你悶騷的個性，我想這個實驗室有了你會更多彩多姿。也謝謝你的細心細膩，讓我在那段難熬的時間裡多了份溫暖的感覺!

當然還要感謝實驗室在不同領域中共同努力以及給予協助的夥伴們: 子銘學長、依蓁、美榕、品麟、舜博、Sri、Jagan、京璋、柏軒、蕙卉。沒有你們的話，我想碩士生活會增添許多難關要過吧!!很開心在這裡能夠遇到你們。

最後，我要感謝我的家人，這兩年裡對我的關心跟包容，讓我充滿勇氣面對所有的挑戰。當然還有你，聽我的抱怨聽我的沮喪忍耐我的壞脾氣，但總是在週末幫我上緊發條，雖然你在最後給了我一個考驗跟挑戰，但很高興在今天 2008 年 6 月 16 日，我大聲可以告訴你: 我做到了!!

謹以此文，獻給我愛的你們!!夏皮兒做到了!!

新穎側向閘極奈米線場效電晶體應用於即時偵測生物感測器

學生：夏德玲　　指導教授：柯富祥 教授

國立交通大學奈米科技研究所碩士班

摘 要

感測元件與生物分子的連結應用在未來的疾病診斷是個重要且具發展性的課題。在此篇論文中，我們選擇甲狀腺乳突癌症相關變異基因 $BRAF^{V599E}$ 以及癌症指標物甲型胎兒蛋白抗原來當作偵測目標。我們以半導體奈米線為元件基礎的裝置做為新穎的生物感測器，可偵測的生物分子或是化學物種包括有低濃度化學成分離子、小分子、抗原抗體反應、檢測蛋白質、DNA 和病毒。在我的研究裡，使用了互補式金氧半場效電晶體的技術來製作新穎側向閘極場效電晶體生物感測器。利用矽的局部氧化製程來製作內縮線寬的奈米線，而此奈米線可以達到優異的高比表面積比以及獲得側向閘極控制，此兩項主要特色對於目前感測元件整合於微流道組件上有極大優勢及應用面。我們量測甲狀腺乳突癌症相關變異基因 $BRAF^{V599E}$ 以及癌症指標物甲型胎兒蛋白抗原對於奈米線元件的電性變化影響，另外還利用了紅外線光譜儀、螢光顯微鏡以及紫外光光譜量測儀確認表面自組裝固定化的技術以及生物分子實驗條件的確立。

最後總結出我們利用矽的局部氧化製程製作出的奈米線通道可使其線寬內縮到 100 nm 以下的線寬，此條件提供元件電性達到優異的 10^5 倍的開關電流比。利用此靈敏度高的元件我們可以偵測到濃度 100 fM 的標的突變 DNA 以及 3 ng/mL 的癌症標誌物抗原分子。結果顯示此新穎的側向閘極奈米線感測元件可以作為未

來的免標定、即時偵測、高靈敏度以及優異專一性結合的場效電晶體生物感測器。另外，此元件具有獨立控制側向閘極的能力更提供了未來感測元件與微流道技術整合上的一大優勢。

Real-Time and Label-Free Detection of the Biomolecules with a Novel Side-Gated SiNW-FET Biosensor

Student: Der-Ling Hsia **Advisor: Prof. Fu-Hsiang Ko**

Institute of Nanotechnology

National Chiao Tung University

Hsinchu 300, Taiwan, ROC

Abstract

It is an important and developing capable issue to combine the semiconductor sensor devices with biomolecules for the future application of disease diagnosis. In the present work, the $BRAF^{V599E}$ mutation gene and cancer marker α-fetoprotein, which have been recently reported to restrict to the papillary thyroid carcinomas (PTCs) and liver cancer, respectively, were chosen as the target biomolecules. The devices based on semiconductor nanowires exhibit high sensitive and selective characteristics for the real-time, label-free, and excellent specificity detection of biomolecules and chemical species. A novel side-gate silicon nanowire field effect transistor (SiNW-FET) is fabricated by using the complementary metal oxide semiconductor (CMOS) FET compatible technology. The shrank nanowires with higher surface-to-volume ratio and individual side-gate for integration are achieved by the LOCOS process. Because of the above advantages, the devices have potential to integrate with microfluidic system for bio-detection application. Therefore, the detection strategy for PTC and liver cancer has been investigated with our SiNW-FET integration with microfluidic system for real-time sensing by measuring the

characteristics of electrical signals. The FT-IR, fluorescence microscopy and UV spectrophotometer are also examined to check out our efficiency of the SAM and appropriate experimental parameters for bio-sensing.

In the conclusion, the width of shrank nanowire by LOCOS process can be thinner than 100 nm. The drain current versus gate voltage (I_D-$V_{G)}$ characteristic of the SiNW-FET exhibits about five orders of magnitude of I_{on}/I_{off} ratio, and the threshold voltage shifts positively after hybridization of 100fM concentrations of $BRAF^{V599E}$ mutation gene and 3ng/mL concentrations of the cancer marker, α-fetoprotein, respectively. The results show that the side-gate nanowire device has the capability of acting as a real-time, label-free, highly sensitive and excellent selectivity SiNW-FET biosensor for important biomolecules. In addition, our approach offers a highly potential possibility to integrate with microfluidic-channel system for future parallel real-time detection of multiple chemical and biological species with controlling the individual side-gate in a single integrated chip.

Contents

List of Tables

Chapter 1: Introduction

Chapter 2: Literature Review

Chapter 4: Results and Discussions

List of Figures

Chapter 1: Introduction

Chapter 2: Literature Review

Chapter 3: Experiments

Chapter 4: Results and Discussions

Chapter 1: Introduction

1.1 General Introduction

Nanotechnology has become a very popular word that is used to describe many types of research in which the characteristic dimensions are below 1000 nm. For example, continuing improvements in lithography have resulted in the reduction of line widths to well below 1 micron. This kind of work is often called nanotechnology. The interdisciplinary study of biology, chemistry, and electronics became more and more important than ever before. Combining biotechnology and semiconductor technology, various types of biochips and biosensors have now been developed to detect the specific binding of biomolecules on the solid-state substrates. As semiconductor devices become scaled down to ever-smaller sizes within the nano-regime, a variety of technological and economic problems arise, the rules of classical physics give way to quantum mechanics, and the term "molecular-scale" becomes more accurate than "nano-scale." At this point, the scaling of sizes that has successfully reduced device features from the micro-scale to the nano-scale reaches its limits, and, therefore, alternative manufacturing methods, materials, device structures, and architectures are required. In this regime, the approach of fabricating nanoelectronic devices and interconnects using a combination of molecular and nanostructured materials with existing and emerging processing technologies promises to allow the continued miniaturization and enhancement in performance of the biotechnology. Nanotechnology is a revolution in science and technology. It distinguishes itself from all previous scientific and industrial revolutions in many ways. Through the new technology, we can't only change the fundamental properties of matter as well as a tailor make materials with desirable attributes but also manipulate the nano-scale objects that conventional technique is impossible to do.

In principle, there are two approaches to nanotechnology: the ''bottom-up''

strategy and the ‘‘top-down’’ approach **[1]**. The pros and cons of the ‘‘bottom-up’’ and ‘‘top-down’’ approaches to nanotechnology are matters of hot debate in the most reports. It is widely held that the present top-down semiconductor technology has not exploited the physics and chemistry of nano-materials on the one hand, and not taking advantage of the development of bottom-up nanotechnology on the other. Many reasons come to mind. Firstly, nanomaterials and their properties in the nanorealm, especially at the interface, are not well understood and still under investigation. Secondly, the fabrication techniques, both at the materials level and at the device stage, are not well defined or fully developed. Thirdly, connection to the macro world remains a real problem. Finally, even if all these problems can be overcome, they are at present not mass producible and cost competitive enough to challenge the existing semiconductor technology. For a stand-alone bottom up nano-device to challenge the top-down nano-device, it must overcome these hurdles and integrate into it. While each approach has its advantages and disadvantages, it is our view that future development of nanotechnology will probably encompass both approaches with their relative contributions depending upon specific applications. In this thesis, we discuss the top-down nanotechnology firstly, followed by the recent developments in biosensors, and finally talked about the importance of detecting biomolecules. While this seems to be a reasonable road to fabricate novel nano-devices, ultimately though, nano-devices will be replaced by traditional molecular, atomic, and nuclear devices, as the size further diminishes, as we shall discuss later in this thesis.

1.2 Introduction to Top-Down Nanotechnology

"Top-down" methods start with patterns made on a large scale and reduce its lateral dimensions before forming nanostructures. This approach seeks to fabricate nanodevices on silicon chips directly using electron beam or X-ray lithography (either photolithography or electron lithography) **[2]**. Indeed, the top-down approach has been the method of choice in the semiconductor industry for making microelectronic and other devices for decades. The semiconductor industry entered the nanotechnology era in the year 2000, and by 2004, the industry was shipping devices with physical gate dimension of less than 40 nm and insulator thickness of less than 1 nm. This is in line with the pace of Moore's Law **[3]**. The current development of the optical lithography at 193 nm wavelength is pushing the limit of 32 nm (half pitch). Dimensions smaller than 32 nm is generally viewed as beyond the capabilities of optical lithography at 193 nm wavelength, unless high-index fluids, high-index lens materials, and higher-index resist can be developed is shown in **figure 1.1**. Another way to extend the lifetime of optical projection lithography with immersion to 32 nm half pitch and beyond is to divide the pattern into two or more masks. It is generally believed that extension of the Roadmap for semiconductor industry beyond 32 nm will probably require the development of ''next-generation'' lithography (NGL) technologies such as extreme ultraviolet lithography (EUVL), mask-less (ML2), and imprint lithography.

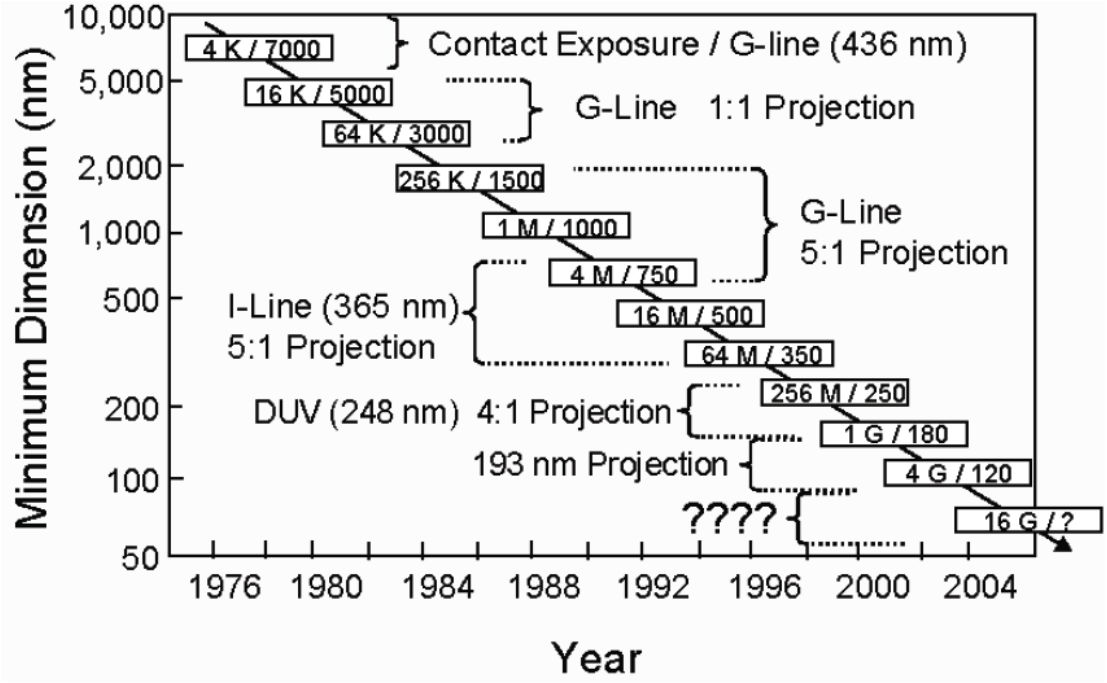

Figure 1.1 The semiconductor industry roadmap of memory technologies and the associated lithographic technologies used to manufacture each generation of devices. Each box displays each device generation's memory size and critical feature size (nm).

A beam of light passes through the mask and a lens, which focuses an image on photoresist placed on a surface of a silicon wafer or a film in **figure 1.2**. The resolution of the photolithographic process determines the width of the channels. In photolithography ultraviolet light is used. The fabrication of spacing smaller than half this length causes blurred features, which can melt together. Various technical improvements managed to reach structural resolutions in the order of 70 nm in experimental setups and about 100 nm in mass production **[4, 5]**. The technical difficulties to make such small structures using light, makes this technique rather expensive. However, the conventional lenses are not transparent to extreme ultraviolet light, they do not focus X-rays and the energy of these radiations easily damages most of the materials used in masks and lenses. Therefore, instead of masks, lithography

technologies based on focused beams are used electron-beam lithography (EBL) and focused-ion beam (FIB) lithography to create nano-channels, e.g., for DNA separation **[6]**. Features of 10 nm in scale can be achieved by top-down methods. Fabricating the high-performance integrated circuits requires increasingly shorter wavelengths of the radiation source to manufacture devices of decreasing critical sizes.

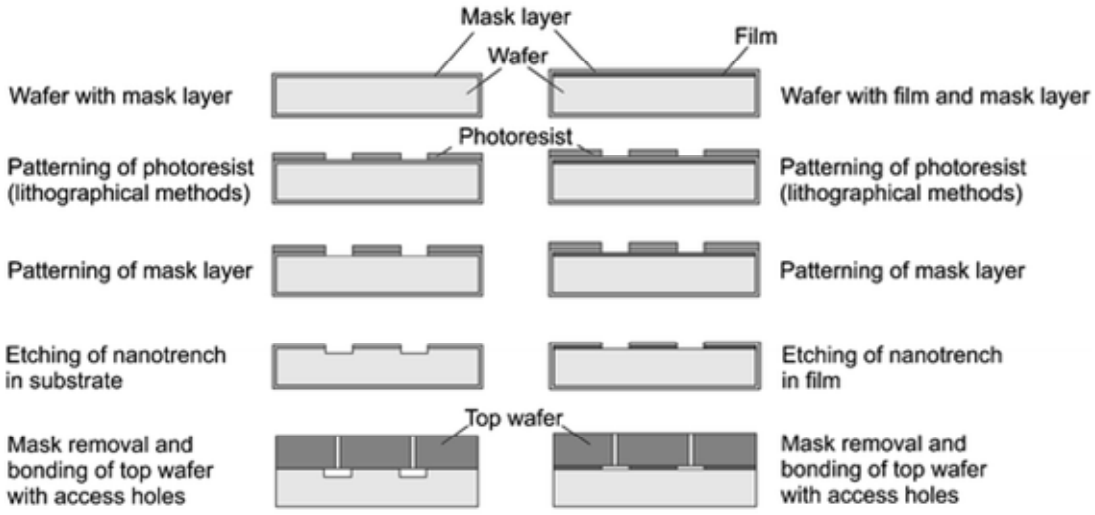

Figure 1.2 The concept of patterning process

Above mentioned have been introduced for the fabrication of electronic devices. Maybe other approaches are all potential "next-generation lithography" (NGL) technologies, but currently they remain expensive and difficult to operate and implement. Because the ''next-generation'' lithographies will most likely require the development of substantially new infrastructure, implementation of these new technologies as viable manufacturing solutions can be a real challenge for the industry **[7]**. Recent development in EUVL is expected to be used in manufacturing starting at 32 nm half pitch. The EUV lithography is a projection optical technology that uses 13.5 nm wavelength. At this wavelength, all materials are highly absorbing, so the imaging system is composed of mirrors coated with multilayer structures designed to

have high reflectivity at 13.5 nm wavelength. For definitions or features finer than 32 nm, it is necessary to use electron beams or X-rays in the so-called ‘‘nanoimprint lithography (NIL) ’’ displayed in **figure 1.3 [8–10]**. High-energy electron beams or X-rays can provide definitions of a few nanometers. The current definition in NIL using electron beams is about 5 nm **[8–10]**. It is obvious that nanoimprint lithography can achieve much better resolution than EUVL discussed earlier. However, it suffers from, among other things, cost effectiveness, mass production capability, and defect tolerance problems. The main reason for this is that NIL is essentially a multilayer mold technology. It is interesting to note that, at or below about 15 nm, quantum confinement sets in, making single-nanowire devices a reality. Indeed, 15 nm wide SiNW channel and 5–10 nm isolated silicon islands were used in the work of Tsutsumi et al. **[11]**. This is a fast-developing technology **[13–28]**.

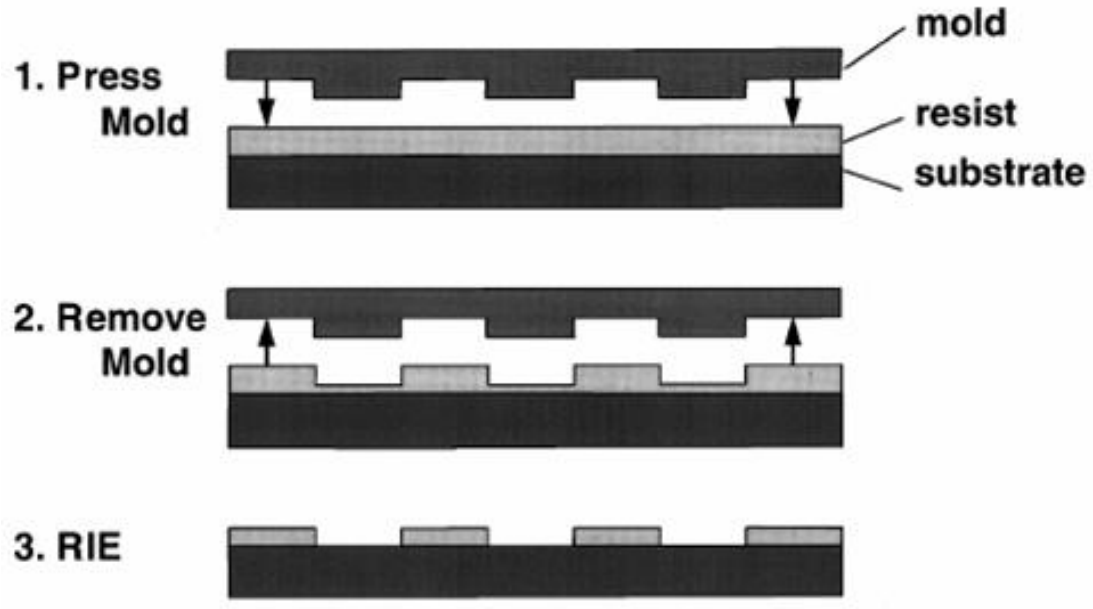

Figure 1.3 The process of nanoimprint method

And then, **figure 1.4** presents the concept of soft lithography **[5]**, which is based on the use of elastomeric polymers to transfer a pattern from a master to a large number of copies having single-layer structures to define the nano-size pattern. Furthermore, soft lithography has great potential because it does not require expensive equipment or a high-quality clean room, but it is ineffective for fabricating multi-layer structures or for allowing precision alignment. In soft lithography in **figure 1.4(a)** the mold is usually made by producing a pattern in a layer of photoresist on the surface by photolithography or electron-beam lithography (EBL) **[1]**. Then a liquid precursor poly-dimethyl-siloxane (PDMS) is poured over it and cured into the rubbery solid. The PDMS stamp is then peeled off the master. Copying the pattern on the PDMS stamp as well as the use of the stamp is, however, cheap and easy. The PDMS stamp is then further used in different ways to make nanostructures: by micro-contact printing **[12]** in **figure 1.4(b)** or micro-molding in capillaries **[6]** in **figure 1.4(c)**. The advantage of the soft lithography is that it does not need to be carried out in the clean room. The nanostructures made by this method can be produced in a wide range of materials and the patterns can be formed on curved and planar surfaces. However, this technique is not suitable for complex nano-electronic devices, i.e., for making multilayered structures due to the deformations and distortions of the soft PDMS stamp that can cause small errors in the replicated pattern and the misalignment of the pattern. The latter limitation can be overcome by employing a rigid stamp in step-and-flash imprint lithography **[13, 14]** and nanoimprint lithography (NIL) **[15, 16]**. Nanoimprint is displayed in **figure 1.5** acting as an emerging lithographic technology that has promise for the high-throughput patterning of nanostructures. The nanoimprint technique can achieve pattern resolutions beyond the limitations set by light diffraction or e-beam scattering in other conventional techniques. NIL is fast and well suited for large-scale fabrication. NIL has also certain limitations in replicating

large-scale and nanoscale patterns simultaneously **[17]**. The key to successful nanoimprint is preventing residual mold attachment after it is removed from the resist coating substrate during the imprinting process.

The pros and cons of the top-down approaches to nanotechnology are discussed. While this approach has its advantages and disadvantages, it is our view that future development of nanotechnology will probably embrace both approaches with their relative contributions depending upon specific applications (e.g. performance enhancement, materials improvement, functionalization, etc.) **[18]**.

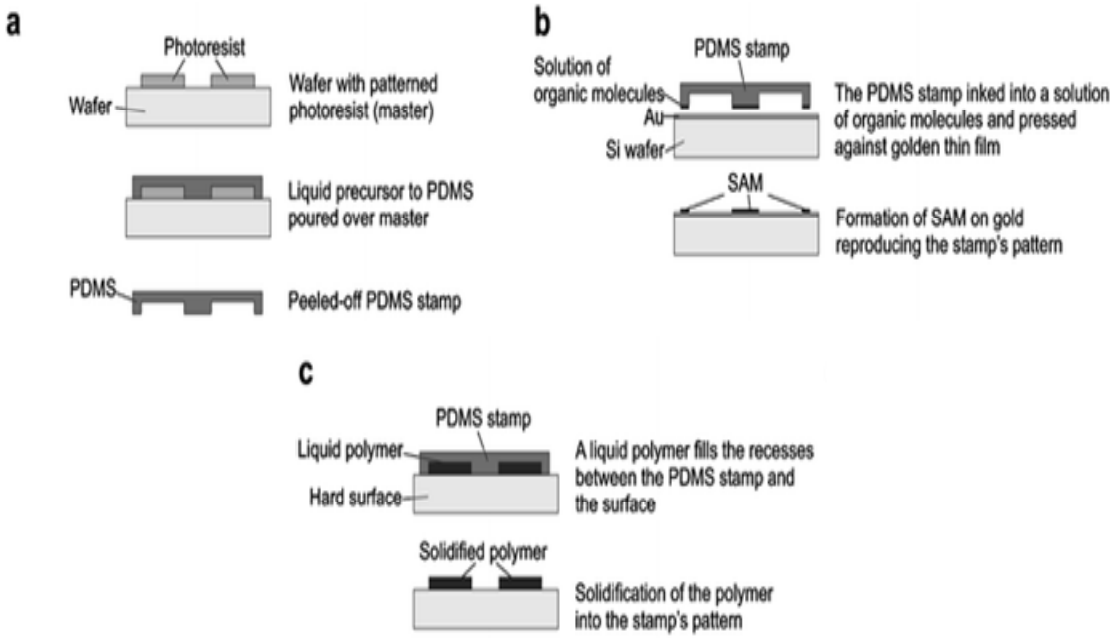

Figure 1.4 Process of the Soft lithography **[5]**; (a) formation of an elastic stamp, (b) micro-contact printing, (c) micro-molding in capillaries

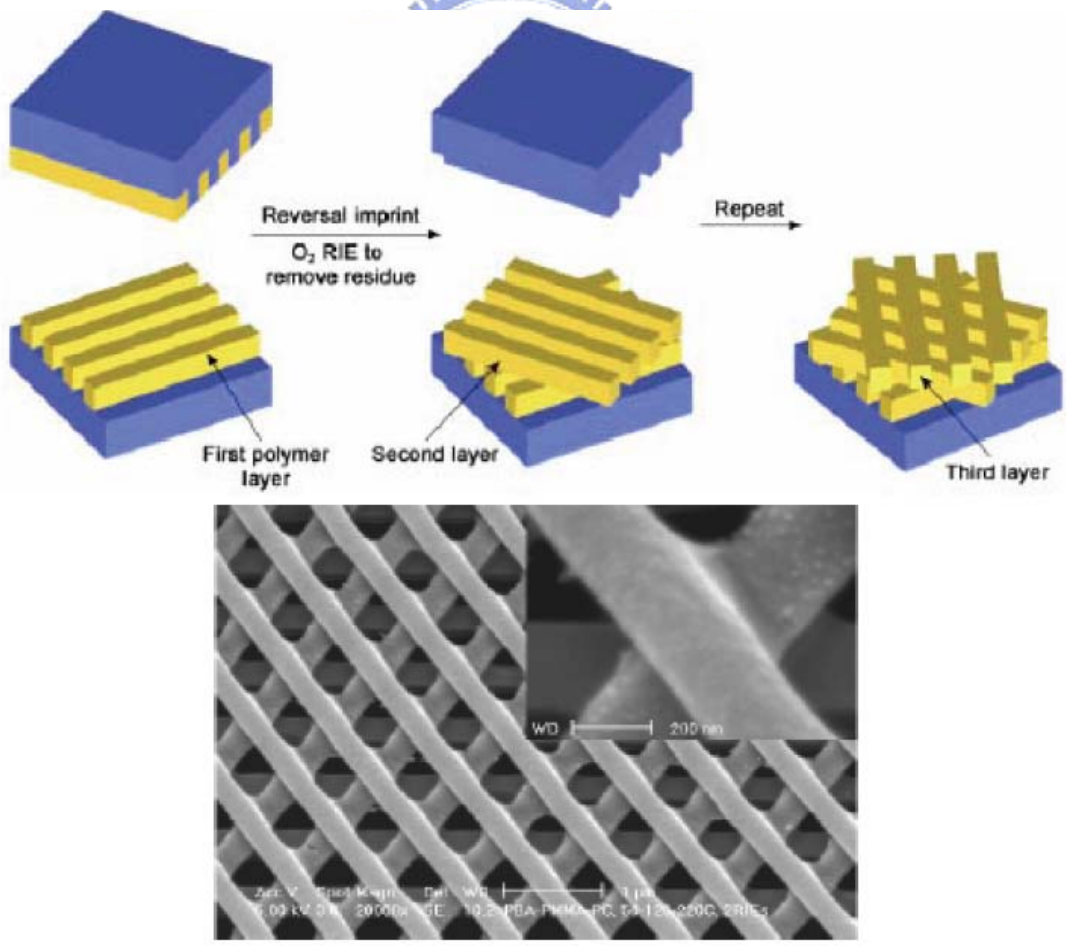

Figure 1.5 Nanoimprint over topographies and multilayer 3D printing

1.3 Introduction to Biosensor

Generally, biosensors are distinguished from one another by the nature of the process and according to their biochemical or biological component, e.g., biocatalytic, immunological molecules and nucleic acid. The transducer is the other component of the biosensor shown in **figure 1.6**, which also plays an important role in terms of converting the bio-recognition event into an electrical signal or other different kind of signal output. The transducers employed for detection include electrochemical, optical, and piezoelectric platforms. The detection strategies of the transducers can be divided into two categories, that is, labeled and label-free. The former relies on the detection of a specific label signal, and the latter is direct measurement of a signal occurring during the biochemical reactions on a transducer surface. The label-free method is more attractive than labeled because the extra label process is unnecessary, and hence research about label-free biosensors continues to grow **[19, 20]**. The biosensors are more common and extremely successful in most of platforms and presenting a selection of the most significant technologies and advances in relation to biological monitoring.

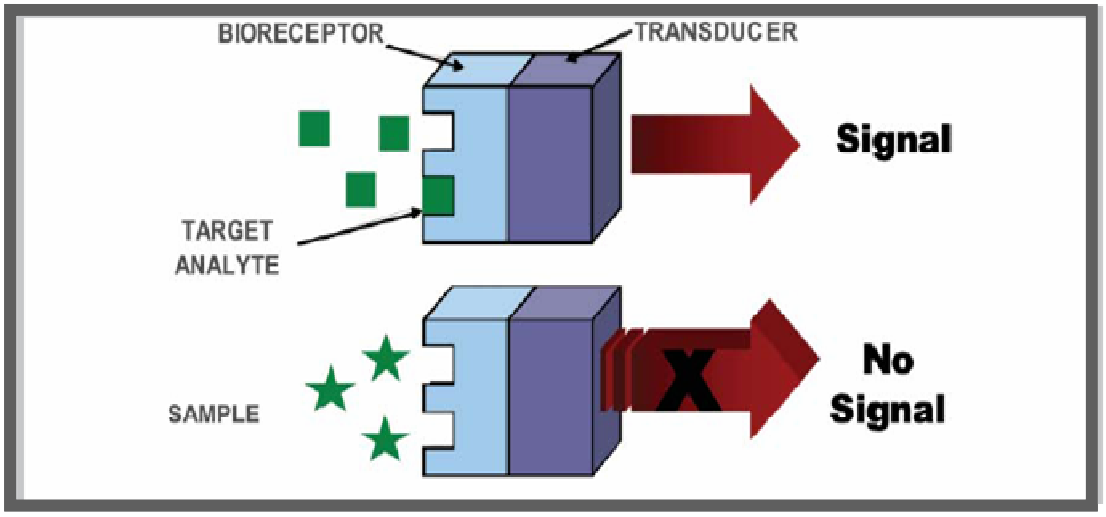

Figure 1.6 Schematic diagram of a typical biorecognition element.

1.3.1 Electrochemical biosensors

More than half of the biosensors used for the detection of biomolecules are based on electrochemical transducers **[21]**. A large amount of reports have demonstrated the importance of the electrochemical biosensors in the field of clinical and environmental analysis **[21, 22].** The electrochemical biosensors have many advantages, such as low cost, high sensitivity, independence from solution turbidity, easily miniaturized and well suited to micro-fabrication, low power requirements, and relatively simple instrumentation **[23].** These characteristics make electrochemical detection methods highly attractive for field monitoring of biological agents. The method used in many cases depends on the type of change along with the properties of the analyte and matrix. A discussion of the electron transfer mechanisms that commonly occur with amperometric-based biosensors are shown in **figure 1.7**.

Despite the features of remarkable sensitivity, rapid response, miniaturization capability, and low cost, the electrochemical biosensors still have problems with long-term stability and selectivity in blood sample. Obviously, further work would be required to demonstrate that the electrochemical biosensors do suffer from biofouling problems. Such problems can be partly addressed by covering the transducer or sensor surface with an appropriate microfluidic system shown in f**igure 1.8**. Notwithstanding, the use of disposable screen printed electrodes appears to be a realistic strategy for target biomolecules detection. Consequently, screen printed electrodes have attracted much attention recently as a platform in DNA, immunoassay and enzyme-based biosensors **[24, 25]**. About this strategy may be somewhat limited to applications that do development accuracy in real-time monitoring.

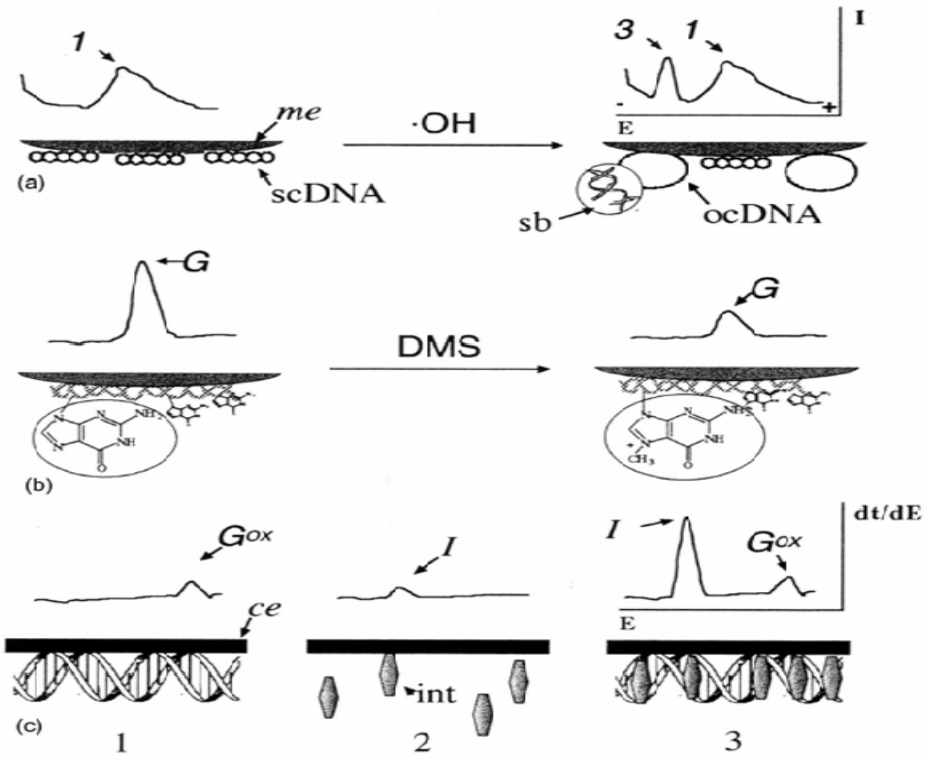

Figure 1.7 Schematic representation of the principle of electrochemical detection of DNA damage and DNA-damaging agents.

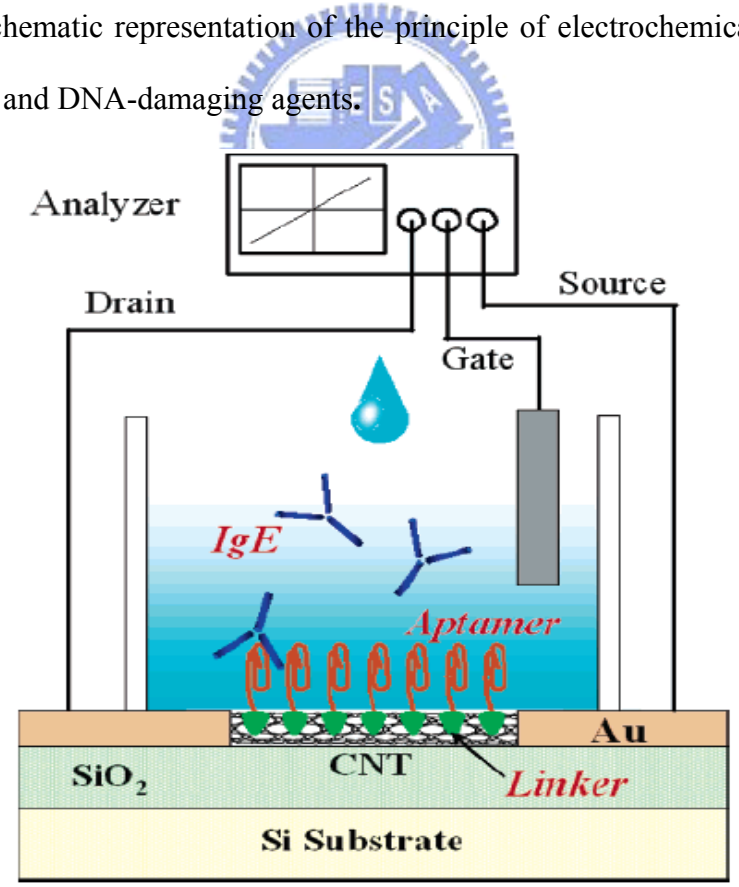

Figure 1.8 Schematic structure of the experimental setup for the detection of IgE using an aptamer-modified FET device integrated with microfluidic system.

1.3.2 Optical biosensors

When a light illuminates onto a sample, a lot of information can be manifested by either reflection or transmission. This phenomenon depends on the wavelength of light, the angle of incidence, the sample composition and sample thickness. By exploiting the energy from the electromagnetic spectrum, it can be used to provide information about the changes in the local environment surrounding the analyte. Optical biosensors, which sometimes referred to considerable interest on the detection of biomolecules **[26]**.Therefore, biosensors based on surface plasmon resonance and fluorescence principles are the most common and promising methods for target molecules detection. Recent reports about related technologies suggest that optical biosensors possibly become a powerful tool in the future for the real-time and biomolecular detections **[27]**. **Figure 1.9** shows the surface plasmon resonance (SPR) being a form of reflectance spectroscopy that has been widely used in biosensor development. It has been demonstrated that SPR plays a significant role in relation to immunogenicity, proteomics, drug discovery, and DNA analysis **[28]**. This method is particularly attractive for direct and label-free detection and many previous works have shown that the SPR-based biosensor is also a tool for target molecules monitoring. SPR is one of very few techniques that are able to provide non-invasive, real-time kinetic data on association and dissociation rates, along with equilibrium binding constants for receptor systems. Although SPR is an interesting and appealing transduction method, the measuring is limited to a very small range. There seems to be developed a hand-held SPR device that can be used to detect biomolecules directly. The development of a technology which can be taken into the field and provide real-time monitoring process in the detection of target molecules directly.

Despite the improvement of sensitivity and reducing analysis time of the SPR, further development is still necessary for the sensor to be performed in a complex

sample such as blood and serum. If these devices are used for the detection of biomolecules routinely, one of the challenges limits the application of SPR for real-time measurement in blood is that the signal is very sensitive to non-specific physical binding on the surface **[21]**. Notwithstanding, the capability to perform real-time measurement is an area of significant interest for the detection of target molecules **[29]**.

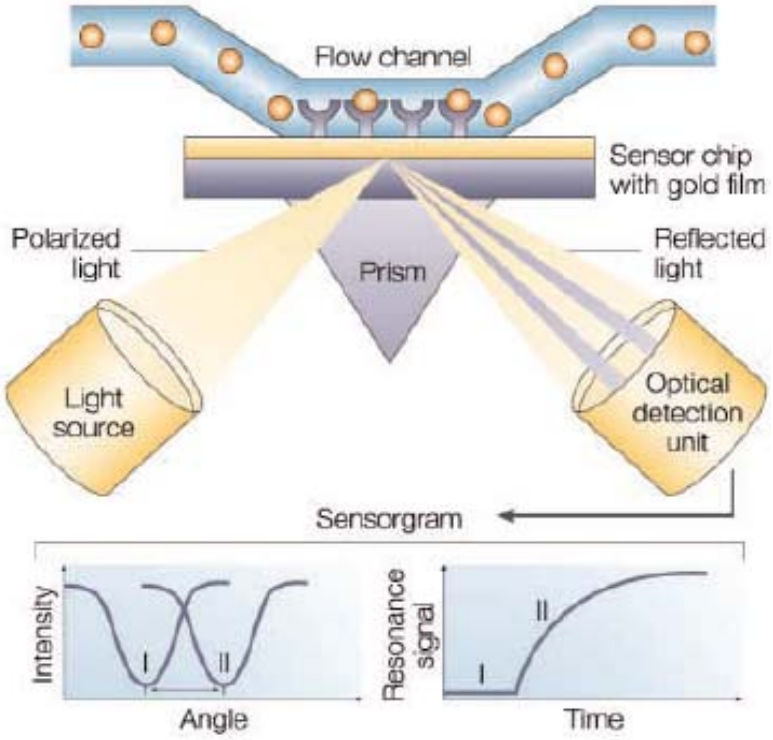

Figure 1.9 Typical setups for an SPR biosensor. Surface plasmon resonance (SPR) detects changes in the refractive index in the immediate vicinity of the surface layer of a sensor chip. The SPR angle shifts when biomolecules bind to the surface and change the mass of the surface layer. This change in resonant angle can be monitored non-invasively in real time as a plot of resonance signal versus time.

1.3.3 Piezoelectric biosensors

Piezoelectric biosensor works on the principle that the frequency variation of an oscillating quartz crystal correspond to changes in mass as a result of a biochemical reaction and bio-recognition event **[30]**, as shown in **figure 1.10**. One of the piezoelectric sensors is quartz crystal microbalance (QCM), which has been used to detect target molecules **[30]**. It has been evaluated the detection limit of various biosensor platforms and concluded that the piezoelectric method is inferior compared to electrochemical and optical detectors **[30].** Notwithstanding, some studies about detection of biomolecules by using the piezoelectric sensor approach increased recently. It was demonstrated that the molecular imprinting technique may be a promising method for solving problems from non-specific interactions. The QCM transduction method is an attractive option for real-time monitoring of target molecules.

Despite the promising analytical performance of the piezoelectric sensor further work still needs to be undertaken to evaluate the stability of the sensor surface in biological fluids. Problems such as crystal regeneration, relatively long incubation times, nonspecific binding of proteins or other biomaterials, and loss of material coating after washing are well known limitations of this technique, **[22, 30]** which still require further attention before this biosensor technology platform is used routinely for target molecules detection.

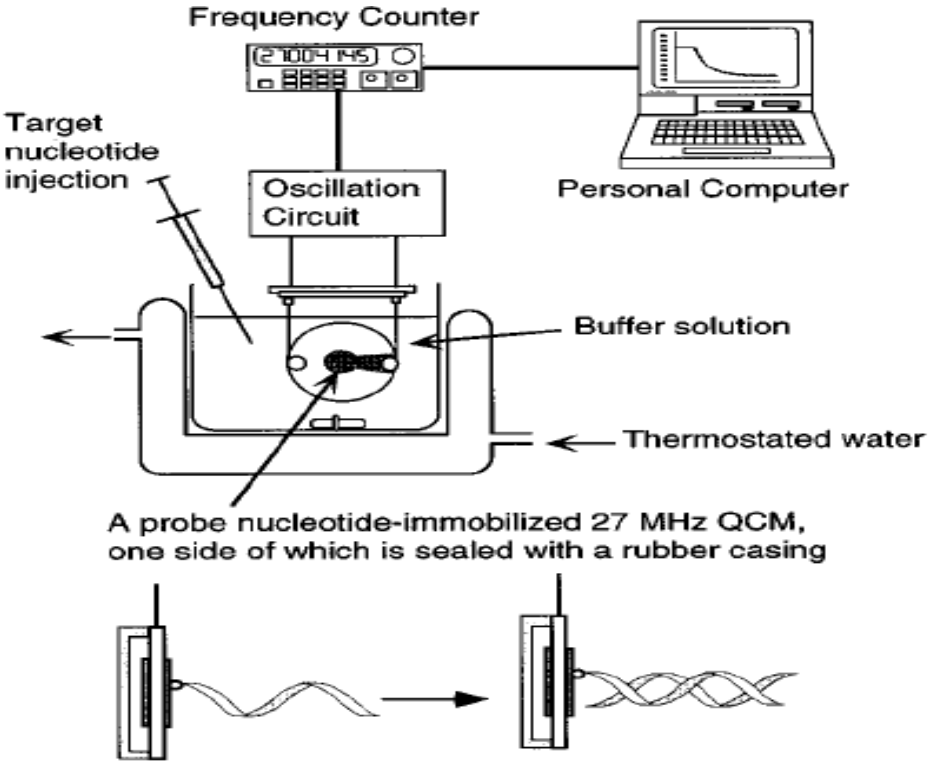

Figure 1.10 Schematic illustration of a highly sensitive 27-MHz QCM

1.4 Introduction to the Importance in Detection of Biomolecules

A number of biosensors have been developed to detected important biomolecules. However, all of them essentially comprise a biological recognition element or bio-receptor, which interacts with the analyte and responds in some manner that can be detected by a transducer, as shown in **figure 1.6.** The biological recognition element is a crucial component, and its function is to impart selectivity so that the sensor responds only to a particular analyte of interest, hence avoiding interferences from other substances. **Table 1.1** summarizes the main analytical features of a wide range of biosensors, noting that a majority of the existing technologies used for detecting target molecules rely on antibodies as the recognition molecule **[5]**. Antibodies are the critical part of an immuno-sensor, since their quality contributes to the sensitivity and specificity **[5]**.

Table 1.1 A summary of selected biosensors used for the detection of biomolecules

Transducer	Analyte	Biosensor format	Detection limit
Amperometric	Newcastle disease	Enzyme-label immunoassay	11.1 ng ml^{-1}
	Forest–Spring encephalitis	Sandwich gold-label immunoassay	10^{-7} mg ml^{-1}
	Japanese B encephalitis	$Fe^{2+/3+}$ probe & label-free immunoassay	6×10^{-9} lg pfu ml^{-1}
	Hepatitis B	Methylene blue probe, PCR & DNA	NA
	Hepatitis B	Osmium complex probe, PCR & DNA	NA
Potentiometric	Hepatitis B	Enzyme label immunoassay	~50 fM
	Japanese B encephalitis	Immunoassay	6×10^{-9} lg pfu ml^{-1}
Light-addressable potentiometric	Newcastle disease	Sandwich enzyme-label immunoassay	2 ng ml^{-1}
	Venezuelan equine encephalitis	Sandwich enzyme-label immunoassay	30 ng ml^{-1}
Impedance spectroscopy	Hepatitis B	Immunoassay	8 ng ml^{-1}
	Hepatitis B	Immunoassay	50 ng l^{-1}
Conductometric	Bovine viral diarrhoea	Sandwich immunoassay	Varied between 10^2–10^4 CCID ml^{-1}
Fiber-optic evanescent wave	Newcastle disease	Fluorescein-label sandwich immunoassay	10 ng ml^{-1}
Surface plasmon resonance	Foot-and-mouth disease	Immunoassay	NA
	Hepatitis A	Immunoassay	NA
	Severe acute respiratory syndrome	Peptide binding	NA
Fluorescence	Various toxins	Immunoassay	~ng ml^{-1}
	Dengue	Immunoassay	NA
	Dengue	Nucleic acid	~Picomolar
Piezoelectric	Foot-and-mouth disease	Immunoassay	NA
	Foot-and-mouth disease	Immunoassay	NA
	Hepatitis B	Nucleic acid	~0.01 μg ml^{-1}
	Severe acute respiratory syndrome	Immunoassay	0.6 mg ml^{-1}
	Dengue	Immunoassay	~μg ml^{-1}

[a] NA = not available.

It is important to note that the success of an immuno-sensor depends heavily on which antibodies, labels, and reagents are used in the assay. Once antibodies of the desired specificity and affinity have been developed, they can be incorporated in a wide range of transducer platforms. DNA is an alternative recognition molecule that has also received some attention for the detection of target molecules. A large number of excellent papers have been reported based on nucleic acid hybridization. And noting that the detection of specific DNA sequences provide the fundamental basis for monitoring a wide variety of genetic diseases and viral infections **[11-16]**. Despite of the great deal of work in this field, the application of a DNA biosensor for target molecules detection is still in its infancy. One of the major requirements in developing a biosensor for target molecules is the need of a sensitive analytical device that can not only achieve low detection limitation easily but also high selectivity. Many infectious diseases will spread rapidly through a community before any symptoms are identified. If a biosensor can detect low levels of antigen easily at the onset of infection will be invaluable. In addition, a biosensor that is relatively cheap, robust, responds rapidly and provides high-throughput is highly desired for applications. However, the type of biosensor used for target molecules will in many cases depend on the properties of the analyte (i.e., size, structure, concentration, etc.) and the matrix (i.e., air, liquid). The most commonly used bio-sensing methodologies for detecting two important biomolecules will be described in detail in next chapter.

Chapter 2: Literature Review

2.1 Silicon Nanowire Field Effect Transisitor (Top–Down SiNW-FET)

Bashir and co-workers **[1]** described SiNW-FET sensor process that was realized using the "top–down" microelectronics processing techniques. A process known as confined was utilized to obtain single crystal silicon nano-plates that are thin as 7nm and nanowires small as 40nm in diameter at precise locations, as shown in **figure 2.1 [2]**. The method allowed the realization of truly integrated dense array of sensor. Initial testing of the device showed that sensitivity towards oxygen ambient, and suggested it possibility of using these sensor**s** for chemical and biological detection shown in **figure 2.2 [1]**.

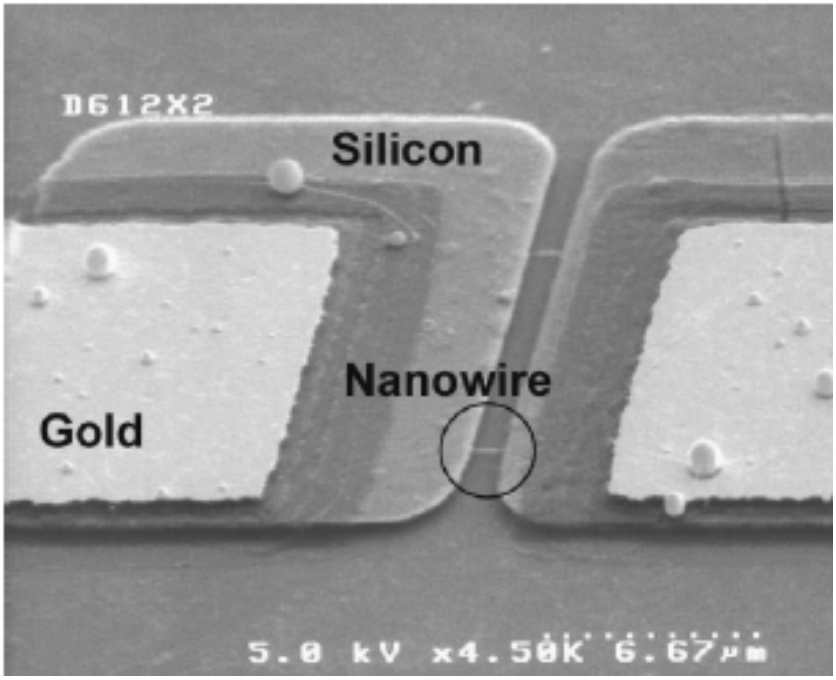

Figure 2.1 Field emission scanning electron microscopy photos of the fabricated devices. There are two nanowires between electrodes.

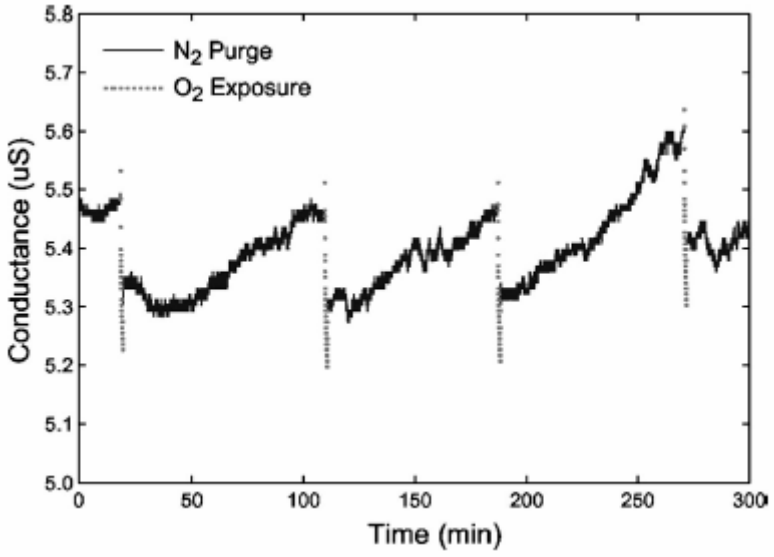

Figure 2.2 Electrical response of the device upon exposure to oxygen and nitrogen.

Li et al. **[3, 4]** fabricated a single crystal silicon nanowire with 50 nm width on SOI wafer by electron bean lithography. They have demonstrated the detection of DNA molecules based on their intrinsic charge by using SiNWs fabricated by top-down semiconductor processes. This method created a pathway for fabricating high-density, high-quality, and well organized nano-scale sensor that can be integrated with communication circuits, as shown in **figure 2.3 [3]**. Sequence-specific and label-free DNA sensors based on SiNW with probe-DNA or PNA molecules covalently immobilized on the surfaces in **figure 2.4 [4]**. Label-free DNA was recognized when the target DNA was complementary with the probe-DNA attached onto the SiNW surfaces, causes the change to accumulate on the surface of the SiNW. But there are two disadvantages blocking the development of this device. One was they use high cost substrate-SOI wafer, the other one was the device lack of individual controlling gate.

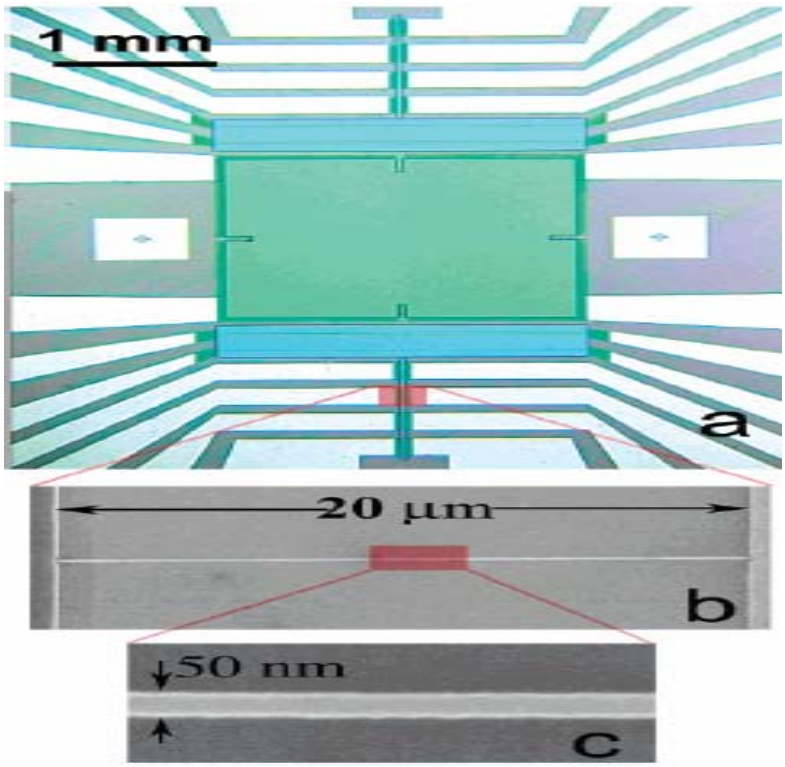

Figure 2.3 (a) The optical image of the central region of a sensor used for the DNA sensing study. (b) and (c) Representative SEM images showing the SiNW bridging two contact leads.

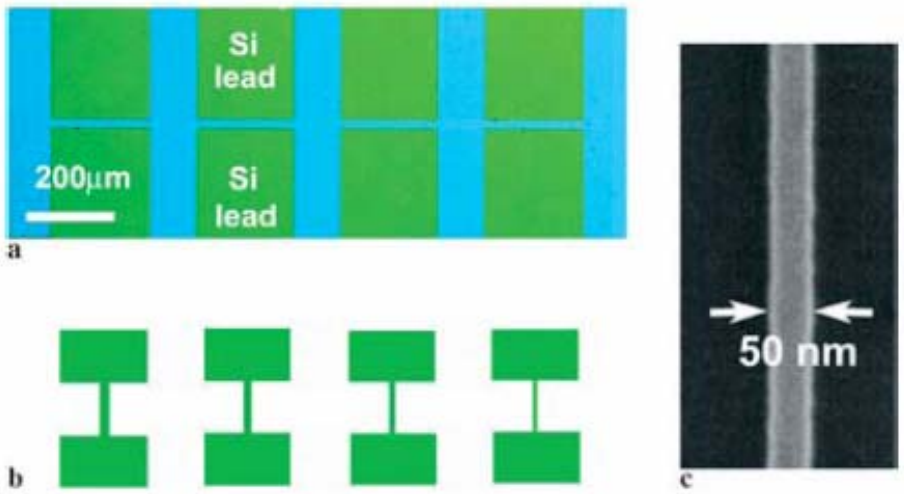

Figure 2.4 (a) Optical image of the central region of a sensor showing a portion of the lead and the bridged nanowire used for the DNA sensing; (b) schematic drawing of the SiNW with varying widths corresponding to the image in (a); (c) a SEM image showing a 50-nm-wide SiNW, which extends between two contact leads.

Sheu et al. **[5]** demonstrated the bio-detection by using the SiNW whose surface was pretreated by APTMS and then selectively deposited with gold nanoparticles, as shown in **figure 2.5 and figure 2.6 [5]**. The GNPs on the surface served as linkers for detection. The target molecules bound with GNPs on the surface of the SiNW and resulted in a voltage shift.

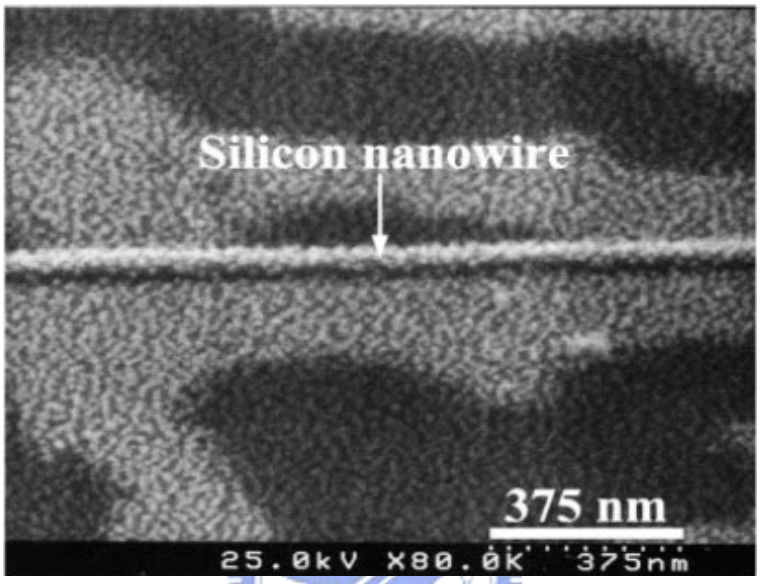

Figure 2.5 SEM image of SiNW after reaction of the GNPs with APTMS.

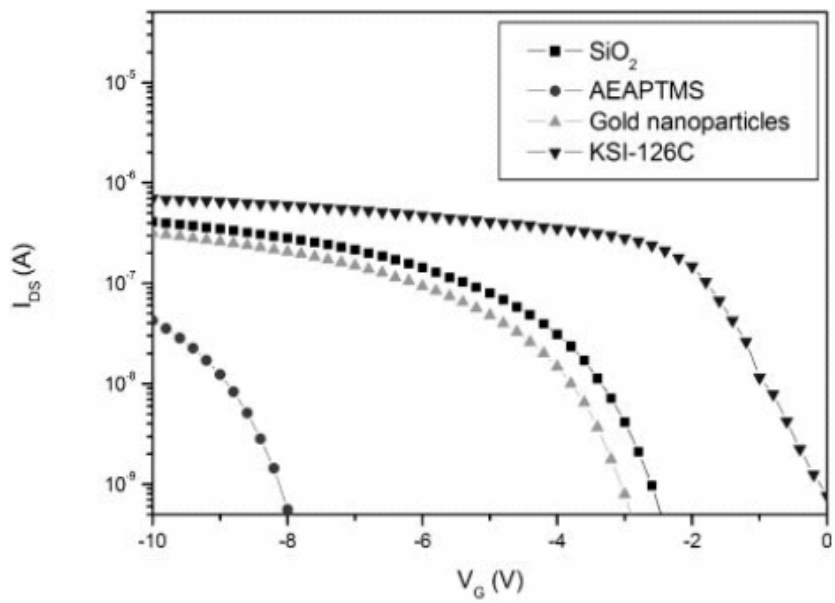

Figure 2.6 I_D-V_G curves of SiNW after binding of different molecules on the surface of SiNW. The turn-on voltage was changed after binding of different molecules

Ko et al. **[6]** developed a self-aligned platinum-silicide nanowire for biomolecules sensing was shown in **figure 2.7.** The immobilization steps of the DNA onto the nanowire are illustrated in **figure 2.8 [6]**. The 40 nm-width nanowire is fabricated through a sequence of electron-beam writing on the poly-Si film, line shrinking by alkaline solution, platinum film depositing, 550°C annealing, and aqua dissolution is performed. The immobilization of capture-DNA on the platinum-silicide nanowire is verified from the fluorescence-labeled technique. The FET can distinguish the complementary, mismatched, and dehybridized DNA via the conductance difference. They can sense the minimal target DNA concentration down to 100fM. Unfortunately, this SiNW-FET device cannot integrate with microfluidic system to detect real-time response.

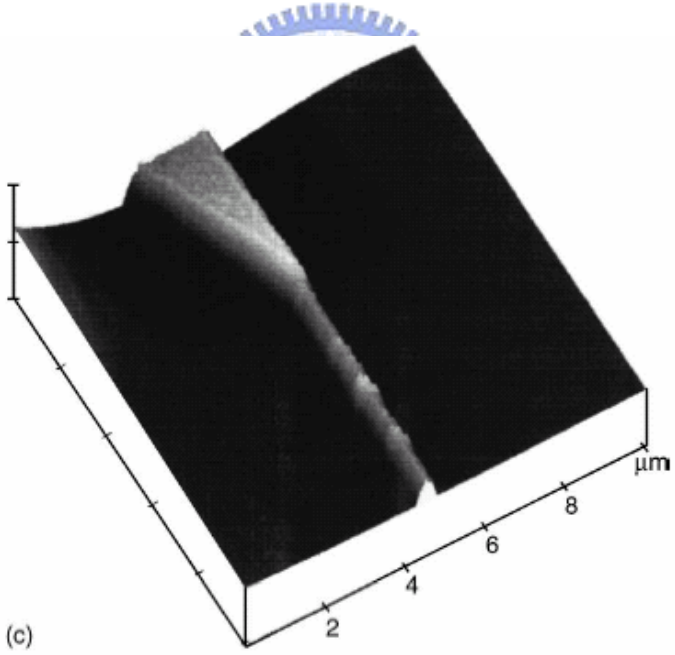

Figure 2.7 The 3-D AFM image of 40 nm width Pt-silicide nanowire.

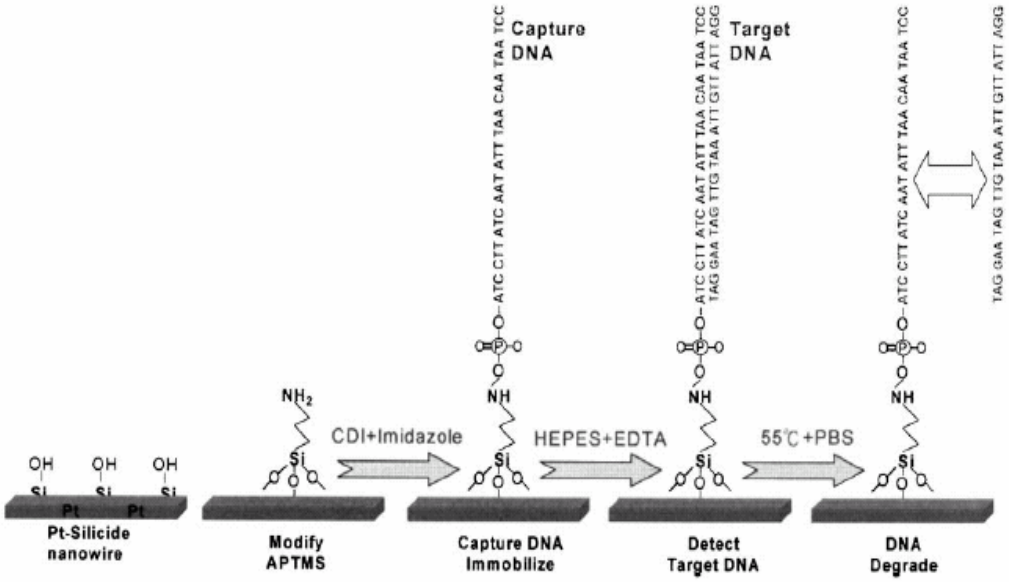

Figure 2.8 The immobilization steps for the DNA on the Pt-silicide nanowires.

Eric Stern et al. **[7]** have demonstrated an approach to realize the characteristic of the SiNW sensors for specific label-free antibody detection. The images and electrical properties of the SiNW sensors are shown in **figure 2.9**. This approach has potential for extending single device to an integrated system, with widely use as the chip-arrays. However, 'top-down' fabrication produced successful solution-phase nanowire sensing has been demonstrated for proteins **[5, 6]**, and DNA **[7**, **8, 9, 10]**. Here they reported the uses of CMOS-FET compatible technology and hence demonstrate the specific label-free detection of concentrations of antibodies as well as real-time monitoring of the response. But this kind of device is without independent controlling back-gate.

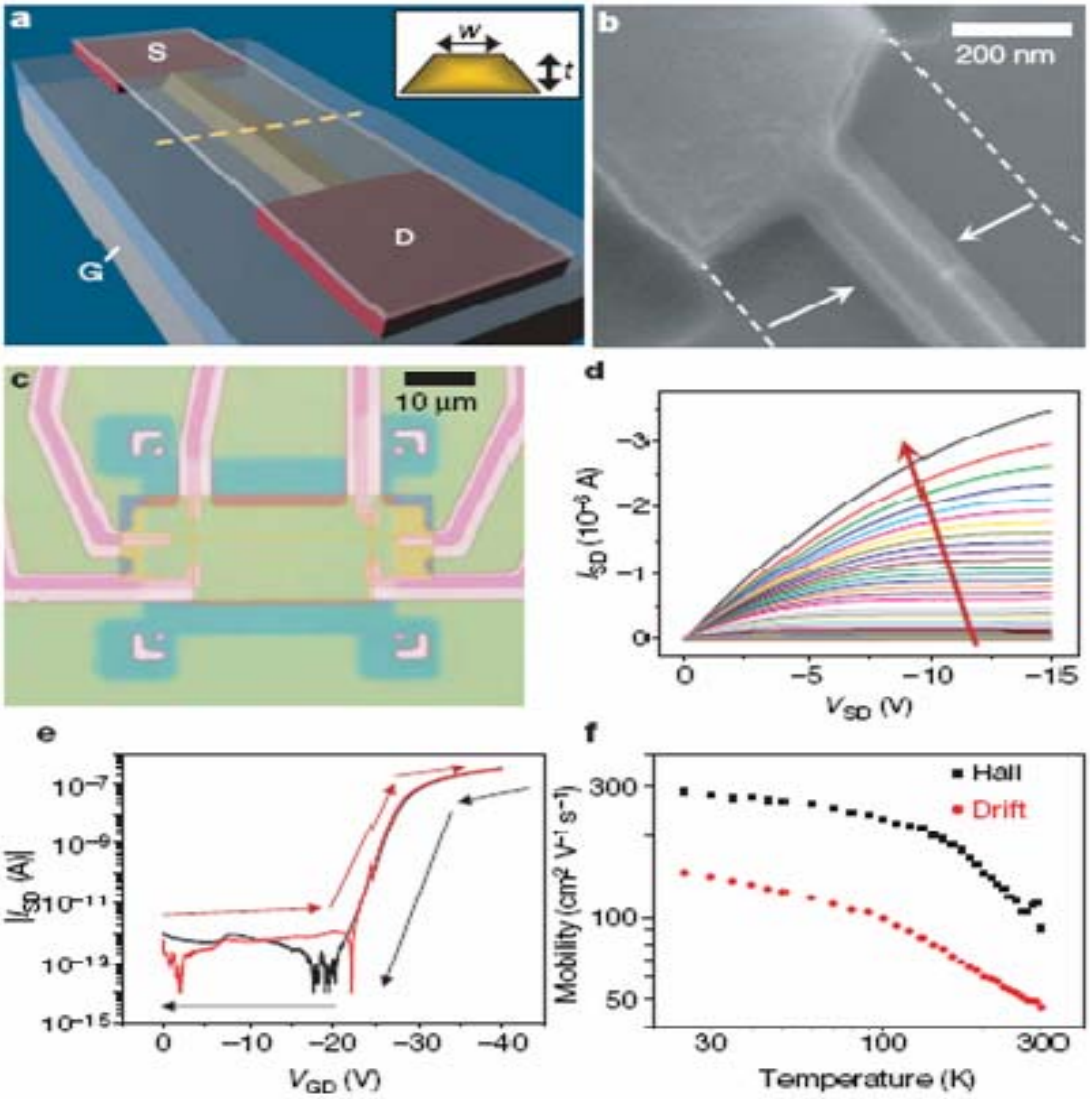

Figure 2.9 Device fabrication and electrical performance. (a) Schematic of active channel. The source, drain, and back-gate are labeled; (b) SEM and (c) OM image of a device; (d) I_{SD} for varying V_{GD}, illustrating p-type behaviour; (e) I_{SD} for V_{GD} for forward and reverse sweep. (f) Hall and drift mobilities versus temperature.

Pritiraj Mohanty et al. **[11]** demonstrated the fabrication, functionalization, and operation of a nano-electronic FET for pH sensor, as shown in **figure2.10**. The SiNW with side-gate is fabricated with standard semiconductor process. The functionalized SiNW can be controlled with local side-gate to induce inversion or depletion layers. This approach offers the possibility of highly parallel detection of ion or charged protein and DNA with control of individual elements. By selective gate-voltage, individual NWs in an array can be turned on or off during sensing process. Therefore, the array contains multiple receptors for the detection of multiple chemical and biological species in a single integrated chip. But this SiNW device is without oxide acting as dielectric layer to level down the field effect characterization. Also their fabrication starts from the high cost SOI wafer.

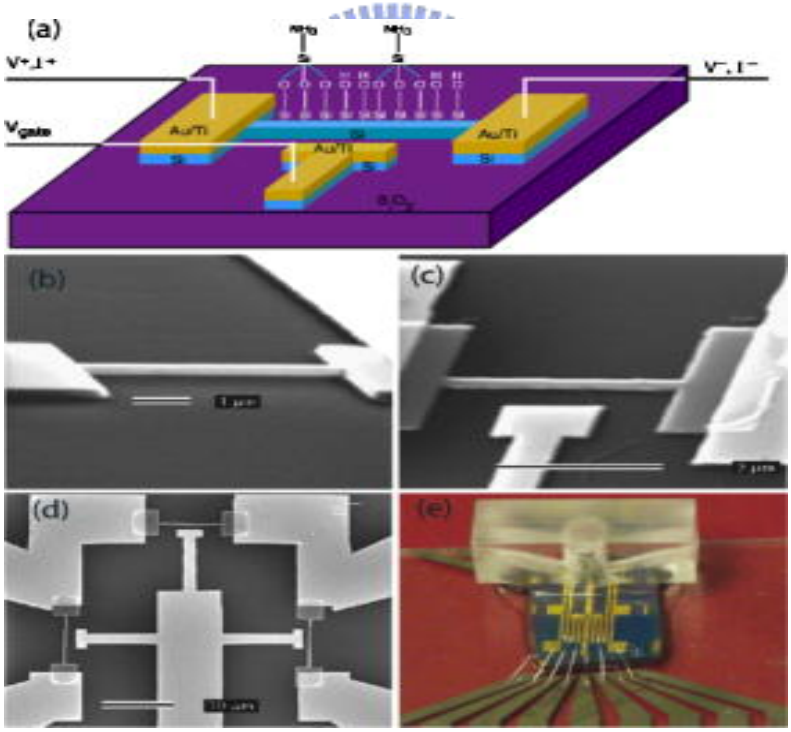

Figure 2.10 Device schematic diagram. (a) The diagram of the SiNW with side-gate; (b) The nanowire shown here; (c) A SiNW with a Au/Ti side-gate. (d) The SEM image displays three SiNW devices on the same chip; (e) An OM image shows the flow chamber sealed on top of the devices.

2.2 Real-time Nanowire Field-Effect-Transisitor Biosensors

Detectors based on semiconductor NWs are configured as FETs, which exhibit a conductivity-relevance change in response to variations in the electric field or potential at the surface **[8]**. The dependence of the conductance on gate voltage makes FET natural candidates for electrically based sensing, because the electric field effect resulting from the binding of a charged species is the effect of applying a voltage with a gate electrode. They can be prepared as p- or n-type materials and configured as FET in **figure 2.11(b)** that exhibits better electrical characteristics achieved for silicon devices **[12, 13, 14]**. The superior switching characteristics of SiNWs are important factor that achieve excellent sensitivity. The binding of biomolecules onto the surface of the NW leads to depletion or accumulation of carriers in the nanometer-diameter structure, versus only the surface region of a device. This semiconductor NWs provides sufficient sensitivity to enable the detection of important biomolecules in solution. However, because these are field-effect devices, detection sensitivity depends on the ionic strength of the solution. A sensing device can be configured from high-performance NW-FET by linking NW receptor groups that recognize specific molecules to the surface of the NW in **figure 2.11(c)**. When the sensor device with surface receptors is exposed to a solution containing biomolecules, such as protein that has a net negative charges in the aqueous solution, specific binding will lead to an increase in the surface and in conductance for a p-type NW device. As a proof of concept, there are some reports have developed a microfluidic system integrated NW sensor that incorporates SiNW with well-defined p- or n-type doping; source and drain electrodes that are insulated from the aqueous reagent environment. And above phenomenon only processes occurring at the SiNW surface contribute to electrical signals and a microfluidic channel for delivery of solutions in **figure 2.11(d)** **[15]**. And then they fabricated electrically addressable arrays by a process that uses

fluid-based assembly of NWs to align them and spacing over large areas. Photolithography and metal deposition define interconnections to a large number of individual NWs in parallel array in **figure 2.12 [15].**

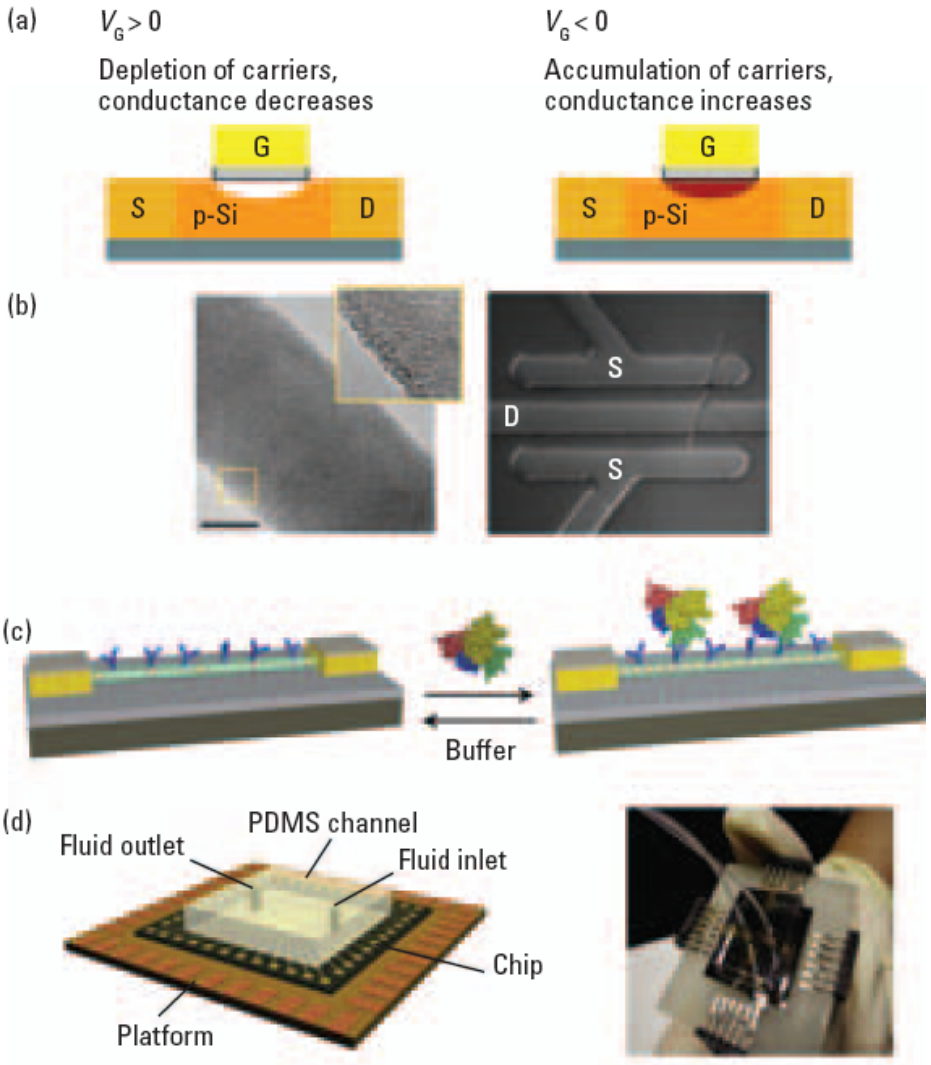

Figure 2.11 NW-FET sensors. (a) Schematic of a p-type FET device. S, source; D, drain; and G, gate electrodes; V_G, gate voltage; (b) (left) TEM images of a 20-nm-diam single-crystal SiNW and (right) an OM image of a device; (c) Schematic of a sensor with antibody receptors (blue); binding of a protein with a net negative charge results in an increase in conductance; (d) NW sensor biochip with integrated microfluidic sample delivery.

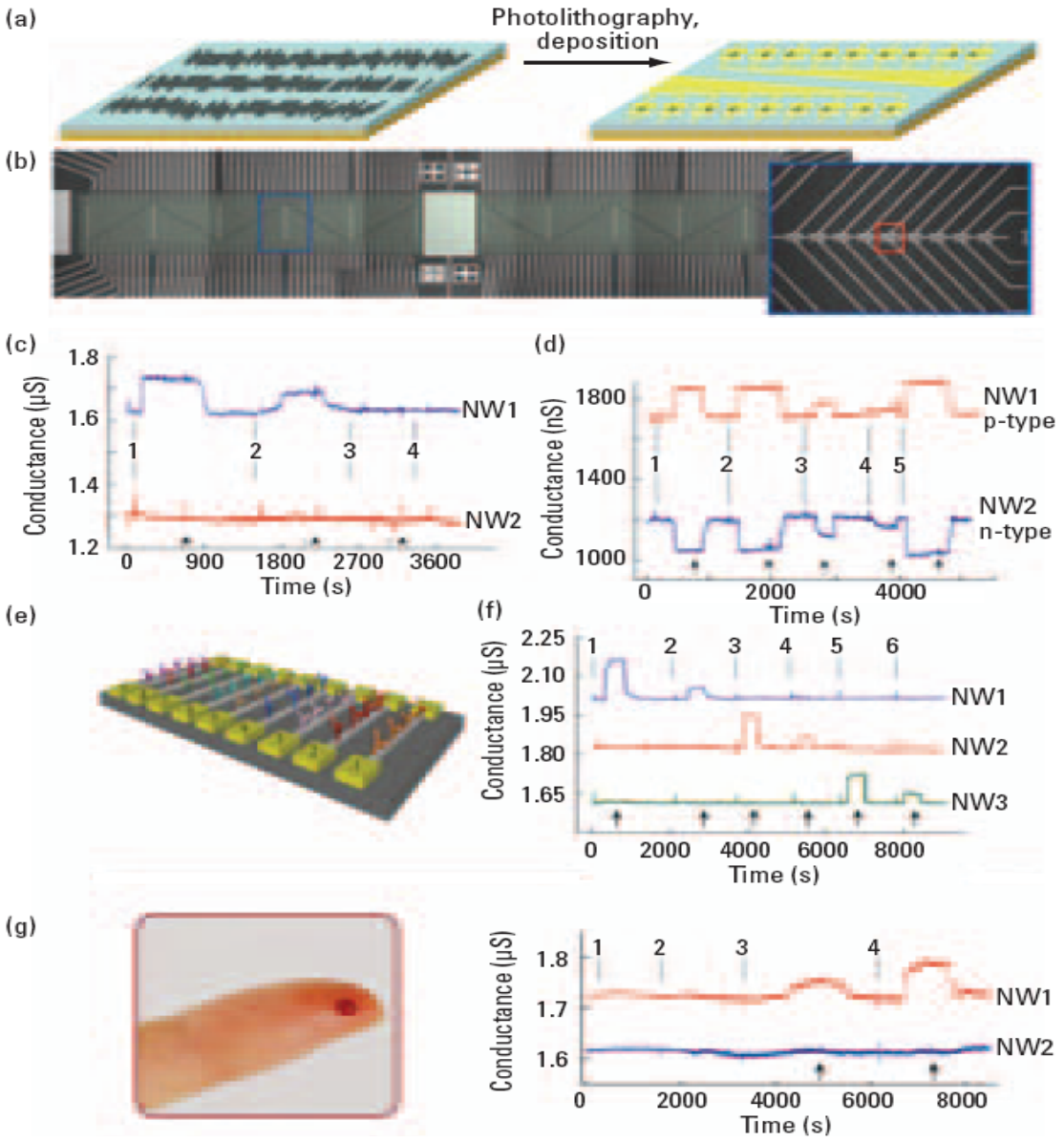

Figure 2.12 NW arrays for multiplexed protein sensing. (a) Illustration of NW array fabrication; (b) Optical image of a NW array; (c) Data recorded from p-SiNW devices; NW1 was immobilized with PSA-Ab1, and NW2 was modified with ethanolamine; (d) Complementary sensing of PSA with p-type (NW1) and n-type (NW2) NW devices; (e) Schematic of array detection of multiple proteins; (f) Detection of PSA, CEA, and mucin-1 with NW1, NW2, and NW3 functionalized with antibodies. Protein solutions of PSA, CEA, and mucin-1 were delivered sequentially to the array. (g) The drop of blood corresponds to the quantity required for analysis. Conductance versus time data recorded for the detection of PSA and PSA. NW2 was passivated with ethanolamine.

Recently, the biosensor has employed increasingly in a variety of applications where continuous measurements in biological media are required by real-time monitoring sensing **[16]**. A biosensor is distinguished from a chemical sensor in that it possesses a biological recognition element, typically a protein, peptide or oligonucleotide. The goal in this subject may measure the rate of uptake or efflux of relevant species or to establish spatial distributions in real-time sensing **[17]**. When a sensor is brought in contact with biological tissues, sensor performance can deteriorate. The exact causes of this deterioration are not clear, but are a mix of passive adsorption of biomolecules on the sensor probe surface and active processes coupled to tissue response **[17]**. For this reason, we will give some attention to approve the microfluidic system that can play key roles in regulation of detection events. This affords a greater range of analytical approaches to analysis, including separations and derivatization not possible with a single real-time sensor array.

2.3 Detection of Important Cancer Markers

2.3.1 Introduction of Mutation Genes-*BRAF*^{V599E}

Cancers arise owing to the accumulation of mutations in critical genes that alter normal program of cell proliferation, differentiation and death **[18]**. Recently, a somatic point mutation in the *BRAF*^{V599E} gene has been identified as the most common genetic event in papillary thyroid carcinoma **[19]**. In a series of 78 papillary carcinomas, 36% of tumors harbored a thymine-to-adenine transversion at nucleotide position 1796, which results in a valine-to-glutamate substitution at residue 599 (V599E). In another study, a higher prevalence (69%) of this mutation was observed in a series of 35 papillary carcinomas **[20]**. Here the paper reports *BRAF*^{V599E} missense mutations in 66% of malignant melanomas and at higher frequency in human liver cancer **[21]**. Nucleotide 1796, the only mutational site in thyroid

carcinomas, the most frequently affects the hot spot in other types of human cancers where $BRAF^{V599E}$ is mutated, such as malignant melanoma and colorectal carcinoma **[21, 22]**. The initial reports indicated that $BRAF^{V599E}$ mutations in thyroid tumors are restricted to papillary carcinoma, because no mutation was observed in other types of well-differentiated thyroid cancer **[20, 21]**. However, it remains unclear whether this gene is also mutated in poorly differentiated and anaplastic thyroid carcinomas, which are the most aggressive types of thyroid neoplasm. In addition, it is important to determine whether $BRAF^{V599E}$ mutation confers papillary carcinomas with distinct phenotypical and biological properties. In this study, they analyzed a series of 320 thyroid tumors and benign nodules for $BRAF^{V599E}$ mutation, report a novel method of screening for the mutation, and provide a detailed comparison of clinical-pathologic features between thyroid tumors according to their $BRAF^{V599E}$ status. The high prevalence of $BRAF^{V599E}$ mutations in papillary carcinomas and the specificity of this alteration to papillary carcinomas or less differentiated tumors developing from papillary carcinoma make it a potentially important marker for tumor diagnosis and prognosis in future real-time biosensors. Testing for $BRAF^{V599E}$ mutations in thyroid tumors is simplified by the fact that virtually all of them are restricted to the nucleotide position 1796. This relatively simple, quick, and sensitive method can be used not only in tissues harvested at the time of surgery but also for the preoperative diagnosis of thyroid specimens. In addition, $BRAF^{V599E}$ may be a valuable target for cancer marker currently being developed to diagnose its activity. This would be of a particular importance for carcinomas that represent a major source to detect the thyroid tumors.

2.3.2 Introduction of Cancer Marker Alpha-Fetoprotein

Hepatoblastoma (HB) is the most common primary liver tumor of childhood but accounts for less than 1% of all paediatric tumors **[23]**. Hepatocellular carcinoma (HCC) is one of the most common causes of cancer-related deaths in Asia, especially in Taiwan **[24]**. The main treatment for HCC is surgical resection, but less than 15 % of patients can benefit from this treatment due to the presence of multi-focal tumors and the risk of post-operative hepatocellular deficiency **[25]**. The introduction of cisplatin into treatment in the early 1980s dramatically improved the prognosis for most children with HB and survival rates have risen to at least 70% in most recent large series **[26, 27]**. The prognosis mainly depends on disease extension at the time of diagnosis and the completeness of surgical resection. However, the level of serum alpha-fetoprotein (AFP) at diagnosis has also been shown to impact the outcome **[28, 29]**. Alpha-fetoprotein, a glycoprotein with an electrophoretic mobility of 1-globulin, is produced in the fetal yolk sac, liver and intestine **[30]**. After birth, production of AFP is almost totally repressed, but it reappears and is over-expressed in about 60 to 70% of patients with HCC, which makes it a useful biomolecule marker in the diagnosis of this malignancy and liver cancer **[31]**. Von Schweinitz et al. were the first team to point out that it would be a negative prognostic factor in suffering from HB when the concentration of serum AFP level was below 30ng/mL **[24, 28]**. This finding resulted in an protocol recommending that future patients with HB and a standard level of AFP at diagnosis should be categorized as high-risk regardless to the extent of the disease at diagnosis, and should be treated with more aggressive chemotherapy. The aim of this work was to investigate the clinical characteristics, histology and outcome of patients with HB and AFP level who have been accrued by biosensor. In conclusion, HB with AFP level is a high subset of hepatic tumors. Even though they are heterogeneous tumors with different histological subtypes, they

nonetheless exhibit some common characteristics such as widespread disease at presentation, chemoresistance and a poor outcome, which signal intrinsically aggressive genetic and biological tumor profiles. Clearly, more investigations and large-scale cooperation among groups involved in HB research are warranted to further improve well-known understanding of these heterogeneous tumors.

Clinical experience and in vitro studies demonstrated that the levels of AFP may vary in patients with HCC. In addition, tumor recurrence rates are rather high in patients with HCC who received surgical treatment. Therefore, novel detection strategy for liver cancer has been investigated. In the current study, we focused on refining the component of tumor receptor-mediated adenoviral vector retargeting using currently varieties of biosensors.

2.4 Motivation

Ultra-sensitive detection of biomolecules is fundamental to the detection of biomolecular analysis. 1-D nanostructures have been demonstrated as good candidates for ultra-sensitive, label-free, miniaturized molecule sensors in the applications. Among the "top-down" systems explored and comparison with previously reported methods is given in **Table 2.1**, the sensors based on SiNW, could be understood in terms of change of surface charge with the presence of molecular species. However, here we demonstrate the detection of important biomolecules based on their charge by using SiNW fabricated by "top-down" processes. This method created a way to fabricate high-density and high-quality biosensor that can be integrated with the following advantages listed in **Table 2.2.** To solve the back-gate problem, the structure of side-gate is configurated in my thesis, addressing all devices on the wafer were the gate be addressed individually of NW-FET. The shrank nanowires with higher surface-to-volume ratio and individual side-gate for integration are achieved by the LOCOS process. The detection sensitivity is therefore greatly enhanced as the signal can be effectively transduced. Our side-gate devices using SOI wafers provide a good quality of gate-dielectric and therefore the electric field was induced effectively by the charged molecule, and the detection signal varied more sensitive. Recently papers have reported about the biological molecules sensing applications, and developed novel real-time biosensors. With the testing sample needs being preceded in an aqueous solution, it usually needs a microfluidic system to carry out. For these reasons, we investigate the process to build the microfluidic system integrating with the SiNW-FET. Our goals are to develop a detection system with real-time, label-free and bio-sensing side-gate devices.

Table 2.1 The characteristics comparison of four kinds of nanowire fabrication

Approach	**Nanowire with back-gate (Top-down)**	**Nanowire with back-gate (Top-down)**	**Nanowire with side-gate (Top-down)**	**Nanowire with side-gate (Top-down)**
Journal	**Nano Letters 2004**	**Nature 2007**	**APL 2006**	**Biosensors and Bioelectronics 2007**
Author	**Z. Li …etc**	**Eric Stern…etc**	**Pritiraj…etc**	**G.S. Wilson…etc**
Sensitivity	**25pM**	**≤ 100fM**	**Not mentioned**	**100fM**
Integration	**Easy (E-beam)**	**Easy (E-beam)**	**Easy (E-beam)**	**Easy (E-beam)**
Advantages	**1. Sensitive 2. Label-Free 3. Sensing array density 4. Real-time detecting**	**1. Sensitive 2. Label-Free 3. Real-time detecting**	**1. Sensitive 2. Label-Free 3. Side-gate for integration 4. Making better Ohmic contact 5. Flow-chamber design for faster throughput**	**1. Sensitive 2. Label-Free 3. Real-time detecting 4. Isolated side-gate for integration 5. Shrinkage Nanowire 6. Good Ohmic contact**
Dis-advantages	**1. Highly cost 2. Lack of a controlling gate**	**1. No isolated -gate**	**1. Highly cost 2. Without oxide dielectric layer**	**1. Highly cost (SOI wafer)**

Table 2.2 The advantages in our fabrication method

1.	**Allows for individually nanowire to be within a single microfluidic channel**
2	**Real-time, label-free, direct-detection of important biomolecules**
3	**High sensitivity & exquisite selectivity**
4.	**Isolated side-gate for integration process**
5.	**Shrinking-effect of LOCOS process**
6.	**Have potential to be a portable device**
7.	**Fabricate single-crystal NW with SOI wafer with high mobility & sensitivity**
8.	**Eliminating expensive labeling steps and simplifying the signal read-out**
9.	**SOI wafer exhibits lower leakage current and excellent field-effect properties**

2.5 Organization of the Thesis

In this thesis, we reported a novel side-gated silicon nanowire field-effect transistor (SiNW-FET) as the cancer marker sensor. We fabricated SiNW on silicon-on-insulator (SOI) wafer with high sensitivity and high detection limitation. Label-free and single-strand DNA and cancer marker anti-AFP were modified onto the SiNW. In order to overcome some challenges in this work, for example, pattern definition, nanowire shrinking, label-free DNA and Anti-AFP modification, microfluidic system integrated with the SiNW and electrical signal detection…etc. In **Chapter 1**, the general overview of the top-down approach of nanotechnology was introduced. There is an overview discussion with varieties of biosensors for detecting significant bio-molecules ex: cancer markers. Literature reviews reported some "top-down" SiNW-FET biosensors and the fabrication of microfluidic system with device and major motivation of this study are introduced in **Chapter 2**. The details of fabrication processes, biomolecules immobilized procedures and characterization of detection analysis instruments are presented in **Chapter 3**. In **Chapter 4**, the electrical property of side-gated SiNW-FET and the application of DNA and protein markers detection were also discussed. Finally, the summary of important achievements and contributions of this thesis are addressed in the **Chapter 5**.

Chapter 3: Experiments

3.1 General introduction

Side-gate nanowire field-effect-transistor (NWFET) by electron beam lithography and shrank SiNW by LOCOS process was fabricated. In the fabrication process, all the experiments were proceeded in National Chiao Tung University (NCTU) or National Nano Device Laboratories (NDL) **[1]**. All the reagents and solvents were of reagent-grade quality, and listed alphabetically in the form of "Name {abbreviation; chemical formula; purity; manufacturer}". Some information will be omitted if not available or not necessary. The experimental reagents were shown in the following text and used the abbreviation of the reagent.

1. (3-Aminopropyl)triethoxysilane (APTES; molecular formula $H_2N(CH_2)_3Si(OCH_2CH_3)_3$; purity 98%; Fluka)

The purpose of APTES molecule is to modify the exposed SiO_2 surface on silicon nanowire. Ethoxy groups of APTES forms covalent bonding with hydrophilic hydroxyl groups attached to the SiO_2 surface to form molecular layer of amino groups in order to bond with biomolecules, ex: DNA and protein.

2.Acetone (molecular formula CH_3COCH_3; purity 99.5%; Sigma)

Acetone was mixed with Ethanol to clean the surface of wafer.

3. Anti-alpha-fetoprotein (human, AFP) from Mouse monoclonal antibody

4. Antigen of Alpha-fetoprotein (human, AFP) from Mouse monoclonal antigen

5. Deionized and distilled water (DI water, ddH_2O)

The water was purified with filters and deionized system until the resistance was 18 MΩ. DI water was used to wash and as the solvent for biomolecules.

6. Deoxyribonucleic acids (OPC grade; MDBio Inc.)

Sequence Name	**Oligonucloetide Sequence**
Capture DNA	**5'-AAATATATTA-TTACTCTTGA-GGTCTCTGTG-3'**
Complementary Target-DNA	**5'CACAGAGACC-*TCAAG*AGTAA-TAATATATTT-3'**
Non-complementary target-DNA	**5'CACAGAGACC-*GCCGT*AGTAA-TAATATATTT-3'**

7. Ethanol (molecular formula CH_3COCH_3; purity 99.5%; Sigma)

Ethanol will diluted APTES to bind onto the SiO_2 surface.

8. Ethylenediaminetetraacetic acid (purity 99%; CALBIOCHEM)

(EDTA; molecular formula $(HOOCCH_2)_2NCH_2CH_2N(CH_2COOH)_{2)}$

The EDTA agent captures the cations, which can induce the activities of some enzymes to digest and destroy the structures of nucleic acids during experimental processes.

9. Glutaraldehyde ($OHC(CH_2)_3CHO$; purity Grade I, 25%; Sigma-Aldrich)

Glutaraldehyde was used as a linker to combine two amine-contained molecules. The chemical needs to be diluted with PBS solution and stored at -20℃.

10. Hydrogen chloride (HCl; ≥99% purity; Sigma)

1 M HCl in DI water was used for pH adjustment.

11. N-2-Hydroxyethylpiperazine-N'-2-ethanesulfonic acid (HEPES; molecular formula $C_8H_{18}N_2O_4S$; purity 99%; CALBIOCHEM)

HEPES is a biological buffer solution and mixed with EDTA to conserve capture and target DNA molecules during the reactions.

12. Phosphate-buffered saline tablets {PBS, 1X; CALBIOCHEM}

PBS, a biological buffer solution, was used to increase the selectivity of the DNA

chips by washing away any non-hybridized nucleic acids. This chemical is dissolved in ddH2O to yield 10mM phosphate buffer, pH 7.4, 140mM NaCl, 3mM KCl.

13. Sodium chloride (NaCl; ≥99% purity; Sigma)

1 M NaCl in DI water was used for pH adjustment.

14. Sodium hydroxide {NaOH; 98% purity; Sigma}

Sodium hydroxide in DI water was used to adjust the pH of the PBS buffer solution.

15. Streptavidin−FITC from *Streptomyces avidinii* {essentially salt-free, lyophilized powder, ≥ 5 units/mg protein; Sigma}

This protein has a high affinity for biotin. The powder needs to be dissolved in the PBS.

16. Sulfuric acid (molecular formula H_2SO_4; purity 98%; Sigma)

Sulfuric acid is mixed with hydrogen peroxide as ratio of 3:1 to clean the sample.

3.2 Experimental Procedure

The experiments are divided into seven six parts: (1) fabrication of side-gate SiNW-FET, (2) microfluidic system integration with SiNW-FET, (3) self-assembly linker layer between probe-DNA and nanowires, (4) characterization of detection of target-DNA, (5) self-assembly linker layer between anti-alpha-fetoprotein and nanowires, and (6) characterization of sensing of interaction antigen-alpha-fetoprotein. They will be discussed in details and described in the following section. During the all experiments, the latex gloves, masks, and protective clothing must be dressed in order to avoid unexpected dangers in the experimental environment.

3.2.1 Fabrication of Side-gate Silicon Nanowire Field Effect Transistor (NWFET)

All experiments were performed with silicon-on-insulator (SOI) wafers. The procedure of device fabrication is illustrated in **figure 3.1**.The details of side-gate SiNW-FET process are listed below.

Fabrication Process in Details:

Step1: Standard RCA cleaning is applied to the silicon wafer.

Step2: Wafers were loaded into APCVD/LPCVD system to deposit SiO_2/Si_3N_4 film as the masking layer for the following LOCOS process, as shown in **figure 3.2**

Step3: The first electron beam resist was spin-coated by TEL CLEAN TRACK MK-8. Next, Leica WePrint 200 e-beam writer was used to pattern nanowire width and length and isolated gate. TMAH (Tetra-Methyl Ammonium Hydroxide) 2.38% reagent was used to develop the unexposed resist.

Step4: The Si_3N_4 layer was etched by TEL dry etching system.

Step5: After the resist was removed, the LOCOS process was executed to form the nanowire structure, isolated gate, and gate oxide at the same time by using APCVD system, followed by the removal of masking layer by wet bench.

Step6: The second electron beam resist was spin-coated. Next, the E-beam writer was

used to pattern the second structure.

Step7: The lithography was used again to pattern the N^+ implantation area which was implanted with As ion by implanter. The As ion was activated at 1050ºC for 30s by rapid thermal annealing.

Step8: The third e-beam lithography process was used to pattern metal pad. The metal pad area was patterned by e-beam lithography and deposited with Cr/Au by PVD sputter system. Lift-off process was performed to remove the resist and unwanted metal by using the NMP (N-Methyl-2-Pyrrolidone) stripper.

Step9: PE-oxide was deposited as the layer.

Step10: The forth e-beam lithography process was used to pattern active area.

Step11: The passivation oxide was wet etched by BOE solution.

Step12: Finally, the shrinking nanowire and individual side-gate are completely finished. The cross sectional diagram was illustrated in **figure 3.3.**

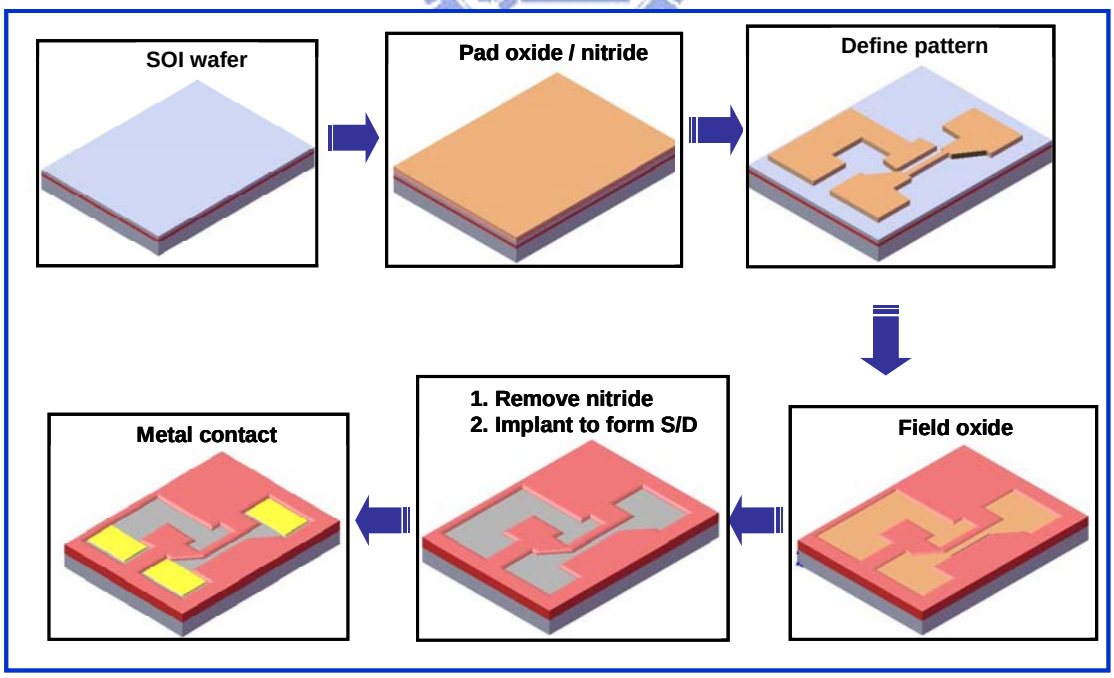

Figure 3.1 Process flow chart of the side-gate SiNW-FET device fabrication on the SOI wafer.

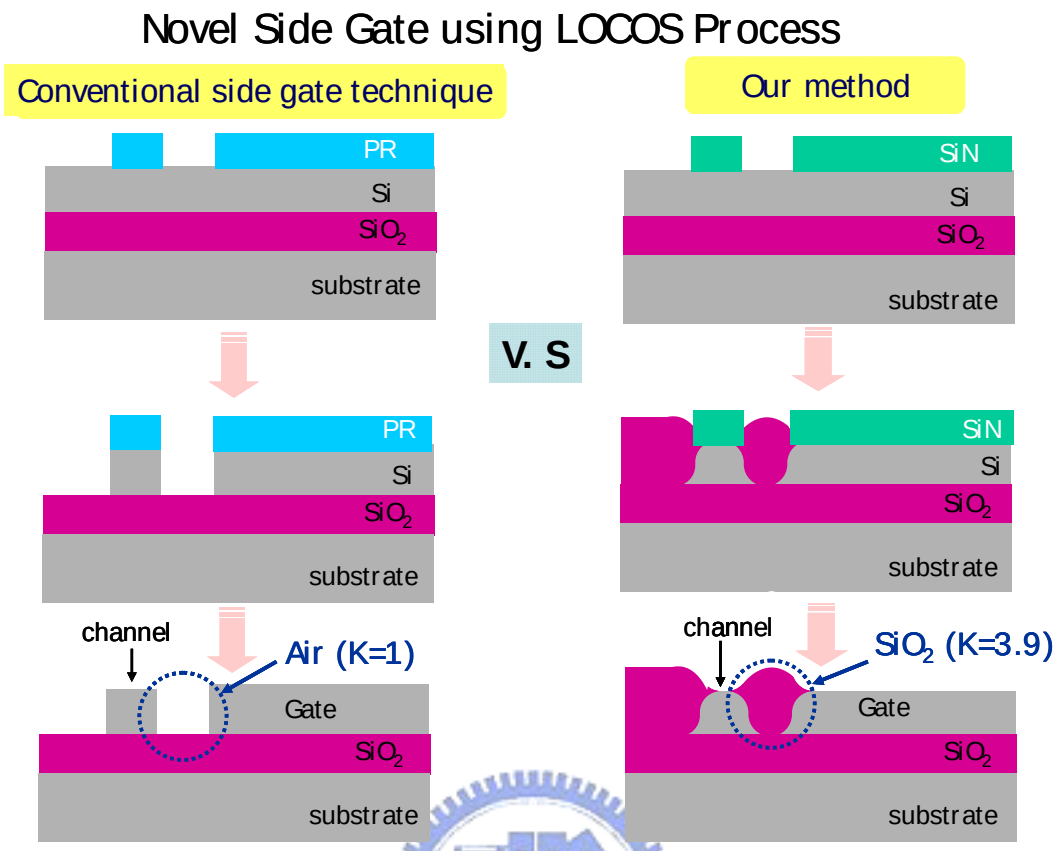

Figure 3.2 Comparison of conventional and modified process flow chart of the side-gate SiNW-FET device fabrication using LOCOS process.

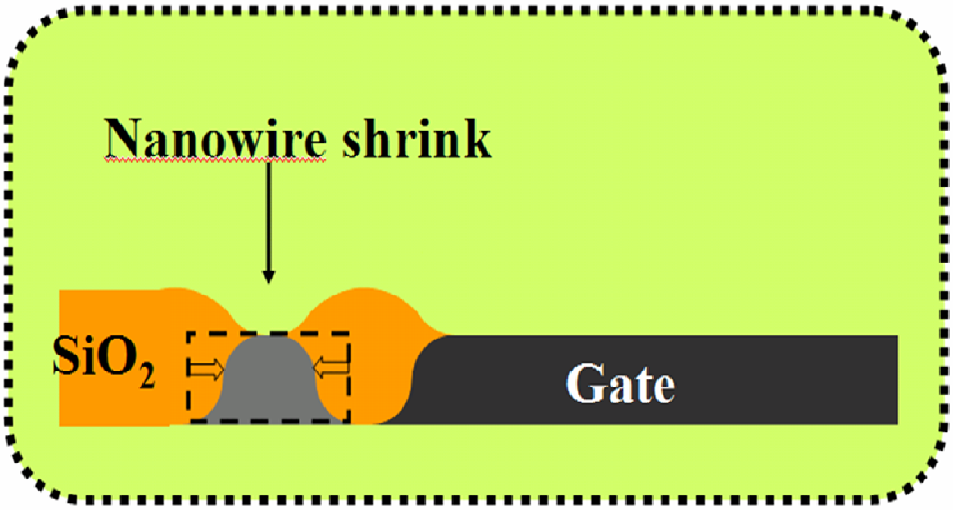

Figure 3.3 The shrank nanowire and individual side-gate are achieved by our modified LOCOS process.

3.2.2 Fabrication of the Microfluidic System and Integration with the SiNW-FET

Process Flow **[2]**:

1) Mixing PDMS (20grams): cure agent=10:1 with stirring rod violently

2) Used a vacuum pump to degas about 30min until all bubbles were gone away

3) Poured it to the mother mode (wafer or glass dish) in **figure 3.4**

4) Cured PDMS at 80 ^{o}C for 20min

5) Peeled off the PDMS structure from the mold carefully

6) Input and output holes punched

7) Cleaned the SiNW surfaces by ethanol/IPA solution

8) O_2 plasma treatment (time=60s) for both SiNW-FET devices and PDMS

9) PDMS mold bound onto the nanowire devices

10) Aligned and pressed the PDMS mold and the SiNW together

11) Baked at 90 ^{o}C for 30min in an oven

12) Inserted the Teflon tubes with syringe pump, as shown in **figure 3.5**

13) Combined the sample onto the clamping holder, as shown in **figure 3.6**

14) The combined microfluidic system with the sensor was shown in **figure 3.7**

And then, **figure 3.8** illustrated the schematic structure of the experimental device being integrated with microfluidic system and combined with transducer analyzer. Furthermore, we also amplified the nanowire active area in **figure 3.8** to account of the reality experimental condition of biomolecules in the microfluidic channel, as shown in **figure 3.9**.

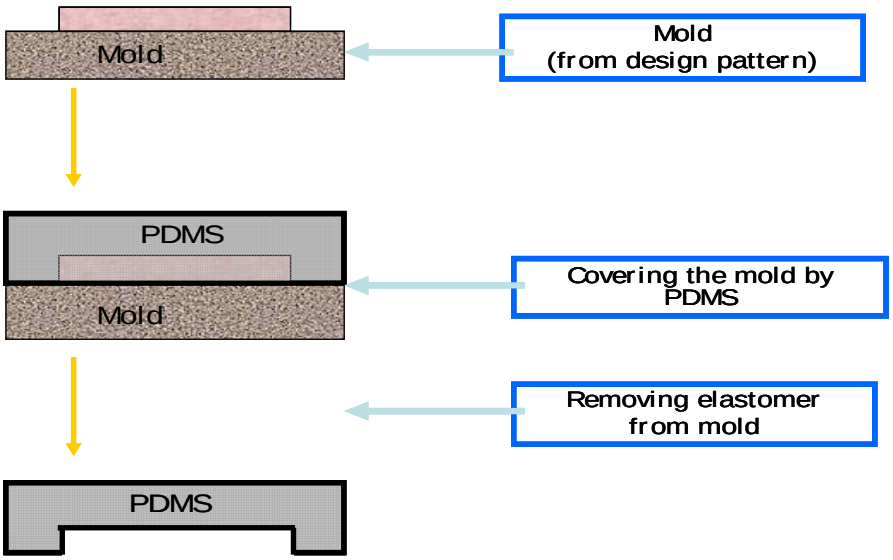

Figure 3.4 The process of making PDMS microfluidic channel.

Figure 3.5 The image of syringe pump (model-120) is used in my studies.

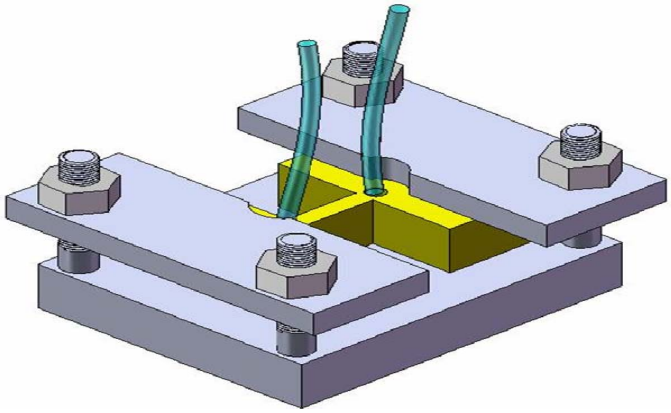

Figure 3.6 The figure of stainless steel clamping apparatus.

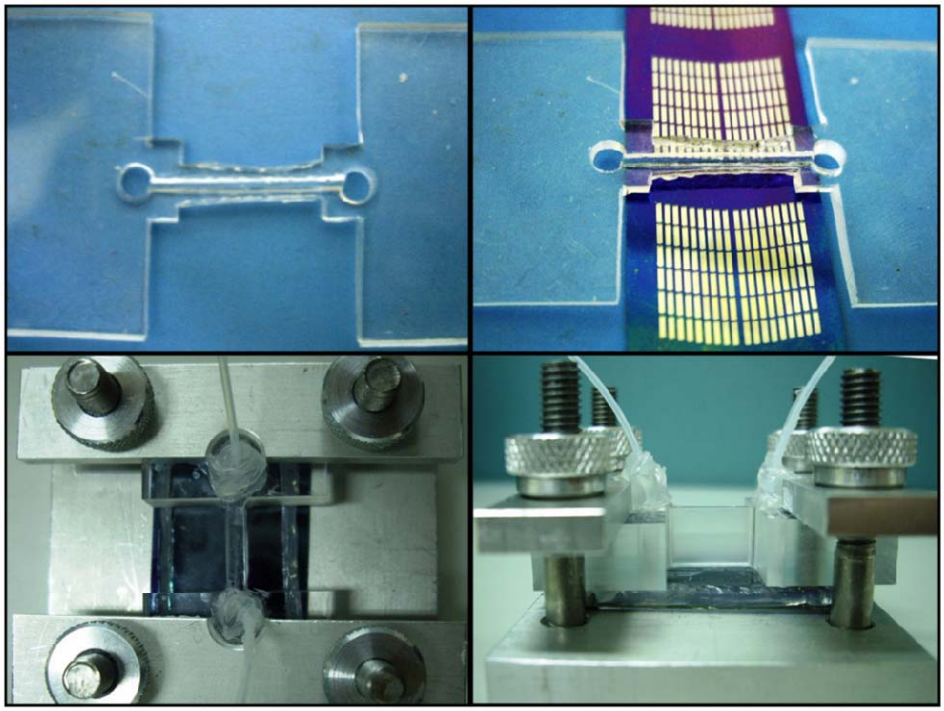

Figure 3.7 The reality image of PDMS mold, clamping holder and integration of the system.

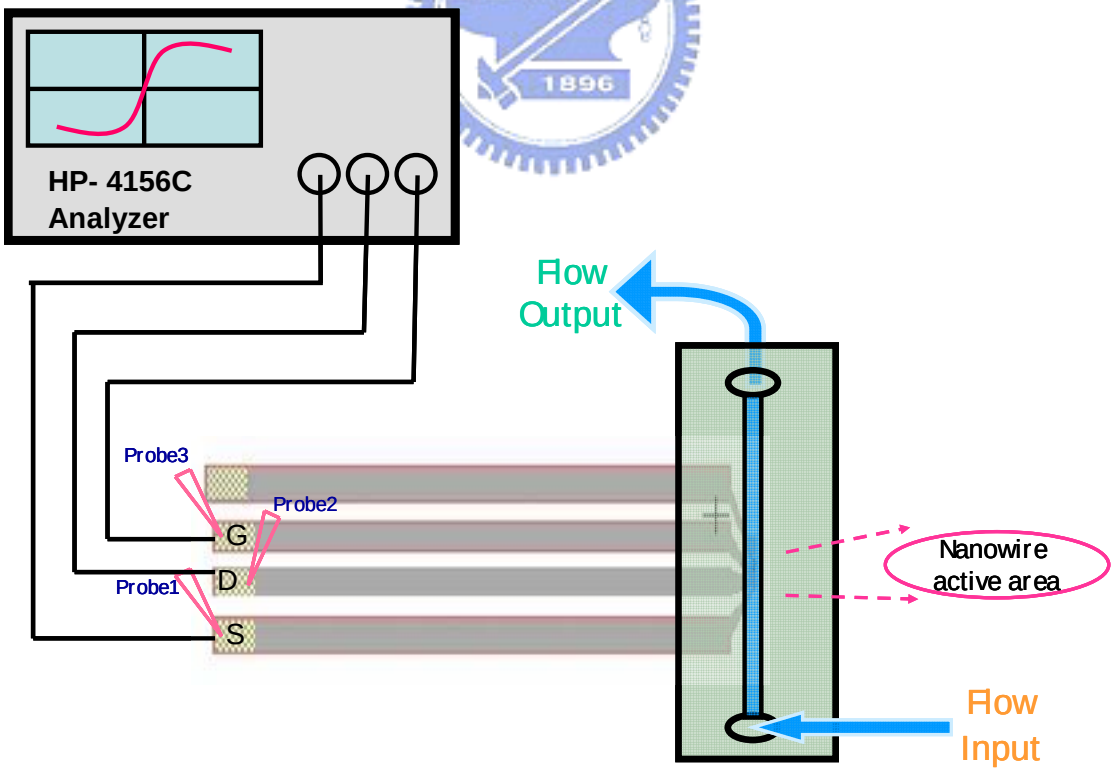

Figure 3.8 Schematic structure of the experimental device integrated with microfluidic system and combined with transducer analyzer.

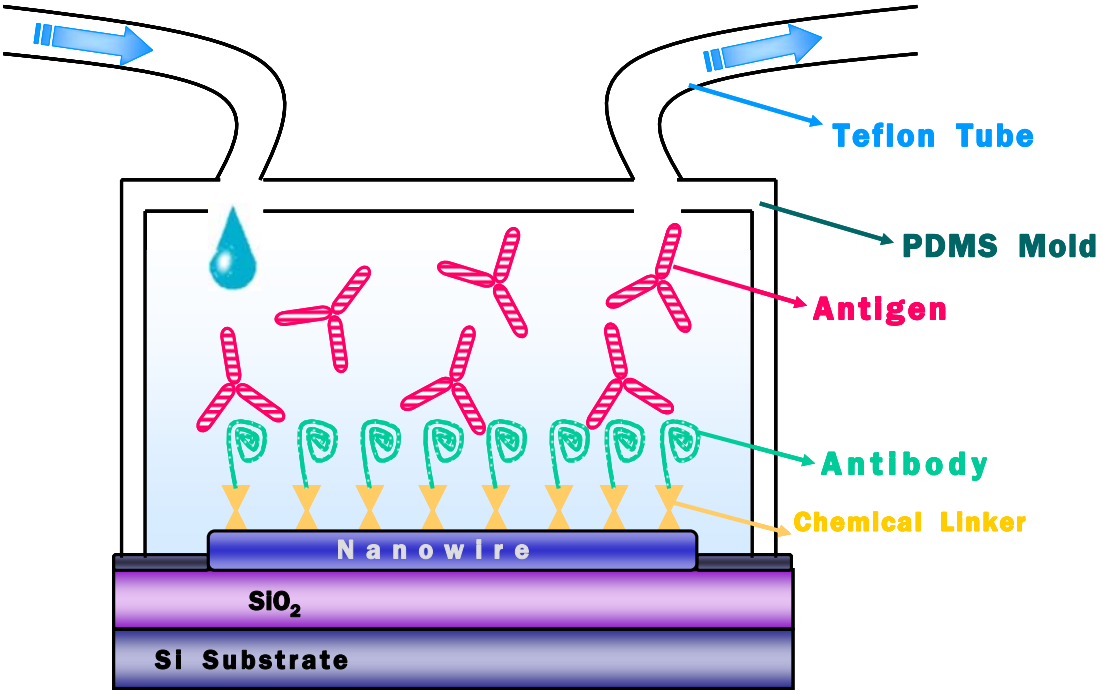

Figure 3.9 Schematic structure of the amplification of the right (nanowire active area) area in **figure 3.8** for the detection of antigen using an antibody-modified FET device integrated with microfluidic system.

3.2.3 Immobilization of the Probe-DNA onto the Nanowire

The interface and system integration must build on the stable immobilization between the nano-electronic devices and biomolecules. The first step was to assemble DNA biomolecules onto the patterned wafer. **Figure 3.10** illustrates the process of the immobilized DNA steps. The procedure of the probe-DNA immobilized was divided into five steps as follows **[3]**:

Step 1: Cleaned patterned wafer with acetone/ethanol solution (C_2H_5OH/Acetone= 1: 1) for 30min

Step 2: The solvent of APTES solution was constituted with the proportion of 110λ of the APTES solution to 5mL of ethanol, and the APTES was added into solvent in the concentration of 5% for 30 minutes at room temperature. The sample was rinsed with ddH_2O after cleaned and dried with N_2 purge.

Step 3: Baked the APTES-modified wafer at 120 °C for 30 minutes.

Step 4: Samples immersed in the 2.5 % glutaraldehyde solution for 30 minutes at room temperature **[4].**

Step 5: The modified wafer was immersed in the solution including the NH_2-DNA for 16 hours at room temperature, and then rinsed with PBS buffer.

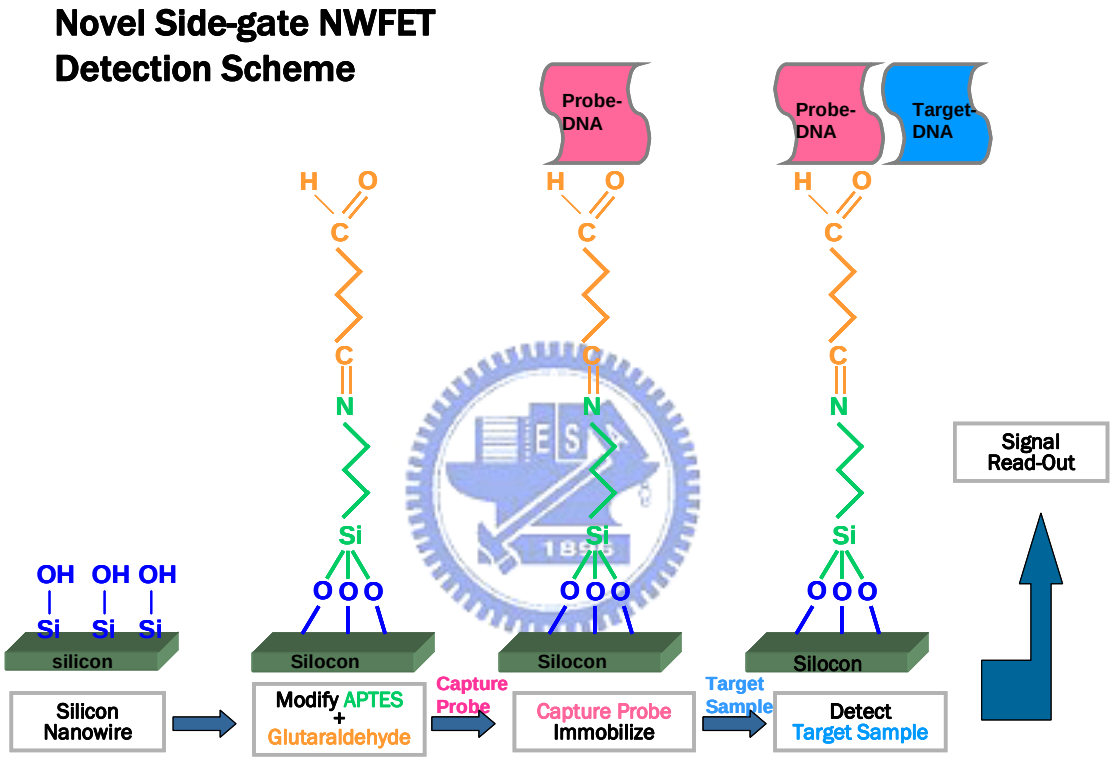

Figure 3.10 The schematic image of overall surface modification and the procedure of detection target-DNA.

3.2.4 Characterization of Detection Probe-DNA, Hybridization with Target-DNA and Non-complementary DNA

After surface modification and probe-DNA binding procedure mentioned above, the complementary target-DNA was applied to complement with the probe-DNA. The schematic diagram of detection target DNA sequences were illustrated in **figure 3.10**. The 30-mer target-DNA was diluted in fresh PBS buffer, and samples were then immersed into the buffer for about 3 hours. After DNA hybridization, DI water was rinsed to remove excess target-DNA and dried with N_2 gun. **T**he electrical characteristics of the DNA sensors were measured using the HP-4156C semiconductor analyzer. The drain-current (I_D) of the SiNW device as a function of measuring time and the drain current versus gate voltage (I_D-V_G) curve were measured every step. After electrical measurement was done, the chips were washed with 100 ^oC DI water to dehybridize the target and mismatch-DNA. The overall procedure was depicted in **figure 3.10**.

After the electrical measurement assay, the fluorescence assay was performed to confirm the immobilization steps. The FITC-labeled probe-DNA and the FAM-labeled target-DNA were prepared. The procedure to evidence the existence of probe-DNA and target-DNA on the nanowire were observed under fluorescence microscope. And then the experimental process was shown in **figure 3.11** and in **figure 3.12**, respectively.

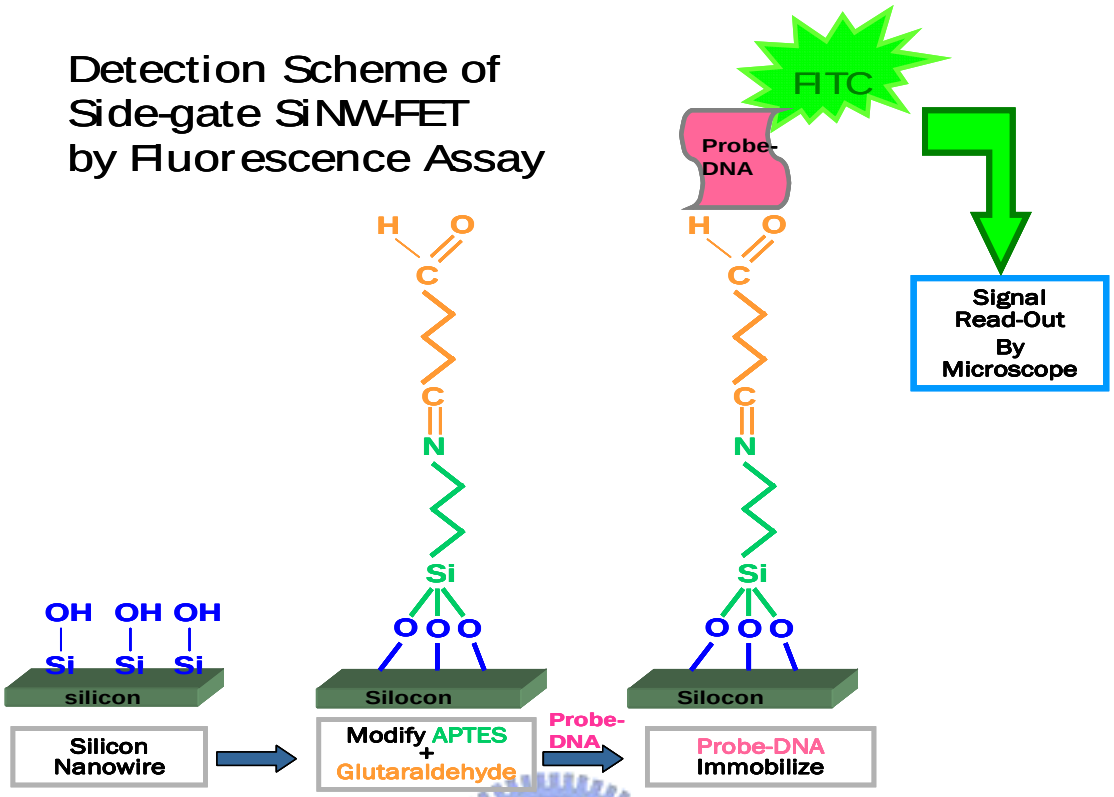

Figure 3.11 The schematic process of detecting FITC-labeled probe-DNA onto the side-gate SiNW-FET by fluorescence assay.

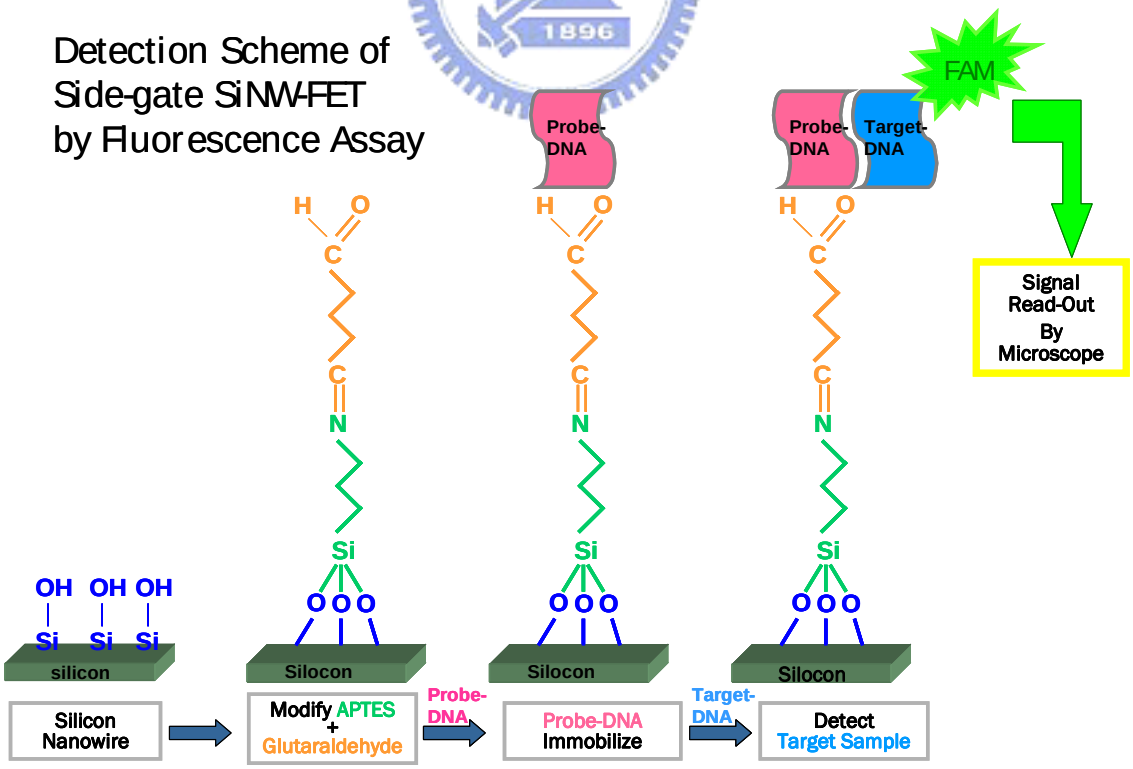

Figure 3.12 The schematic process of detecting FAM-labeled target-DNA hybridizes with the side-gate SiNW-FET by fluorescence assay.

3.2.5 Immobilization of the Anti-alpha-fetoprotein onto the Nanowires

For the detection purpose, the nanowire was modified with the anti-α-fetoprotein. Samples were prepared by the following four main processes **[3]**:

(1) Pre-cleaning of the SiNW surface.

Samples were cleaned by the fresh prepared acetone/ ethanol solution at 25^{o}C for 30min. And then washed by DI water and purged by N_2 gun.

(2) Immobilization of APTES and glutaraldehyde molecules.

Samples were immersed with APTES solution with the proportion of 110λ of the APTES solution to 5mL of ethanol, and then rinsed by ddH_2O and dried by N_2 purge.

(3) Anti-alpha-fetoprotein immobilized.

Covalent immobilization was used to bind the terminal amine-group of the Anti-alpha-fetoprotein to the carbonyl group of glutaraldehyde on the surface of SiNW. The solution was mixed with 10nM anti-alpha-fetoprotein, and the wafers were immersed it on the above mixture solution for 16 hours to ensure the complete binding. The overall process is depicted in **figure 3.13.**

(4) The FT-IR spectrophotometer assay was also carried out to confirm the evidence of the existence anti-alpha-fetoprotein on the SiNW.

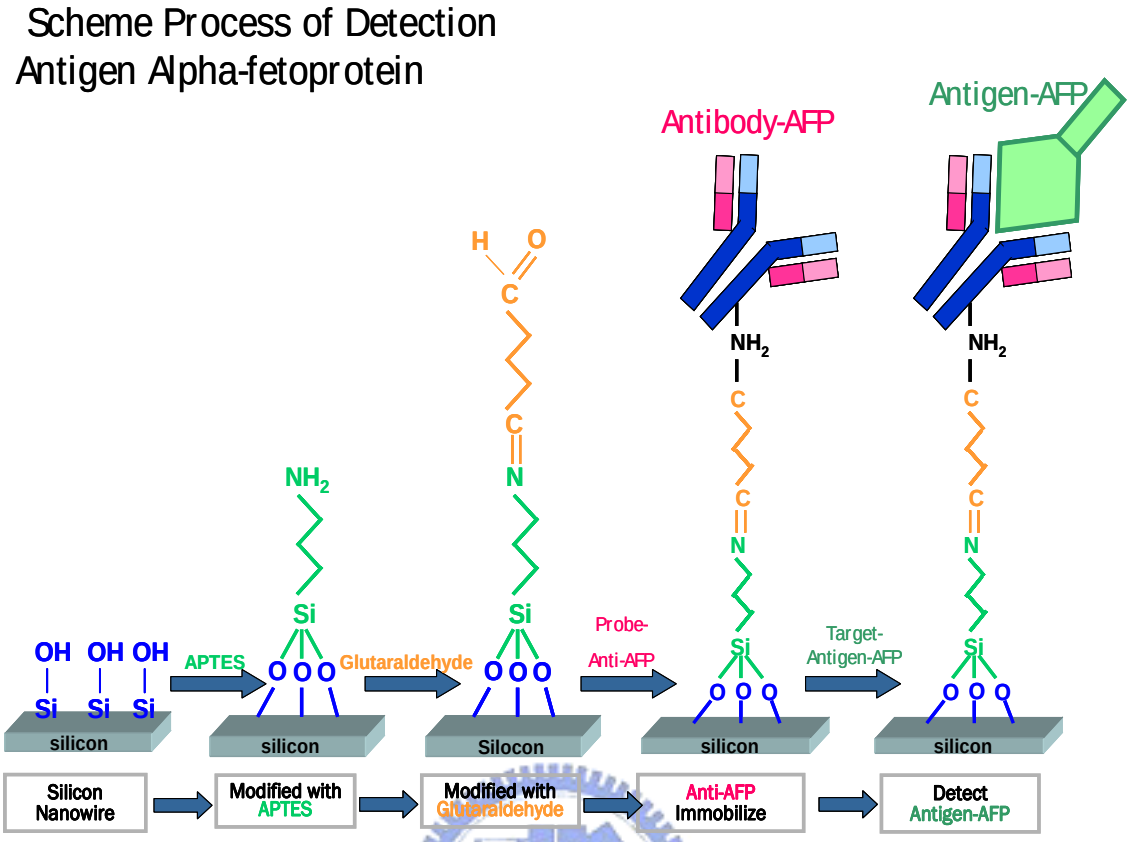

Figure 3.13 The schematic process of detecting anti-alpha-fetoprotein and antigen-AFP onto the side-gate SiNW-FET.

3.2.6 Characterization of Detection Interaction of Antigen-Alpha-Fetoprotein to the Antibody onto the Nanowires

After surface modification and anti-alpha-fetoprotein binding procedure, the antigen-alpha-fetoprotein was applied to interact with the anti-alpha-fetoprotein **[3]**. The schematic diagram of antibody bound to antigen was illustrated in **figure 3.13**. The detail procedure was described as below:

Step 1: The antigen-alpha-fetoprotein was diluted in prepared PBS buffer.

Step 2: Wafers were immersed in the solution including AFP for about 2 hours.

Step 3: Rinsed by DI water to remove excesses antigen molecules.

Step 4: And then the unreacted surface with aldehyde group was blocked by reaction with ethanolamine

Step 5: The electrical characteristics of the protein sensors were measured using the HP- 4156C semiconductor analyzer. The drain current (I_D) of the SiNW device as a function of measuring time and the drain current versus gate voltage (I_D-V_G) curve were measured every step. We measured not only the I_D-V_G curve of antigen-AFP, but also the protein BSA. After measurement the chip was washed with 100 °C DI water to denature the interaction of antibody and antigen-AFP. The overall procedure is depicted in **figure 3.13**.

Chapter 4: Results and Discussions

We have successfully evaluated the capability of immobilization on the SiNW substrate. The fluorescent images and UV spectrophotometer results demonstrated that the suitable experimental parameters were for bio-sensing. We also successfully fabricated side-gate SiNW-FET by using the traditional LOCOS process and integrated with microfluidic-channel system for detection of the important disease marker.

4.1 Physical and Electrical Properties of the Side-Gate SiNW-FET

The layout structures of the side-gate SiNW FET are illustrated in **figure 4.1(a), (b), and (c).** The length of nanowire is 1000nm and the width is 100nm. **Figure 4.2-1 and 4.2-2** show the plan view of SEM images for the FET device. As the n-channel FET, the gate-voltage (V_G) is applied a positive voltage to induce negative charges on the surface of the nanowire to cause the device to the "ON" state. When a negative bias is applied on gate-voltage a relatively small drain current is observed, which is called the "OFF" state. When the gate-voltage is high enough to construct the conducting inversion layer and "open" the channel, the drain-to-source current (I_{DS}) increases obviously and the gate-voltage is called "threshold voltage (V_{th})". Finally, the currents (I_{on}) reach different saturations with different drain-to-source voltages (V_{DS}). The I_D-V_G and I_D-V_D characteristics of the nanowire FET (1μm length and 100nm width) are shown in f**igure 4.3-1 and 4.3-2**.

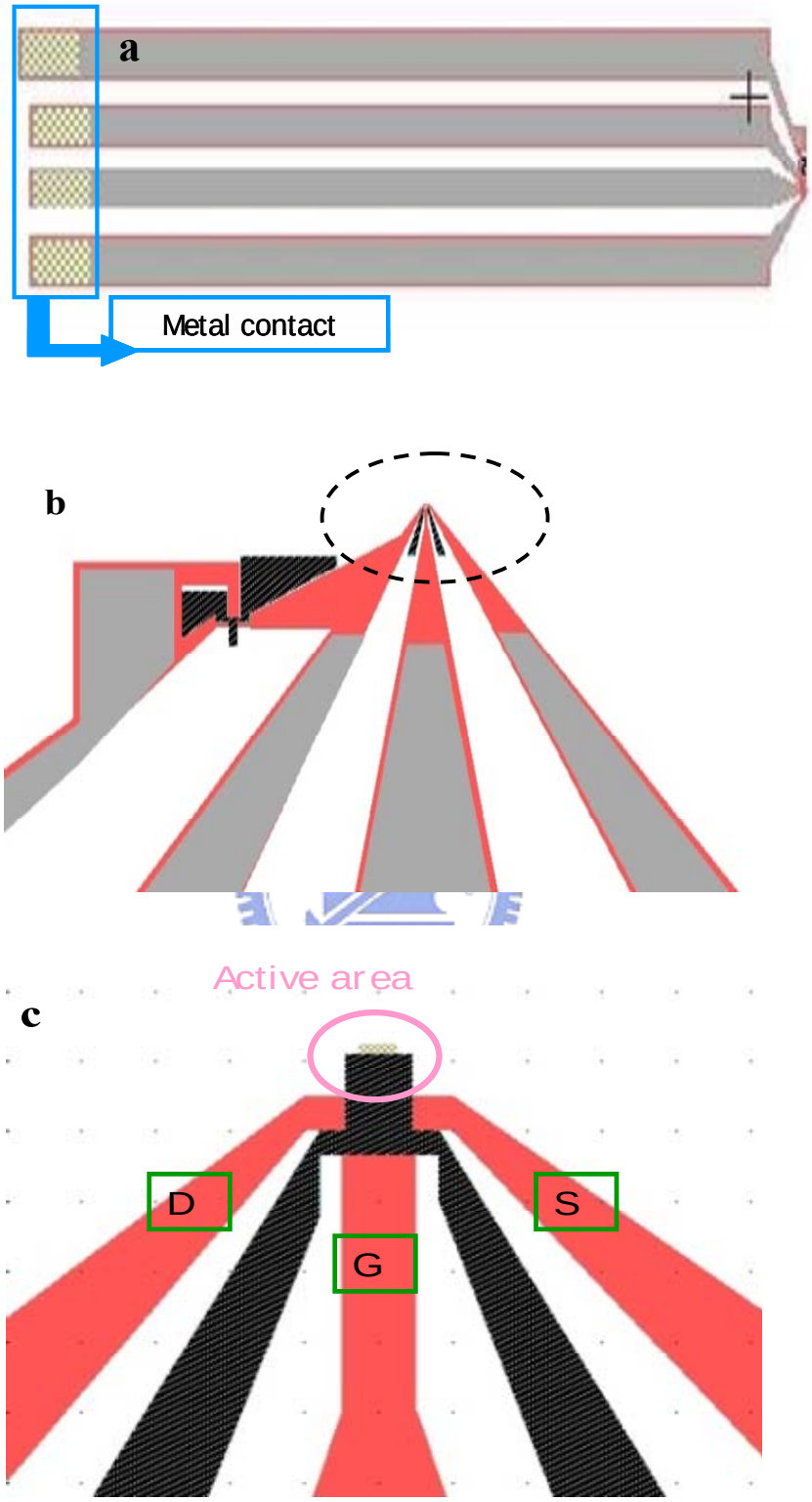

Figure 4.1 (a) Top-view layout of a side-gate SiNW-FET. **(b)** Amplification of the left area in (a). **(c)** Amplification of the area dotted in (b)

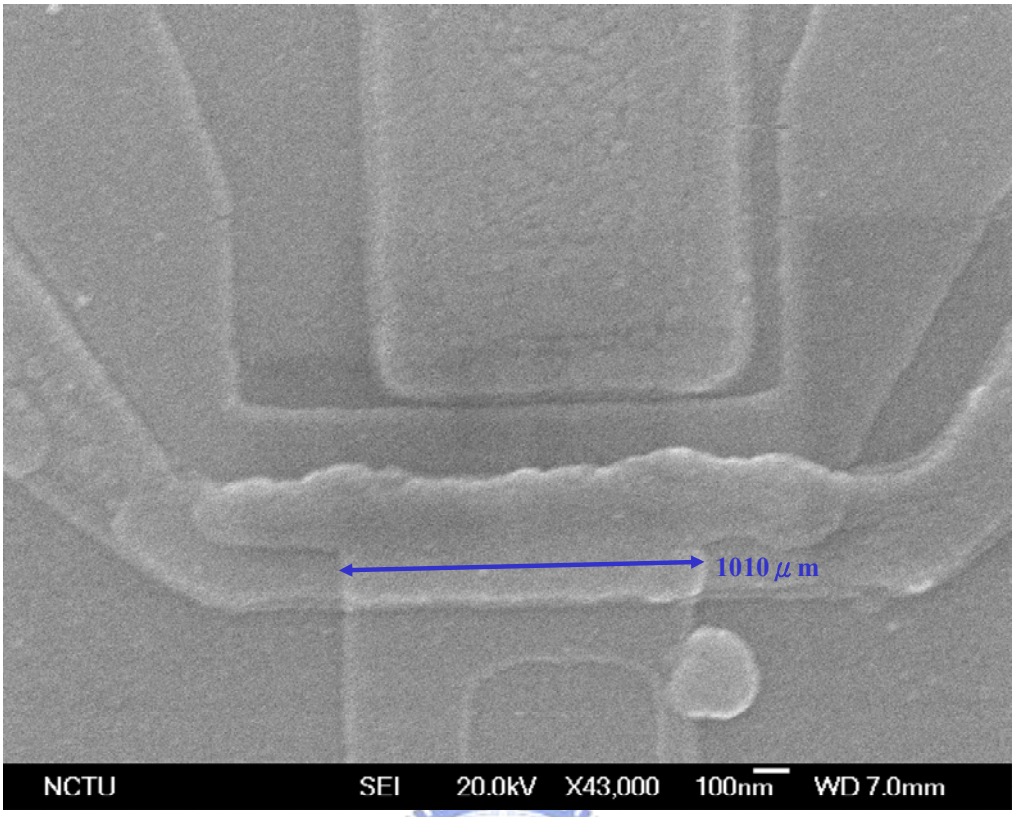

Figure 4.2-1 SEM images of side-gate SiNW-FET with channel length = 1μm

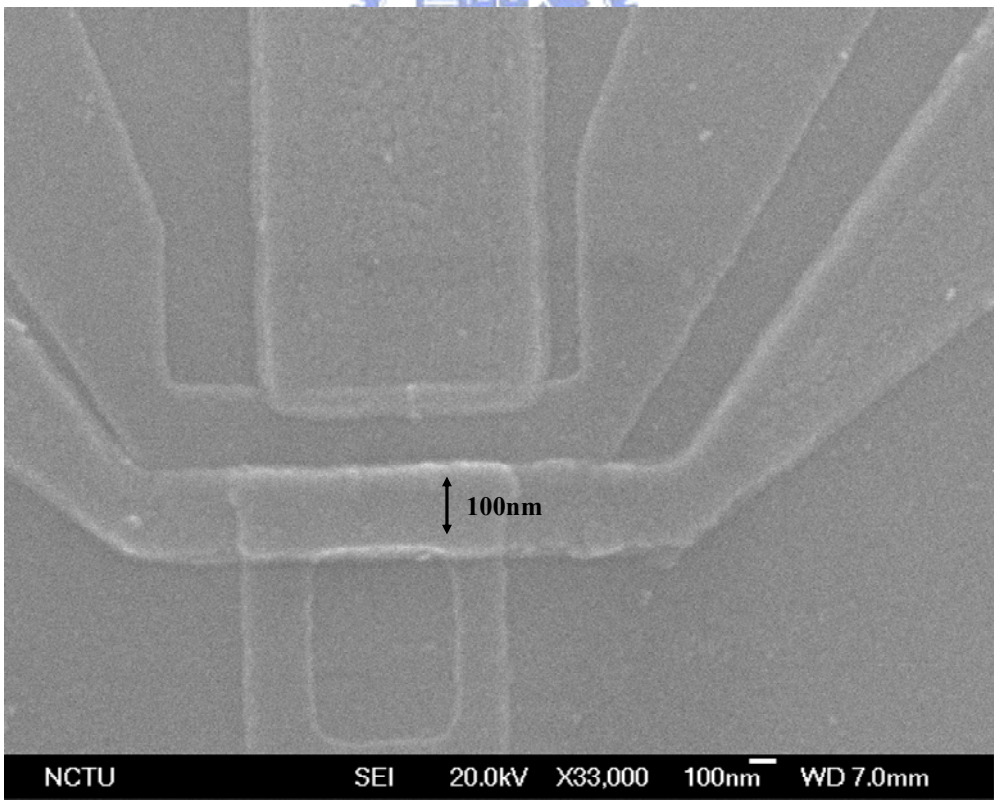

Figure 4.2-2 SEM images of side-gate SiNW-FET with channel width =100 nm

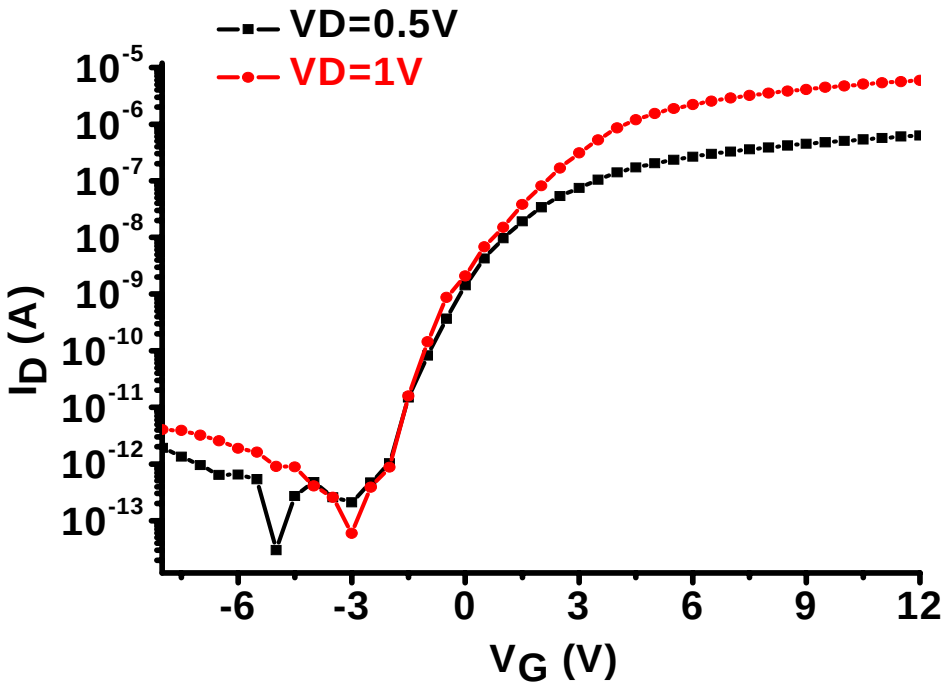

Figure 4.3-1 The I_D-V_G characteristic of the SiNW-FET.

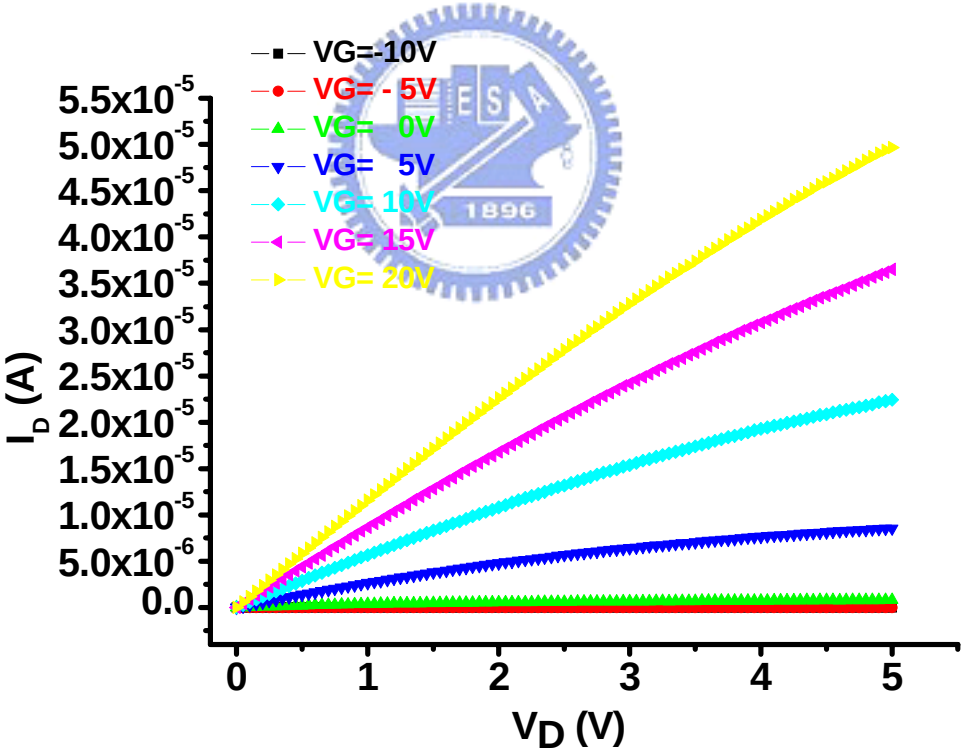

Figure 4.3-2 The I_D-V_D characteristic of the side-gate SiNW-FET.

4.1.1 Determination of the Threshold Voltage

V_{th}, is the most important parameter of semiconductor devices. In MOSFET, the method to determinate the threshold voltage is *constant drain current method* **[1]**. The V_{th} is usually defined a fixed drain current scaled by the device dimensions:

$$I_{DT} = I_{DN} \times \frac{W}{L}$$

I_{DT}: The threshold current to determine the threshold voltage.

I_{DN}: The normalized threshold current defined as 10nA in this thesis.

W: The channel width. L: The channel length.

4.1.2 Determination of the Sub-threshold Swing

Sub-threshold swing (S.S.) is a typical parameter to describe the control ability of gate toward channels. It is defined as the amount of gate voltage required to increase and decrease drain current by one order of magnitude. The sub-threshold swing is related to gate-voltage due to undesirable factors such as serial resistance and interface state. The threshold current is specified to be the drain-current when the gate-voltage is equal to the threshold voltage.

4.1.3 Determination of On/Off Current Ratio

On/Off current ratio is another important factor for SiNW-FET. High On/Off ratio represents not only large turn-on current but also small off current (leakage current). The practical method is defined as the maximum current as on current and the minimum leakage current as off current.

4.1.4 Determination of the Field-effect Mobility

The field-effect mobility (μ_{FE}) is determined from the transconductance ($g_{m)}$ at low drain voltage. The transfer I-V characteristics of SiNW-FET can be expressed as

$$I_D = \mu_{FE} C_{ox} \frac{W}{L}\left[(V_G - V_{TH})V_D - \frac{1}{2}V_D^{\,2}\right]$$

Where:

C_{ox}: The gate oxide capacitance per unit area

W: The channel width L: The channel length

$V_{TH:}$ The threshold voltage

If V_D is much smaller than V_G-V_{th} (i.e. $V_D << V_G$-V_{th}) and $V_G > V_{th}$, the drain current can be approximated as:

$$I_D = \mu_{FE} C_{ox} \frac{W}{L}(V_G - V_{TH})V_D$$

The trans-conductance is defined as

$$g_m = \frac{\partial I_D}{\partial V_G}\Big|_{V_D=\text{const.}} = \frac{WC_{ox}\mu_{FE}}{L}V_D$$

Therefore, the field-effect mobility can be obtained by

$$\mu_{FE} = \frac{L}{C_{ox}WV_D}g_m$$

Table 4.1 Device parameters with channel width = 100nm and channel length = 1μm

Device Parameters	**The amounts extracted at V_{DS}=1V**
V_{th}, Threshold voltage	**V_{th}= 0.75 V**
S.S., Sub-threshold swing	**S.S= 375 mV/dec**
I_{on}/I_{off}, On/Off current ratio	**I_{on}/I_{off}=8.33×10^5**
g_m, Transconductance	**g_m=5.12×10^{-7} S**
μ_{FE}, Field-effect mobility	**μ_{FE}=445.59 $\frac{cm^2}{V\cdot s}$**

4.2 Real-Time Detection of Multi-Steps-APTES Immobilization and BRAF^{V599E} Mutation Genes for Hybridization and Dehybridization Assay

To characterize liquid-phase sensor response, a micro-scale channel was designed specifically to avoid the well-characterized limits on sensitivity and response time inherent in diffusion-limited systems such as micro-channels **[2].** Our design in **figure 4.1 wa**s experimentally simple and induced mixing during fluid exchange, and was used for all following solution-based sensor measurements.

4.2.1 Real-time Detection of the Different pH Value Solutions

APTES-functionalized onto the SiNW-FET was characterized as a pH sensor. The oxide surface of the NWFET that coats the APTES can be protonated and deprotonated by varying pH value, thereby modulates the drain-current **[3, 4]**. And then SiNWs evaluates by fabricating a system consisting of a microfluidic channel formed between a poly-dimethylsiloxane (PDMS) mold **[5, 6]** and the nanowire. The changes in pH value was we could carry out continuous flow experiments and could read-out the different current response of three solutions with pH values varying from 4.0 to 9.0 was displayed in **figure 4.4 ~ figure 4.7**. The I_d decreased with changes in pH from 7 to 9 was shown in **figure 4.4.** The real-time I_D changes as the pH from 7 to 4 was shown in **figure 4.5**. A typical real-time detection curve plot of the different pH value solution current versus time was shown in **figure 4.6.** The variation was dependent to the pH value and suggested that the modified SiNW could be acted as the nano-scale pH sensors.

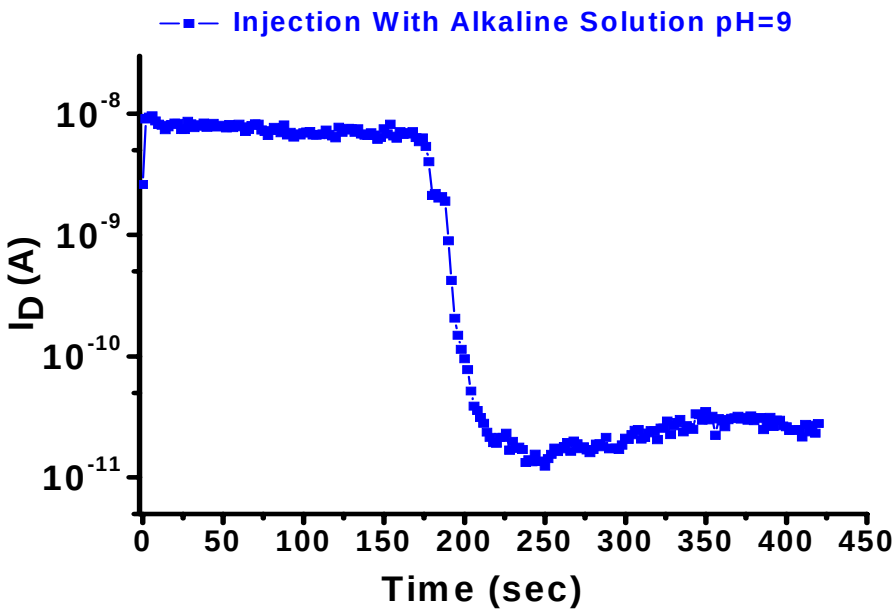

Figure 4.4 The real-time versus I_D detection curve acquired from alkaline (pH=9) solution

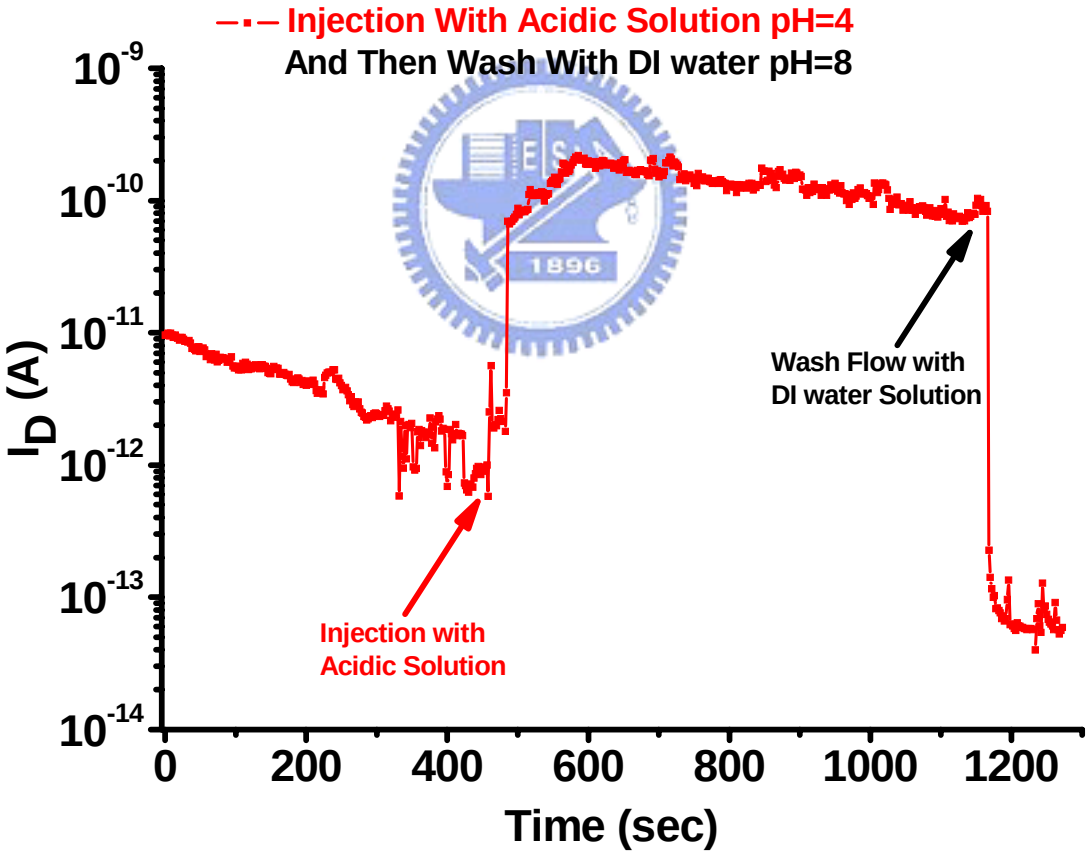

Figure 4.5 The real-time versus drain-current detection curve acquired from acidic (pH=4) solution

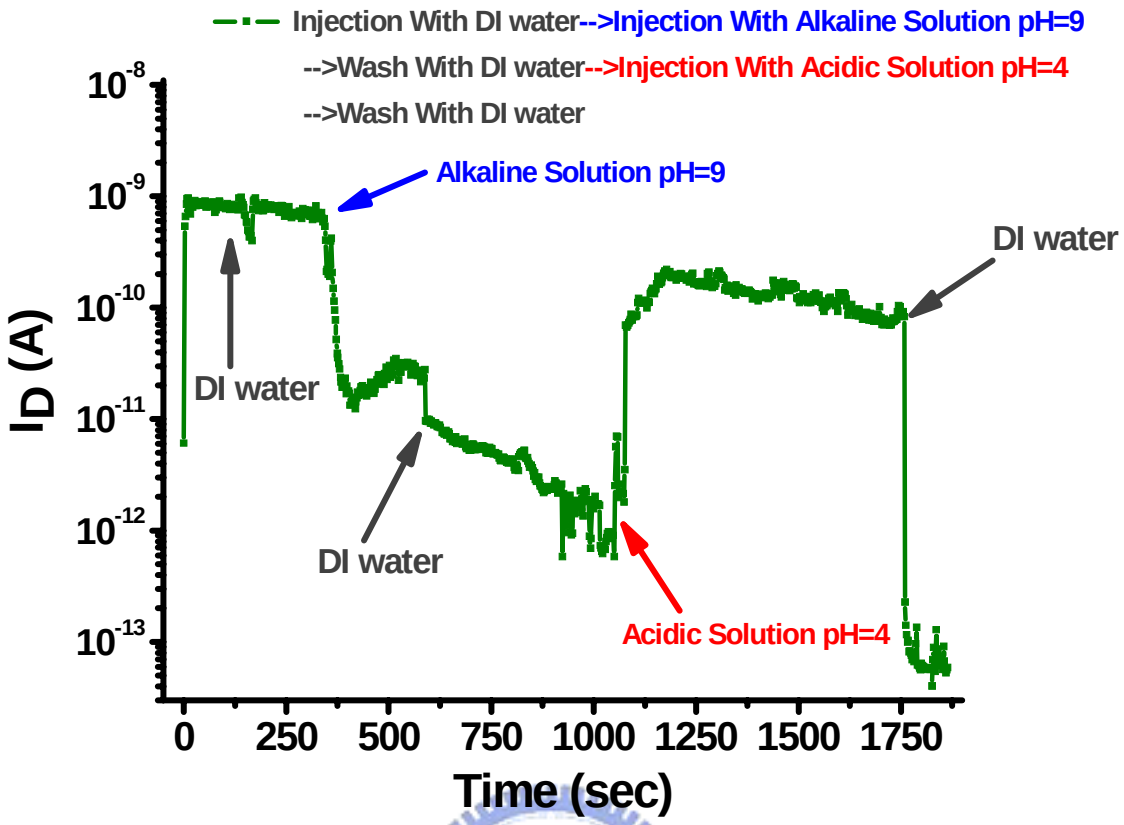

Figure 4.6 The real-time versus drain-current detection curve acquired from alkaline (pH=9) to acidic (pH=4) solution

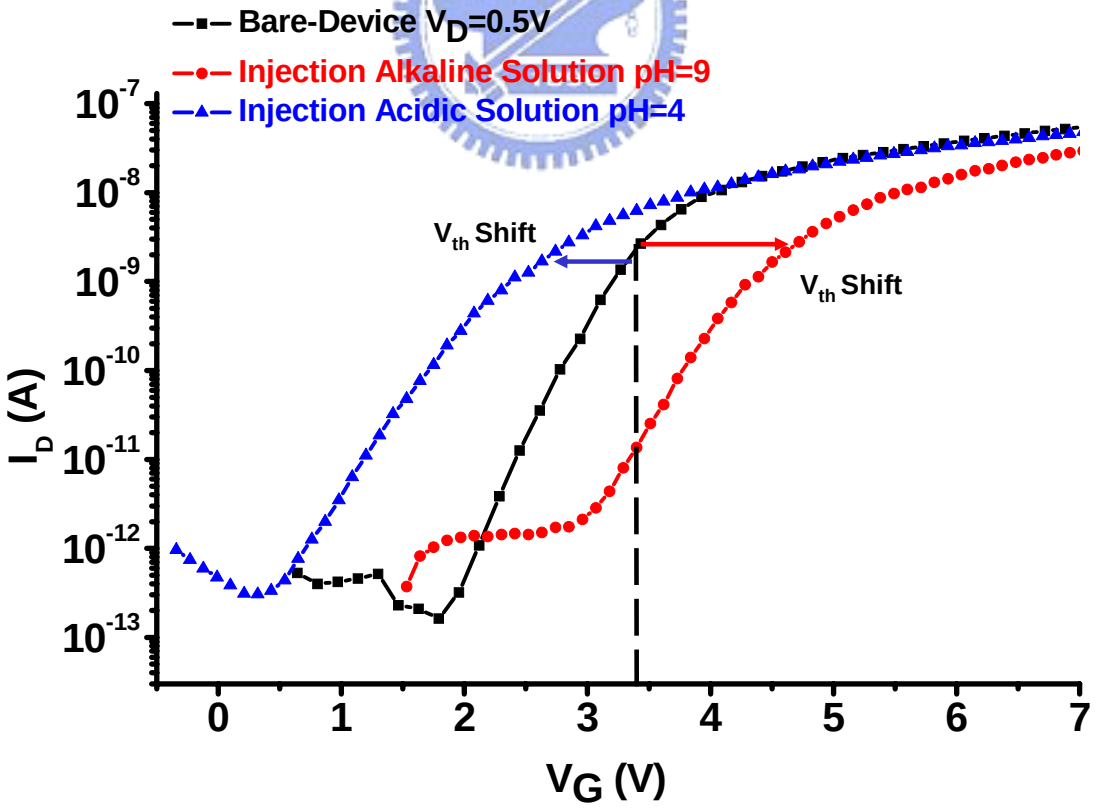

Figure 4.7 The I_D-V_G curve of alkaline (pH=9) solution and acidic (pH=4) solution detection.

These results can be understood by considering the surface functionality of the APTES-modified SiNW-FET. Covalently linking APTES onto the SiNWs oxide surface resulted in a surface terminating in both NH_2 and SiOH groups, which was shown in **figure 4.8 [3]** and has different dissociation constants, p*K*a **[7, 8, 9]**. In an n-channel SiNW-FET, an increase in the density of oxide charge would cause such a shift in threshold voltage towards more negative value. Protonation of the surface would lead to an increase in positive charge at the surface, and resulted in an increase in the electron charge density in the device channel, as displayed in **figure 4.8**. The resulting increase in current indicates that the device required a lower threshold voltage to achieve the same current, as observed in **figure 4.5 and figure 4.7**.

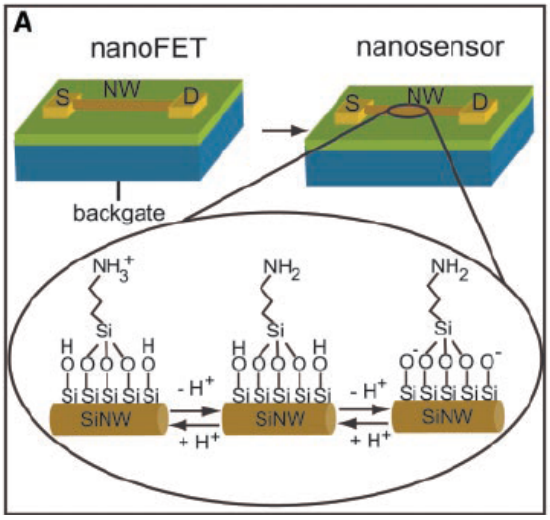

Figure 4.8 SiNW-FET for pH detection. Schematic illustrating the SiNW nanosensors for pH sensing. Zoom of the APTES-modified SiNW surface illustrating changes in the surface charge state with pH value **[3]**.

On the other word, deprotonation of the modified surface would lead to a decrease in positive charge at the surface, resulted in a decrease in the electron charge density on the channel. The decrease in drain-current indicated the device requires a high threshold voltage to achieve the same current, also as observed in **figure 4.4 and**

figure 4.7 [10]. Notably, these pH measurements on modified SiNWs are in excellent sensitivity with present measurements of the pH-dependent surface charge density derived from APTES-modified shown in **figure 4.6**. It is speculated that the disilanols (= $SiOH_2$) are exhibited approximately 9.3 in pKa values **[11],** while the APTES surface is reported to have a pKa value approximately 4 **[16]**. Therefore, it is expected that the modified surface would be fully protonated and deprotoned over the pH value ranging from pH=4 to pH=9 and the significant variation current was dominated.

4.2.2 The Confirmation of Effect between Debye Length and Detecting DNA Hybridization Signal

The properties of the SiNW biosensor is affected by many factors, such as Debye length screening **[12]**, nanowire size **[13]** and surface chemistry **[14]**. These factors will result in the change of detection sensitivity. Debye length, which depends on the ionic strength of solution, is one of the significant factors to affect the detection sensitivity. To effectively detect the target-DNA which located at more than a few nanometers from the SiNWs, 1mM PBS buffer solution was employed because it had a Debye-length of about 10 nm, which allowed the distance of hybridization to be detectable. The strict adjustment of ion conditions is necessary for sensitive detection of biomolecules using SiNW-FET based sensors in my experiment. The length of the probe-DNA (30mer) was estimated to be 10.2 nm, and the length of target-DNA (30mer) was reported to be about 10.2 nm **[15].** Thus, the hybridization of DNA complex would ensure close to the Debye-length in this study as illustrated in **figure 4.9**. The charges of the DNA may be “screened” by the layer, and their effect on the equilibrium carrier distribution would then be guaranteed to detect signal.

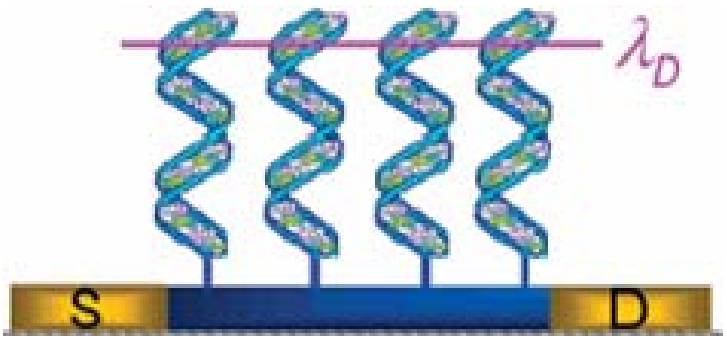

Figure 4.9 Specific detection of DNA. Schematic λ_D=10 nm from the device surface. Target-DNA strands will be screened, while the majority of the charge of hybridized strands be close to the Debye-length.

4.2.3 Real-time Detection for Hybridization and Dehybridization of Target-DNA on Immobilized Probe-DNA Modified Surface

Generally, most biological processes including DNA hybridization involved electrostatic interactions and charge transfer, which allowed electronic detection using SiNW-FET devices. However, the exact mechanism of the nanoelectronic detection principles is illustrated clearly in **figure 4.10**. DNA molecules attached to the SiNW will mostly influence the FET characteristics by changing electron density. As a result, the drain-current in real-time assay and V_{th} in I_D-V_G measurement of the SiNW-FET were changed through the different gate voltage. After confirmation the effect of the Debye-length, the effect of different buffer solution in DNA hybridization assay was also examined. Two kinds of buffer solution were used in the experiment that one is HEPES+EDTA solution and the other is PBS solution, as a solvent for DNA sample in hybridized and dehybridized process. Compared between in **figure 4.11 and figure 4.12**, we found that the HEPES+EDTA solution affected the background signal in UV spectrophotometer assay, while the signal still unchanged for the PBS solution. That was a reason why we used the PBS as a solvent for DNA sample that not to make a significant signal disturbance during UV assay and electrical measurement.

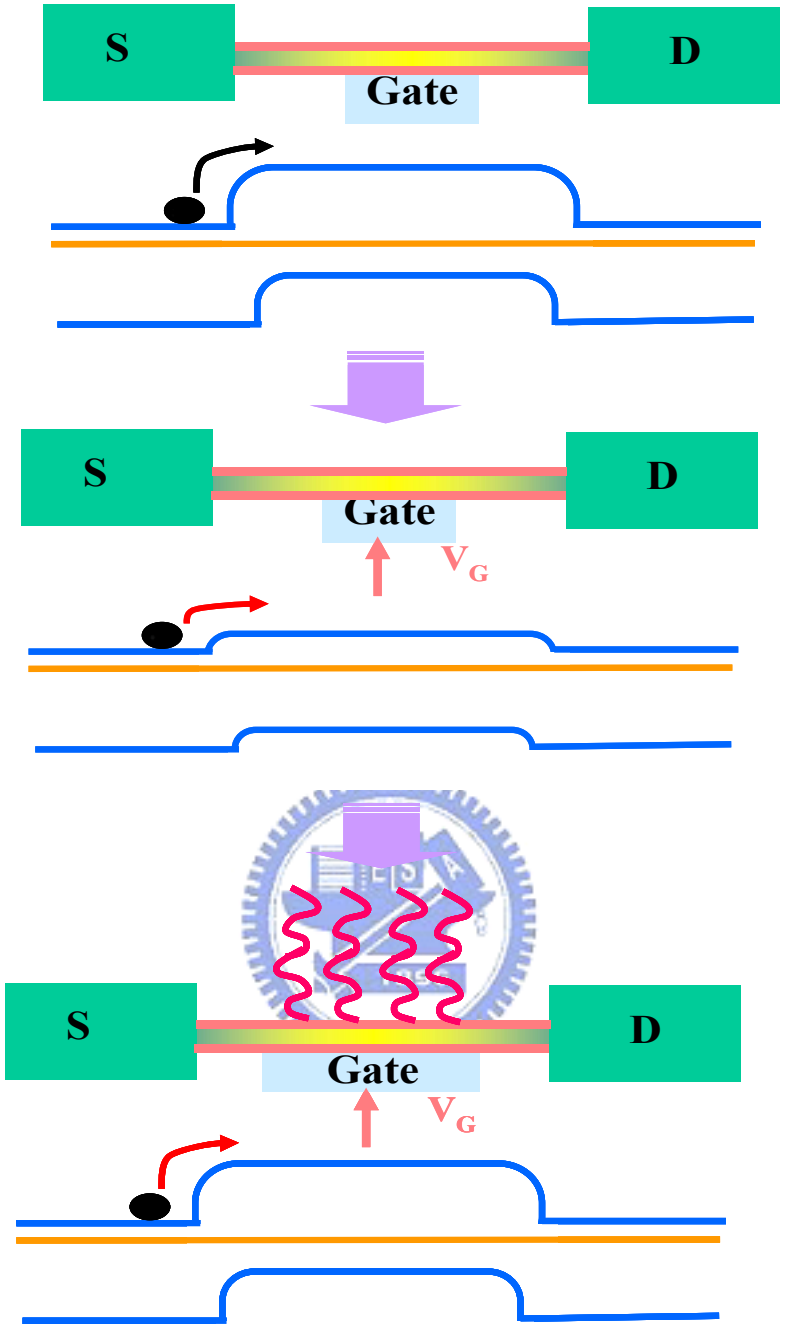

Figure 4.10 The mechanism of the SiNW-FET for detection of biomolecules

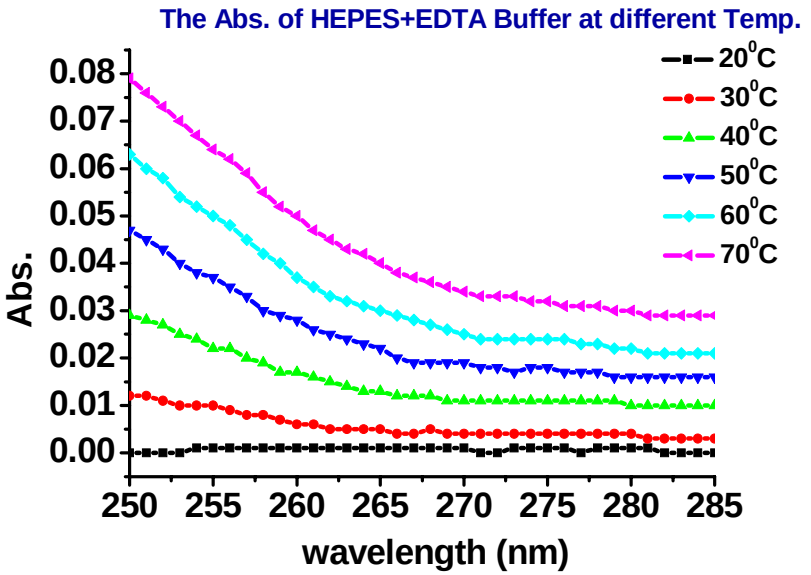

Figure 4.11 The noise level of HEPES+EDTA solution during different temperature measured by UV spectrophotometer.

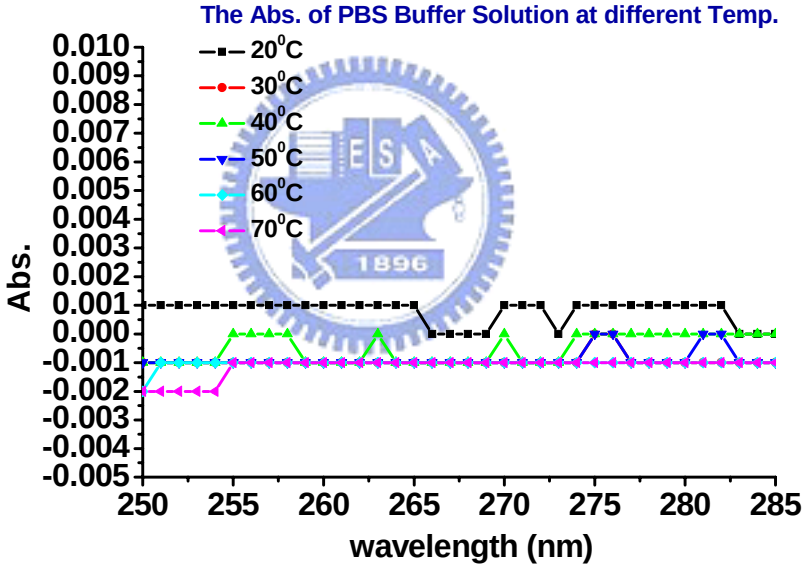

Figure 4.12 The noise level of PBS solution during different temperature measured by UV spectrophotometer.

The SiNW-FET sensors were functionalized with the probe-DNA receptors which was able to distinguish the wild-type DNA of the *BRAF*^{V599E} mutation gene. More generally, the development of sensors capable of the facile detection of DNA sequence variations for disease. The probe-DNA was chosen as a recognition sequence in our studies, since it was known to bind the target-DNA with greater

affinity and stability **[16, 17]**. The probe-DNA acted as the receptor for detection of the target $BRAF^{V599E}$ mutation gene and non-complementary oligonucleotide. The sequences of the probe-DNA, target-DNA and non-complementary were displayed in **Table 4.2 [3]**.

Table 4.2 The sequences of the probe-DNA, target-DNA and non-complementary

Sequence Name	**Oligonucleotide Sequence**
Probe-DNA	**5'-AAATATATTA-TTACTCTTGA-GGTCTCTGTG-3'**
Target-DNA	**5'CACAGAGACC-*TCAAG*AGTAA-TAATATATTT-3'**
Non-complementary DNA	**5'CACAGAGACC-*GCCGT*AGTAA-TAATAtATTT-5',**

Before real-time measurements, the noise level of the SiNW-FET was around 35nA, revealing that unobvious substantial change in the drain-current versus time was obtained in **figure 4.13**. **Figure 4.14** showed a dramatically decrease in drain-current by addition the 100fM target-DNA sample solution onto the SiNW surface. This drain-current change included a rapid (<20min) response in the region 3 of **figure 4.14**, followed by a longer time scale decrease occurring over hundreds of seconds at region3. The decrease in drain-current for this device was because of an increase negative charge density on the surface associated with hybridizing of negatively charged target-DNA **[3]**. Several control experiments have been carried out to assess further the nature of the observed change. First, addition of samples with only PBS buffer solution exhibited no substantial change in drain-current, as shown in the region 2 of **figure 4.14**. Specifically, the addition of 100pM target-DNA solution following the 100fM target-DNA injection functionalized-device that has been exposed to probe-DNA also leads to a significant decrease in the region 4 of **figure 4.14,** and then the drain-current continued to decrease to the lower level until

saturated when 10nM target-DNA solution is injected, as shown in the region5 of **figure 4.14**. These results demonstrated that the longer term decrease in drain-current was unique to the target-DNA samples, and thus the current decrease can be used as a measurement of hybridized DNA complex formation onto the SiNW surface. The specific drain-current changed due to DNA-DNA hybridization were obtained from the time-dependent drain-current recorded following different target-DNA samples injected into the same SiNW device. The results were recorded in **figure 4.14** that demonstrated that the target-DNA could be effectively and selectively detected for the concentration as low as 100fM by using the SiNW device without any labeling.

In addition, there are several features of our DNA biosensors that deserved further comment. First, the 100fM detection limit determined in our study was not an absolute limit since it should be possible to improve electrical sensitivity of SiNWs through variations in effective improvements in the contacts **[4]**. Second, the curve of the current changed as a function of the target-DNA concentration for two independent devices showing a very similar systematic decrease in net drain-current with increasing DNA concentrations will be discussed in **Chapter 4.3.2.**

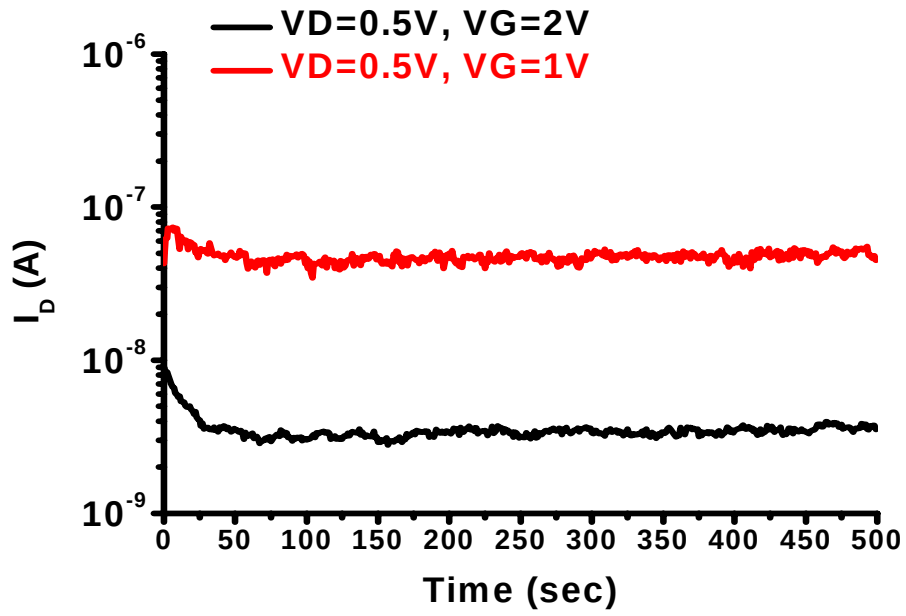

Figure 4.13 Noise of SiNW-FET device in real-time detecting by HP-4156C analyzer

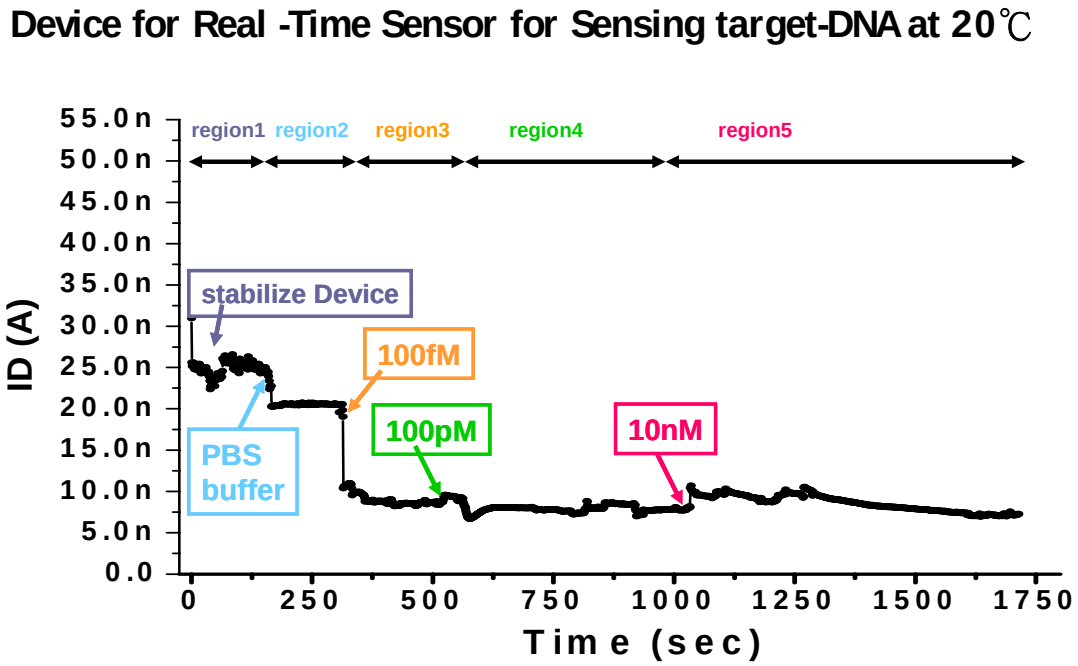

Figure 4.14 Real-time detection of target-DNA hybridizing with probe-DNA at 20°C. (Plot of drain-current versus time for modified SiNWs, where **region1** corresponds to stabilize device, **region2** corresponds to the buffer solution, **region3** corresponds to the addition of 100fM target-DNA, **region4** corresponds to addition of 100pM target-DNA and **region5** corresponds to addition of 10nM target-DNA).

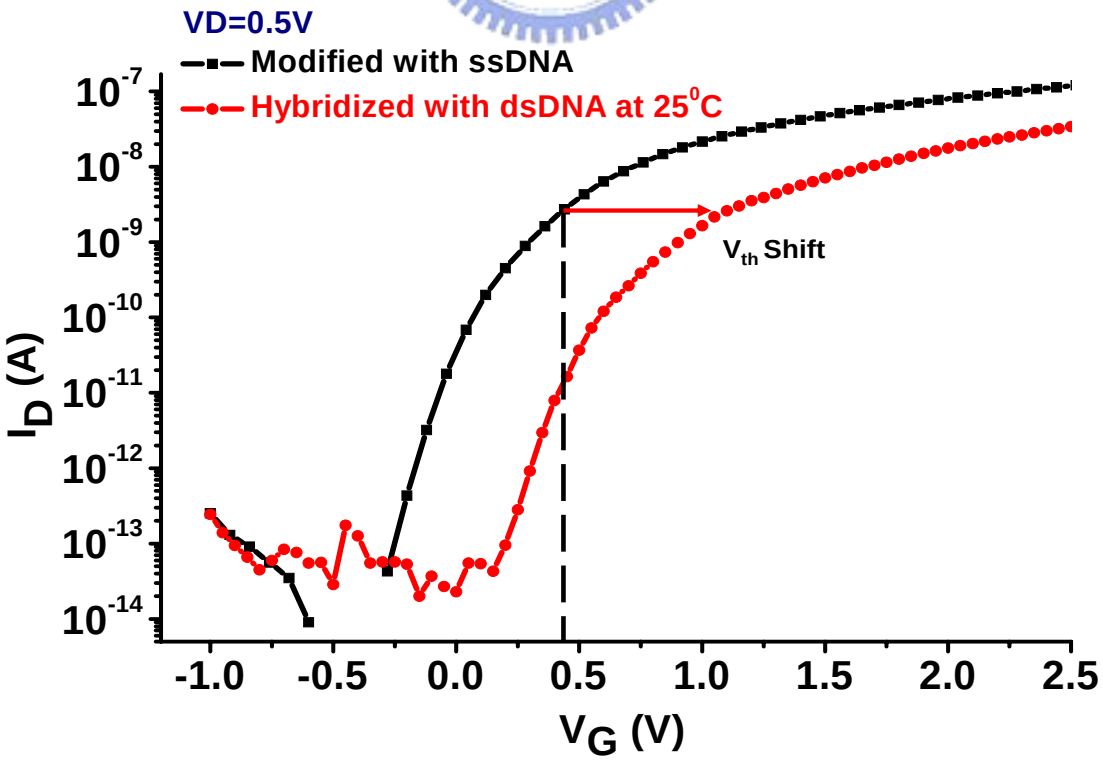

Figure 4.15 The I_D-V_G curve of detection for DNA hybridization assay at 25 ℃

The I_D-V_G characteristic curve during every experimental step were also measured to examined the stability of the device. The threshold voltage the device with 1 μm length and 100 nm in width was shown in **figure 4.16**. At first, the threshold voltage shifted right because the probe-DNA attached, which was equal the negative charges to the surface of SiNW. The target-DNA was applied at the next step to hybridize with the probe-DNA, and hence the threshold voltage shifted to more positive. It can be explained that the more negative charges were applied onto the SiNW. The shift of threshold voltage is about 0.76V about the target-DNA was applied. From the results of threshold voltage shifted during DNA hybridization, the potential of applying this type of nanowire to biomolecular sensing was working out. In order to test the dehybridization process the complex-DNA pairs were washed at 100 °C with DI water in this experiment. After the dehybridization process, the threshold voltage of sensor device recovered to the original value, as shown in **figure 4.16.** This result depicted that the more positively shift of threshold voltage at hybridization step was totally contributed by the target-DNA. An alternate control of experiments used with non-complementary DNA as the target-DNA was performed. In addition, the mismatch-DNA was also examined to hybridize with probe-DNA onto the SiNW. A positive threshold voltage shift (~0.43V) was observed as the mismatch-DNA was hybridized to the probe-DNA, but the shifting was smaller than complementary DNA. This result indicated that the mismatch-DNA was also hybridized to the probe-DNA but the hybridization efficiency was less than the complementary DNA. The I_D-V_G characteristic curve of above assay was shown in **figure 4.16**.

In summary, we reported the use of SiNW-FET to employ the label-free, direct real-time electrical detection of the target-DNA and mismatch-DNA. DNA hybridization could be detected by measuring the electrical characteristics of the

SiNW-FET. The SiNW-FET could be a charge molecular indicator because of their field-effect characterization, and the I_D-V_G curve was sensitive enough to detect biomolecules on the surface shown in **figure 4.16**.

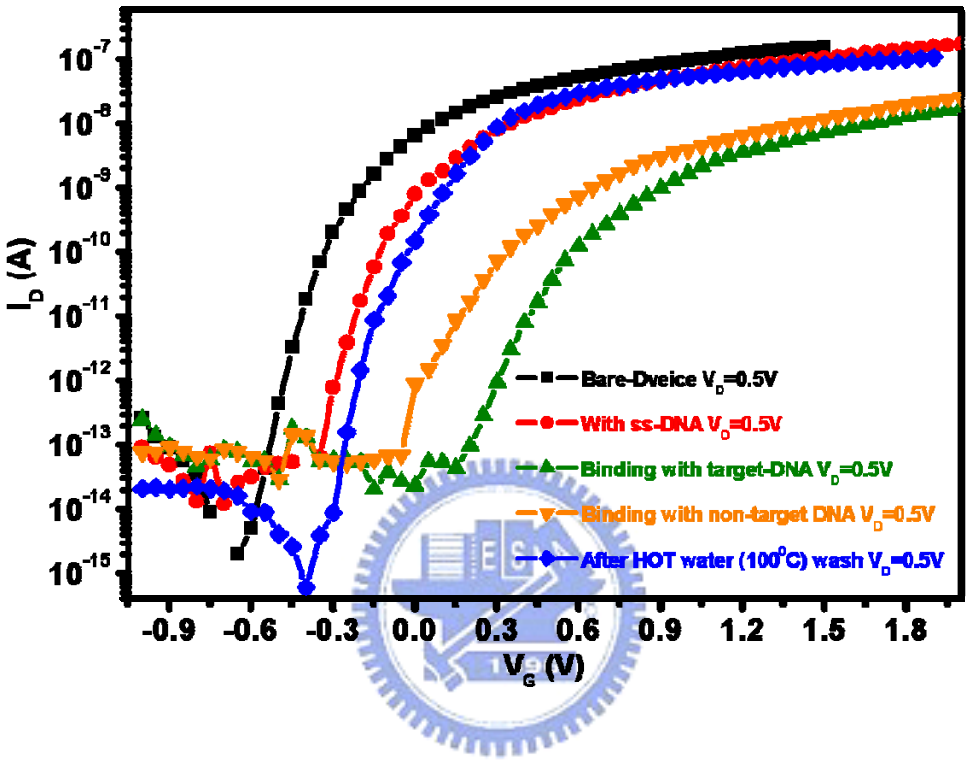

Figure 4.16 The I_D-V_G curve of detection for DNA hybridization assay.

4.2.4 The Influence of Temperature on Efficiency of Hybridization and Dehybridization Assay

As we mentioned in **Chapter 4.2.3**, the threshold voltage shifted as the probe-DNA and target-DNA hybridized together. In this section, we reported the improvement of hybridization efficiency by changing the temperature. The PCR assay was used to examine the hybridization efficiency. **[18]**. The PCR process contains three steps, including dehybridization, annealing and extending. The controlling parameter is decided by temperature factor, a gradient temperature decreasing from 65 to 20 ^{o}C was performed during the hybridization process, and the hybridization

efficiency was better than that in room temperature. Single-strand DNA has specific absorption peak at wavelength of 260 nm using UV photometer because of the aromatic-ring structure of the single strand-DNA which was displayed in **figure 4.17 [19].** On the other word, DNA remained at the hybridized state could be easily detected by the absorption peak of UV photometer. **Figure 4.18** shows the absorption peak value during hybridization process at various temperatures. From 20 to 70 °C and then cooling down to 36 °C continuously, it is realized which conformation will be at the different temperature using OD260-curve shown in **figure 4.18 and 4.19**. As a result, we can make a brief conclusion on the best experimental parameter by controlling the temperature. We can provide more suitable experimental condition during DNA hybridization assay in real-time detection and recorded out-put signal by electrical analyzer.

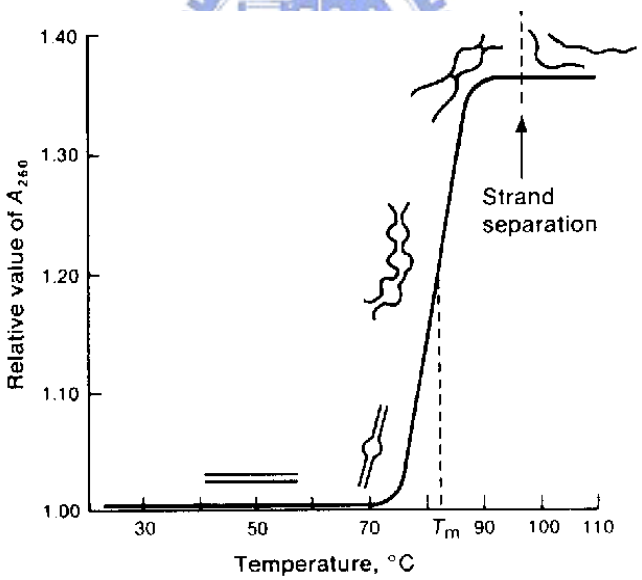

Figure 4.17 The Hyperchromic-Effect in DNA hybridization assay

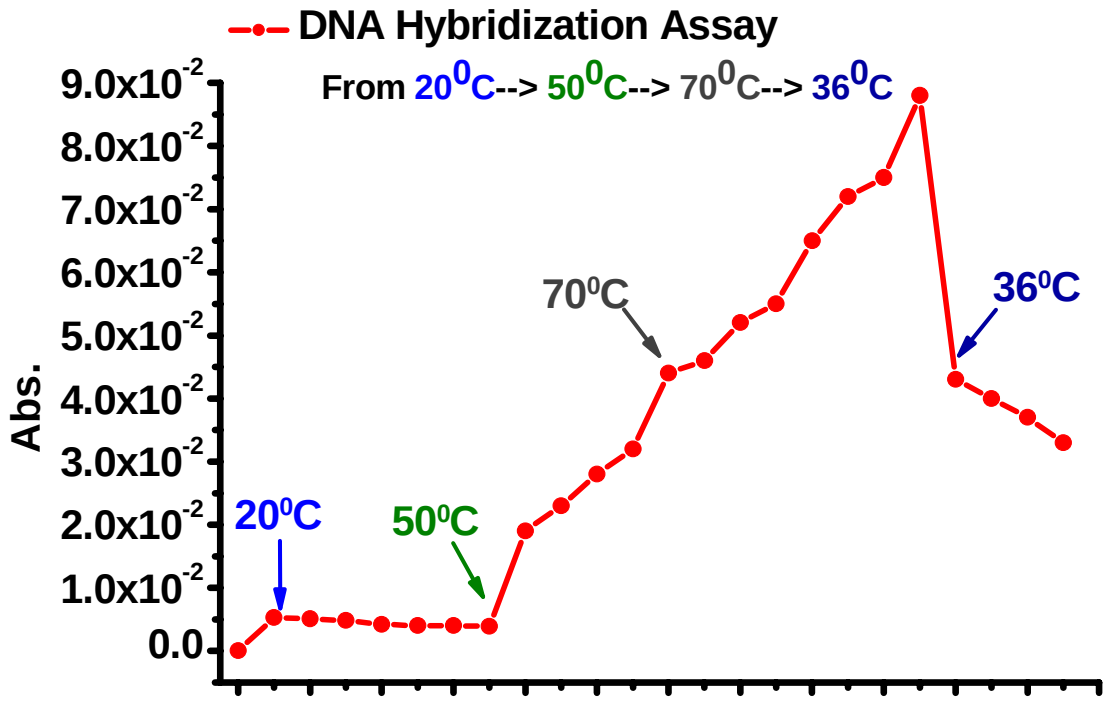

Figure 4.18 The OD260-curve recorded during DNA hybridization assay with variation temperature continuously.

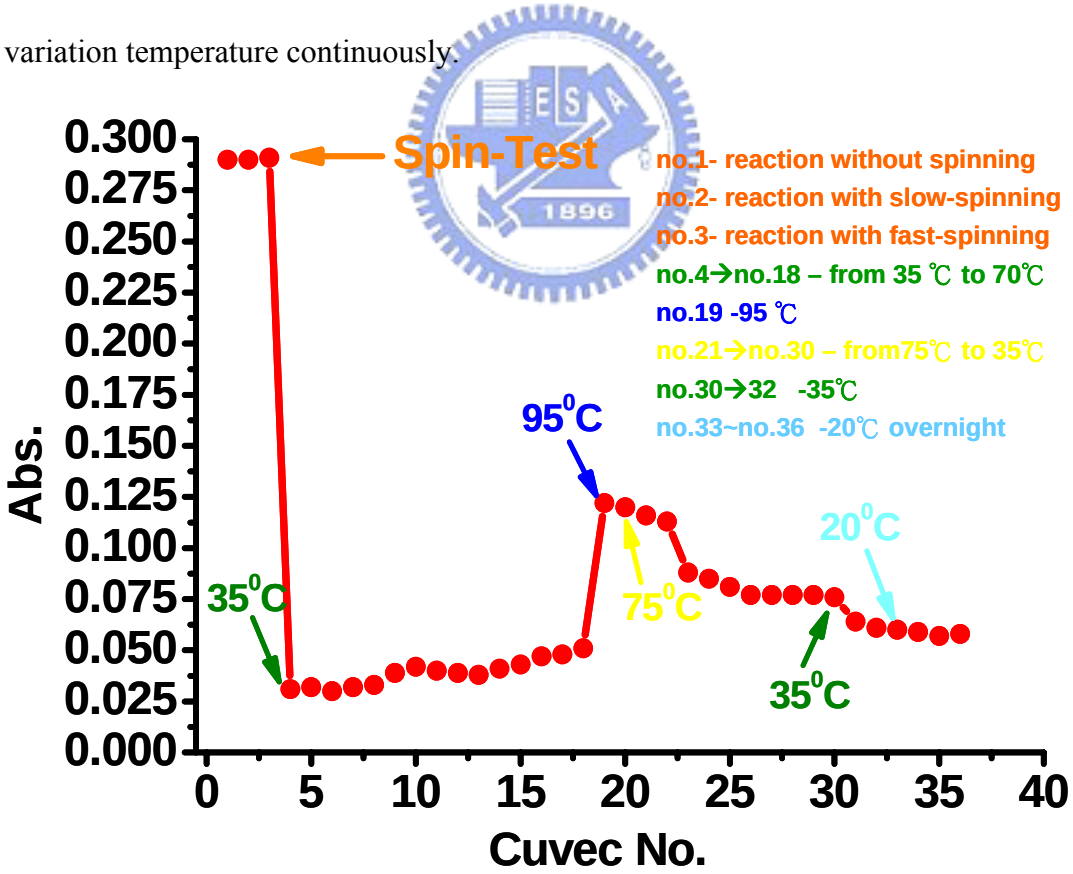

Figure 4.19 The OD260-curve recorded during DNA hybridization assay with variation temperature continuously.

After UV spectrophotometer assay, we tried to proofed that the gradient temperature curve was making better efficiency of hybridization assay and the condition for effectively dehybridization process. The whole procedures for the model of probe-DNA conjugated FITC and target-DNA conjugated FAM molecules onto the modified surfaces have been described in **figure 3.8 and figure 3.9**, respectively. In **figure 4.20**, the appearance of fluorescent FITC and FAM molecules on the silicon dioxide was detected. An alternate controlling sample was used by the unmodified surface, that is, APTES only and APTES with glutaraldehyde only were performed. The surface with APTES and glutaraldehyde could make a selective assembly. The fluorescent images under optical microscope were the direct view of the different modified surface. The images under fluorescent microscope shown in **figure 4.20 (a) and (b)** are with FITC-conjugated probe-DNA, FAM-conjugated target-DNA, respectively. From these images, we could discover the oxide surface, APTES only and APTES with glutaraldehyde only were negative in fluorescent assay. On the contrary, surface with APTES and glutaraldehyde modified reacted with the FITC-conjugated probe-DNA, and hence the fluorescent image was shown in **figure 4.20**. The following step was trying different hybridization temperature, one was from 60 to 20 °C and the other was kept at 20 °C. We found that the hybridization assay in gradient reduced temperature was achieved excellent fluorescent image than that kept at 20 °C. The quantitative data by Image-Pro Plus is also shown in **figure 4.21**. In addition, the dehybridization assay used with the gradient temperature from 60~20 °C was also demonstrated, which is shown in **figure 4.22**. We found that the dehybridization was more efficient for sample after treatment overnight than others. The calculated quantitative analysis by IPP is shown in **figure 4.23**. Finally, we found the best experimental parameter in hybridization and dehybridization assay to be applied in our real-time detection disease genes assay with electrical analysis.

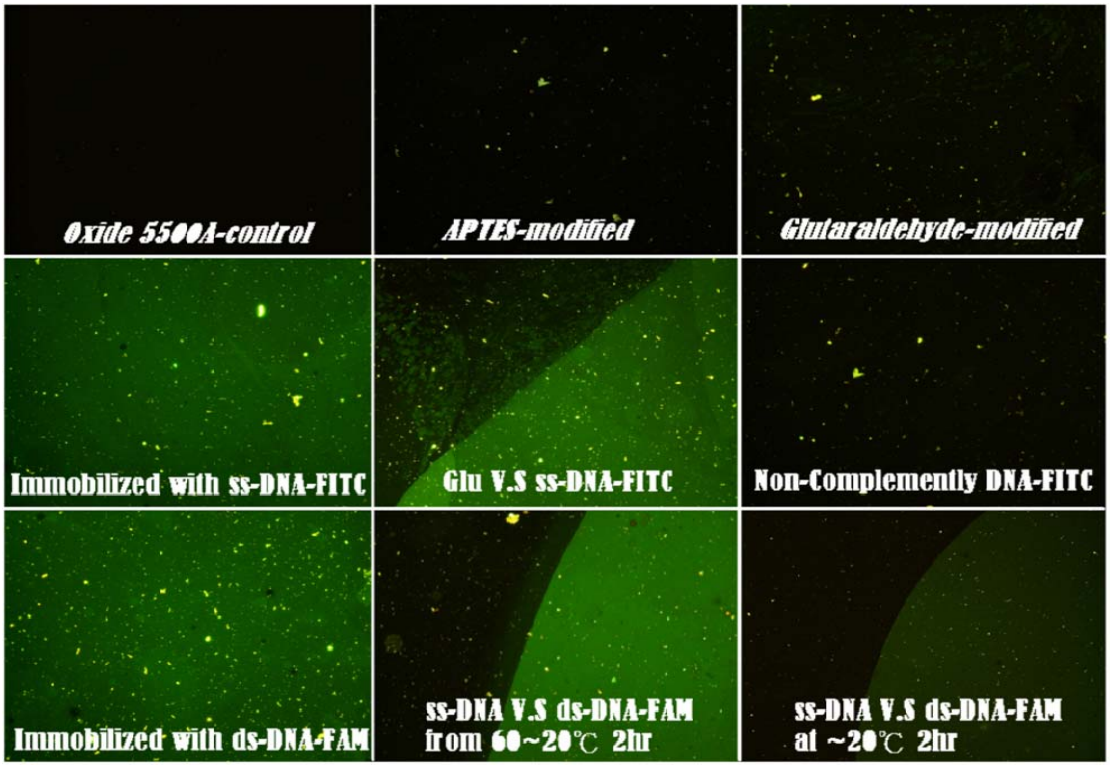

Figure 4.20 The fluorescent images under treated different hybridization experimental conditions with the same oxide substrate.

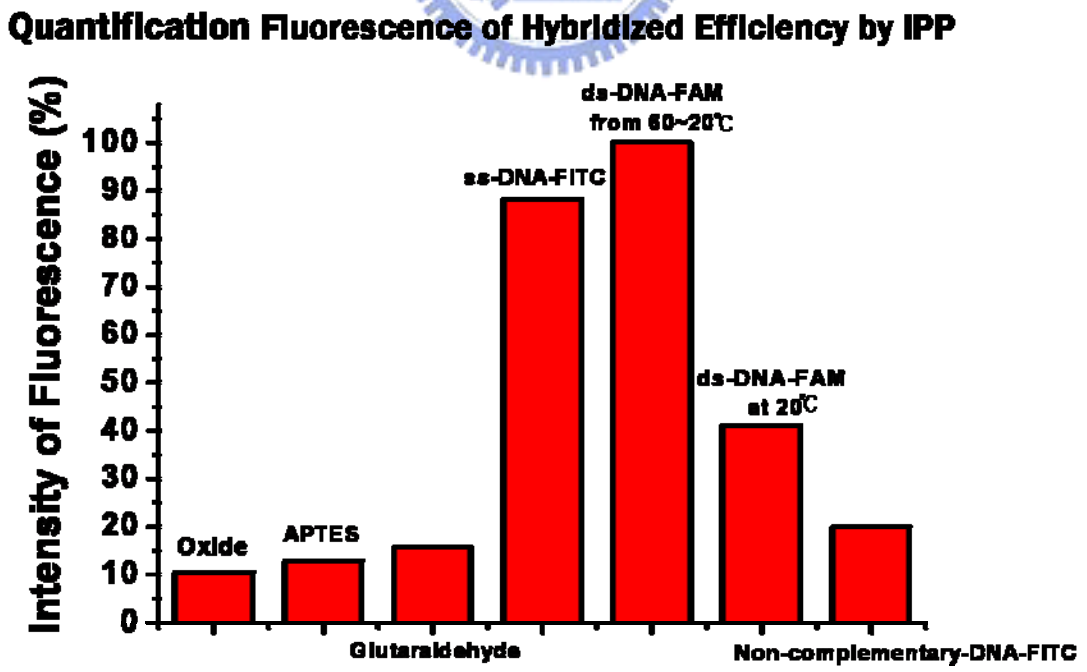

Figure 4.21 The quantification of each one condition in Figure 4.20 by IPP analysis.

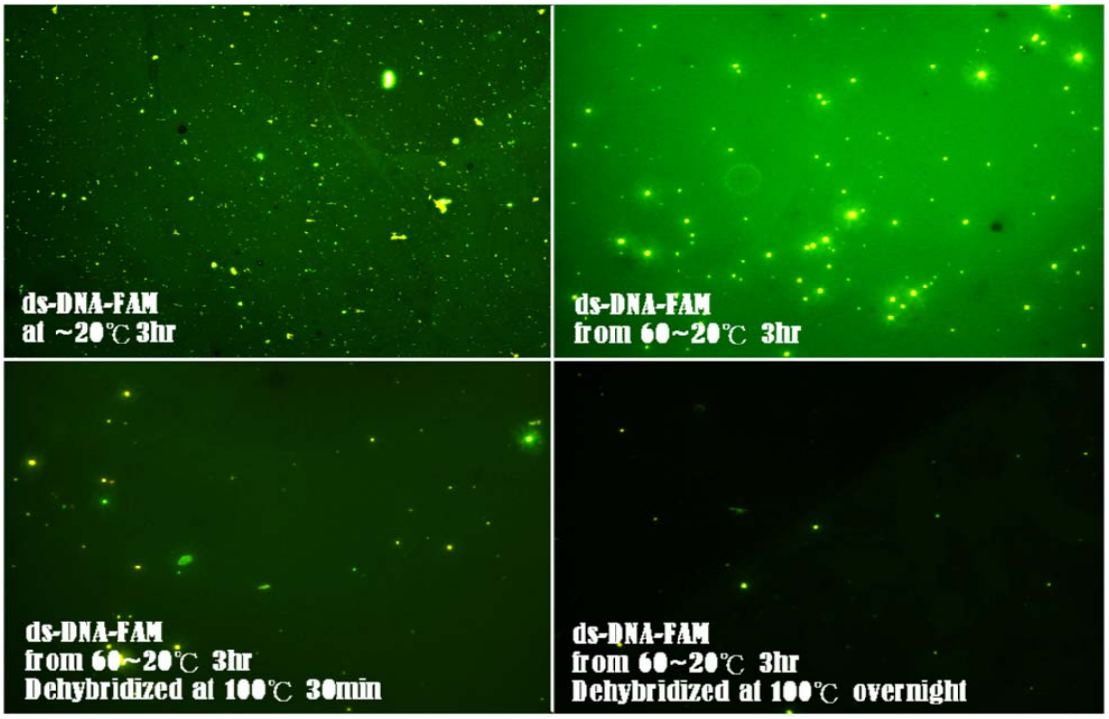

Figure 4.22 The fluorescent images under treated different dehybridization experimental conditions with the same modified oxide substrate.

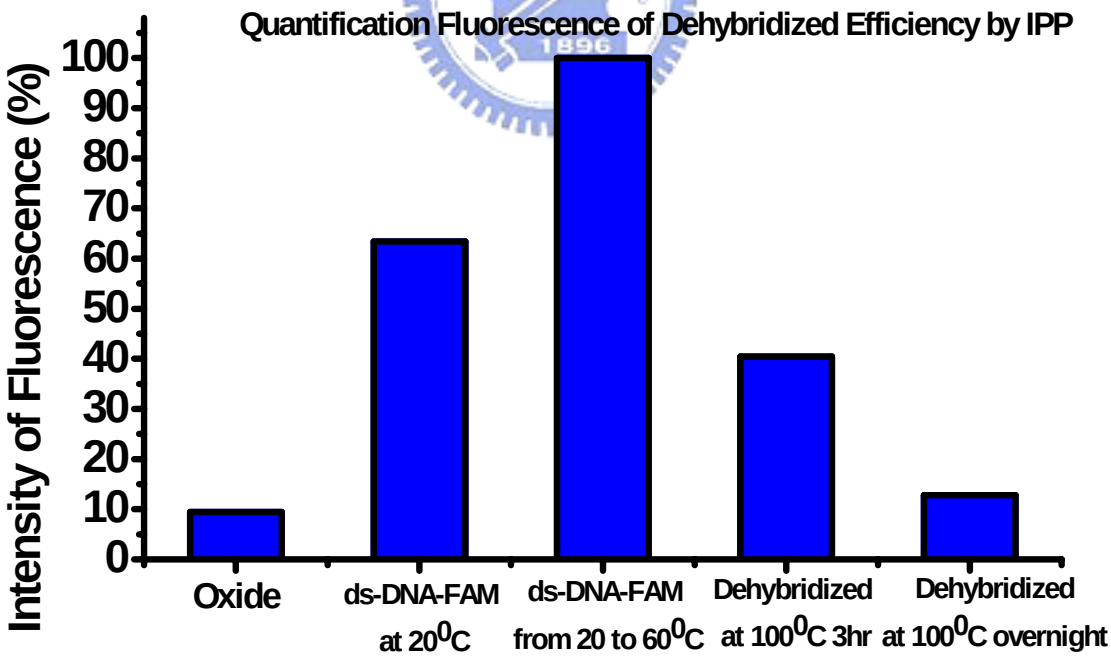

Figure 4.23 The quantification of each one condition in Figure 4.22 by IPP analysis.

After the experimental condition of the DNA hybridization in microfluidic sytem of SiNW-FET had been confirmed. A buffer solution was introduced into the side-gate sensor. The solid line in **figure 4.14** and **figure 4.24** show the drain-current I_D versus time characterizations when the buffer solution, complementary-DNA with various concentrations were poured. The decrease of the drain-current has significant difference between **figure 4.14 and figure 4.24**. **Figure 4.24** shows the change of drain current with different concentration of target DNA injected into the SiNW sensor. The sensitivity of the sensor was better than previous experiment shown in **figure 4.14** because of the gradient temperature was used at the hybridization process. When the complementary-DNA solution with the concentration from 100fM to 10 nM was injected, the drain-current I_D in **figure 4.24** decreased from 35nA to less than 5nA, which is better than in **figure 4.14** from 2nA to 10nA at V_G= +0.5 V. Finally, we decided the suitable experimental parameter for DNA hybridization assay and dehybridization process.

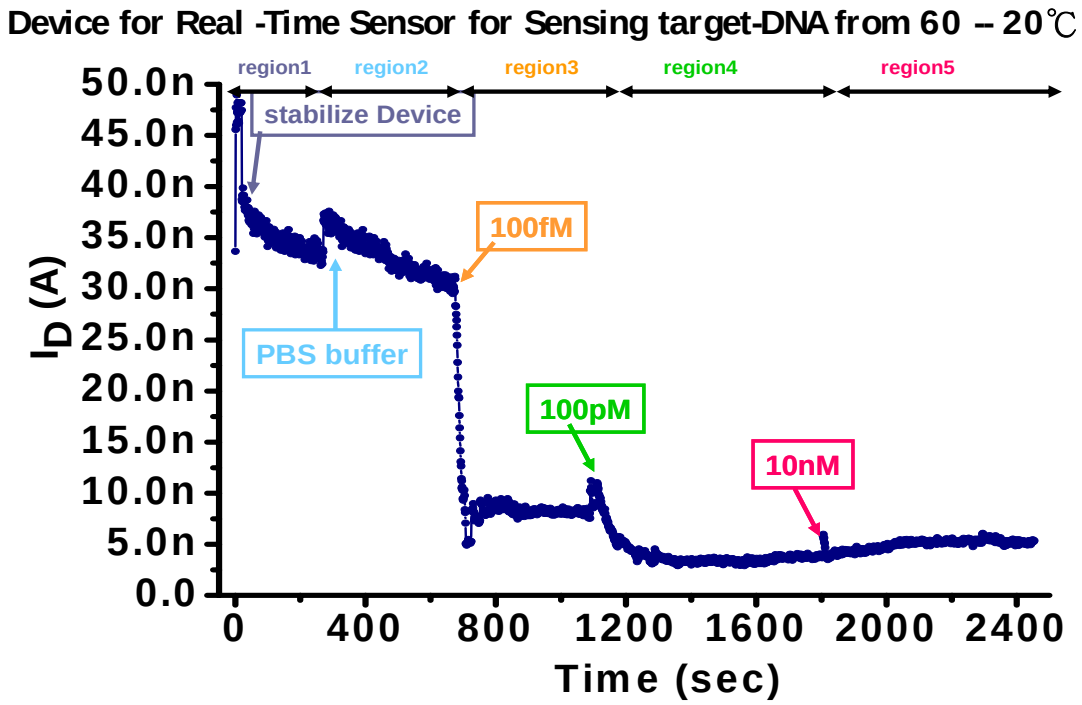

Figure 4.24 Real-time detection of target-DNA hybridizing with probe-DNA at from 60 to 20 °C. (Plot of I_D versus time for modified SiNWs, where **region1** corresponds to stabilize device, **region2** corresponds to the buffer solution, **region3** corresponds to the addition of 100 fM target-DNA, **region4** corresponds to addition of 100 pM target-DNA and **region5** corresponds to addition of 10 nM DNA.

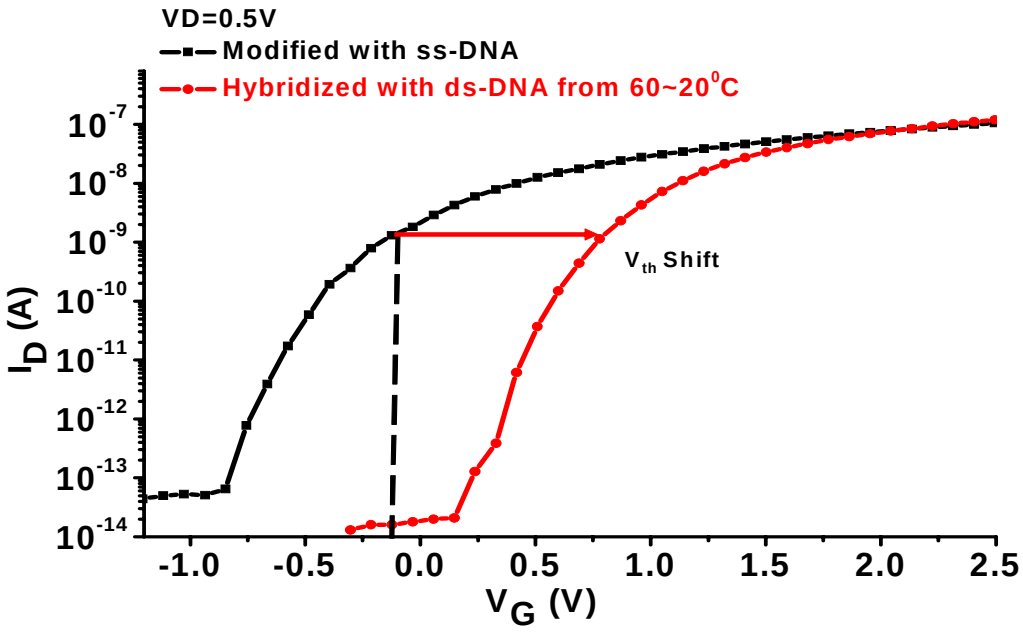

Figure 4.25 The I_D-V_G curve of detection for hybridization assay from 60 to 20 °C

4.2.5 Quantification of Detection Target-DNA

The charge of target-DNA, Q_e, causes the threshold voltage shift ΔV_{th}, which is linearly proportional to Q_e as

$$\mathbf{Q_e = C^* \Delta V_{th} = C^* \Delta I_D/gm\text{----------(1)}}$$

Where C is the gate capacitance of the SiNW-FET biosensor **[20]**. Therefore, the amount of the adsorbed target-DNA is proportional to ΔV_{th}. In the present SiNW-FET biosensor, the drain current I_D was related to the side-gate bias V_G as shown in **figure 4.16**. Hence, we regard *g*m as a constant in our measuring range according to **equation 1**. Therefore, Q_e is linearly proportional to ΔI_D. Hereafter, the properties of the target-DNA detection are characterized by the drain-current decreasing ΔI_D. For the target-DNA detection, the dependence of ΔI_D on the concentration of the target-DNA solution is shown in **figure 4.26**. **Figure 4.26** is a kind of adsorption isotherm because ΔI_D was positive related to the amount of target-DNA hybridized with probe-DNA. The mechanism would be site-selective and monolayer adsorption. The ΔI_D is proportional to the logarithmic scale of target-DNA concentration below 10 fM, as shown in **figure 4.26**. As target-DNA concentration increased, the increase of ΔI_D became gentle and almost saturated. Direct comparison of these data highlights the substantial net drain-current change associated with hybridization of the DNA complementary to the probe-DNA receptor.

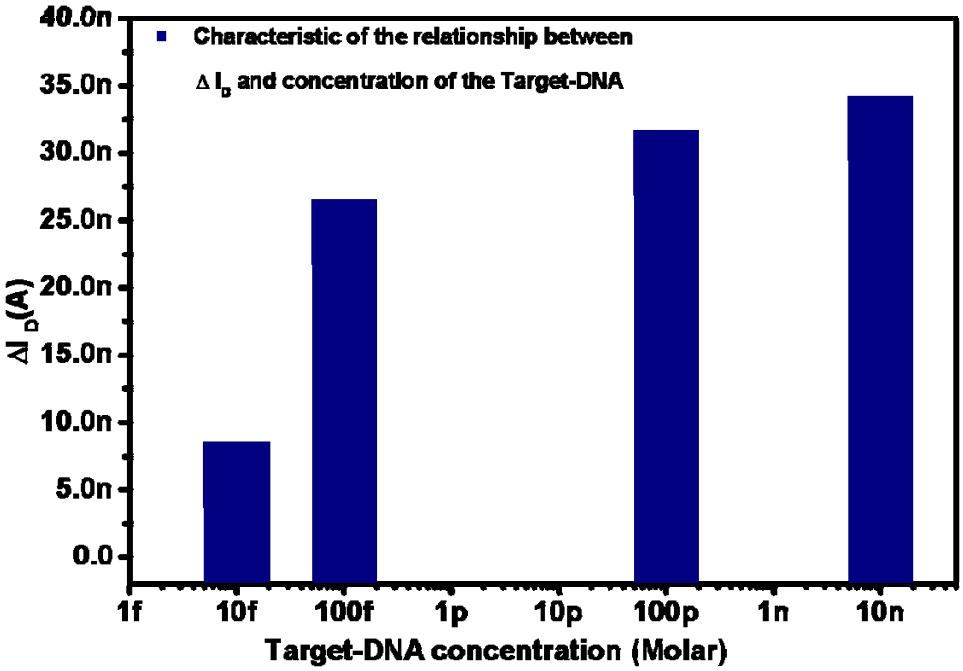

Figure 4.26 Characteristic of the DNA sensor measured in PBS buffer solution containing target-DNA, V_D=0.5V. It shows the ΔI_D positive related to logarithmic scale of target-DNA concentration.

4.3 Detection of Immobilized Anti-Alpha-Fetoprotein and Interacted with Alpha-Fetoprotein

More recently, we explored the use of SiNW devices for the detection platform. One important application is the detection of protein biomarkers, which are thought to have the potential to greatly improve the diagnosis of diseases **[21]**. The availability of cancer markers is believed to be especially important in the diagnosis of cancers because disease makes single-marker tests, such as the analysis of alpha-fetoprotein, inadequate **[22]**.We chosen the SiNW for this experiment according to the previous accuracy results of the measurements of mutation DNA. The AFP plays an important role in inspecting pathology of liver as a cancer marker. **Figure 4.27** and **figure 4.28**

shows the FT-IR analysis after sample was immobilized with anti-AFP. The absorption spectrum in **figure 4.27** and **figure 4.28** shows the anti-AFP exactly on the SiNW. The interaction of the anti-AFP and AFP onto the nanowires was too tiny to be seen in the images. The electrical properties of the samples were shown in **figure 4.29 ~ figure 4.31**. And then, we discussed in more details in next section.

4.3.1 Detection of Anti-α-fetoprotein by FT-IR Assay

FT-IR nondestructive optical technique allows for the characterization of the structure, and the extraction of information concerning the interfaces, the nature of the bonds in the material and on the interface. With regard to the spectra of the immobilized antibody, they were carried out after immobilized sample on the silicon wafer. The antibody was immobilized on the silicon oxide. The spectrum of the antibody of AFP obtained according to the procedure of subtraction described in **figure 4.27** and **figure 4.28**, is characteristic of a protein, for C-N bond is present around 1095 cm^{-1} **[23-25]**, as well as the N-H bond around 3300 cm^{-1} convoluted with the backbone S-S bond at 462 cm^{-1}. There are very strong and cumulate bonds of amino-acid combination around 2000~3000 cm^{-1}. The main outline of this spectrum is the presence of the peaks of the antibody of AFP. This presence is discussed as a result to achieve our immobilized assay for antibody of AFP onto the SiNW.

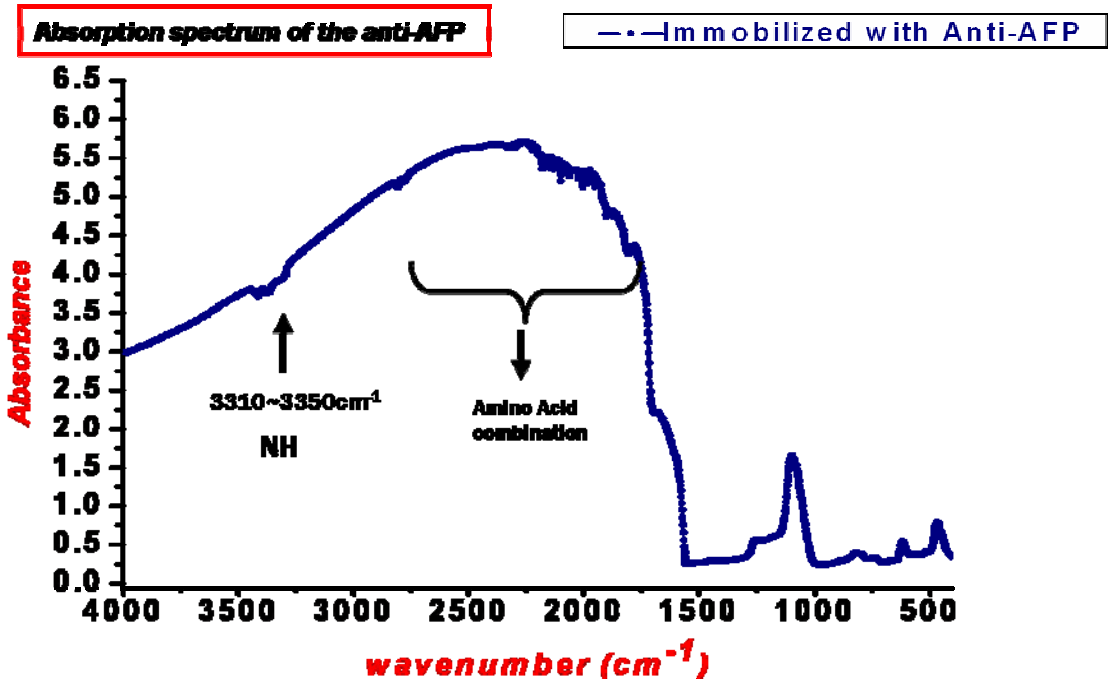

Figure 4.27 Absorption spectrum of the antibody of AFP heterostructure between 4000 to 500 cm^{-1}

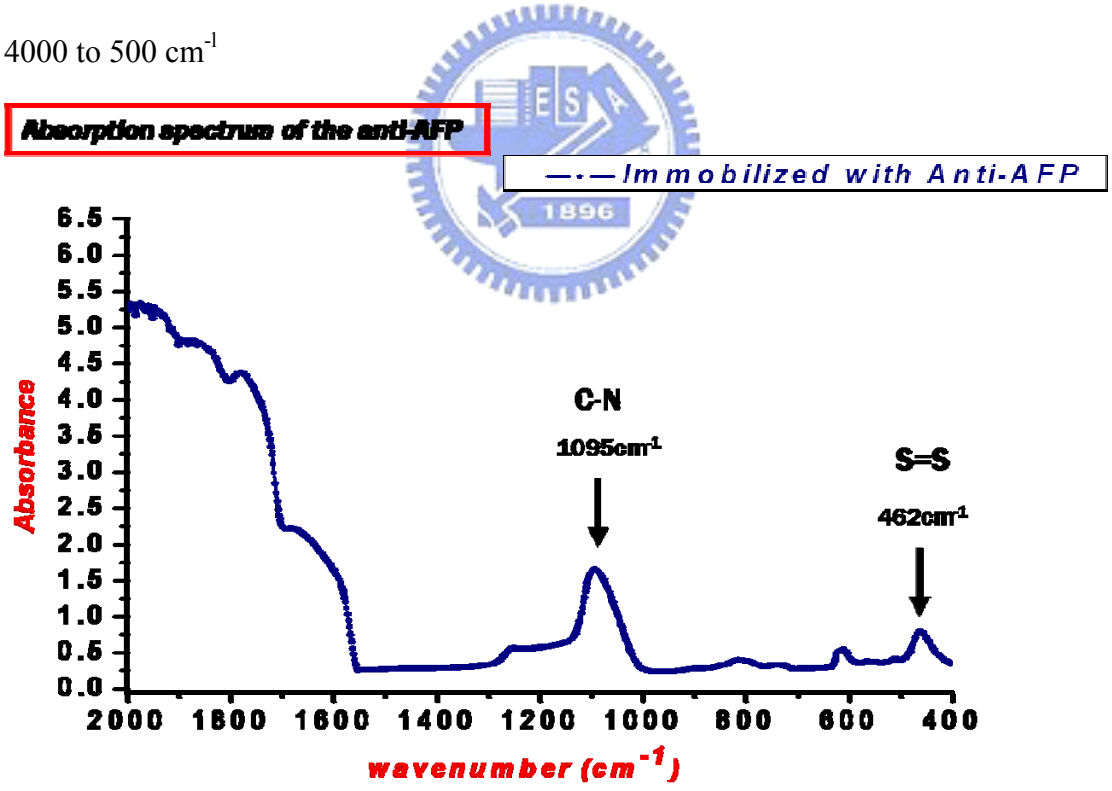

Figure 4.28 Absorption spectrum of the antibody of AFP heterostructure between 2000 to 400 cm^{-1}

4.3.2 The Real-Time Detection of Antigen-Alpha-Fetoprotein

Debye length is one of the significant factors, which affects the detection sensitivity. It depends on the ionic strength of solution. To effectively detect the interaction of antibody and antigen which were located at more than a few nanometers from the SiNWs in the charged molecules, 1 mM PBS buffer solution was employed which allowed the interaction distance effect detectable, as illustrated in **figure 4.9**. Thus, the charges of the protein might be "screened" by the layer, and their effect on the carrier distribution would then be guaranteed to detect signal. Moreover, detection of markers associated with further facilitating early detection, which is especially important for successful cancer treatment. The cancer biomarker was detected by modified SiNW with the antibody of AFP. Sensitivity was determined by measuring drain-current changes as the solution concentration of AFP was varied in **figure 4.29**. And the decrease in drain-current with α-fetoprotein interaction with antibody with negative overall charge, as expected from the isoelectric point of α-fetoprotein was 6.4, and the buffer with pH=7.4, in our experiments **[26].** The data recorded in **figure 4.29** shown a decrease in drain-current versus time when α-fetoprotein solution was delivered to the devices and a subsequent returned to the baseline with the delivery of hot water solution. Firstly, the drain-current decreased as the α-fetoprotein concentration was increasing. Plot of drain-current versus time in **figure 4.29**, where **region1** corresponds to stabilize device, **region2** corresponds to the PBS buffer solution without obviously current decreased, **region3** corresponds to the addition of 3ng/mL AFP with decrease ~2nA current signal, **region4** corresponds to addition of 15ng/mL AFP continued down to ~11nA, **region5** corresponds to addition of 30ng/mL AFP interaction with antibody caused the decreasing current to 8.5nA, **region6** corresponds to addition of 300ng/mL AFP down to the lowest current value ~7nA, **region7** corresponds to addition of 600ng/mL AFP remains the saturation state

and **region8** corresponds to addition of hot-water flow solution makes the current reverse to the original level. **figure 4.29** shows a well-defined drain-current decreasing and a subsequent return to baseline when α-fetoprotein solution (**region3**), only buffer solution (**region2**) and hot-water (**region8**) are alternately delivered through the microfluidic channel to the devices. Notably, the data shows that direct detection of AFP is achieved with detection limit for concentration down to 3ng/mL. The limitation concentration fits for the standard value in clinical diagnosis which reveals that our device exhibits excellent sensitivity for clinical application.

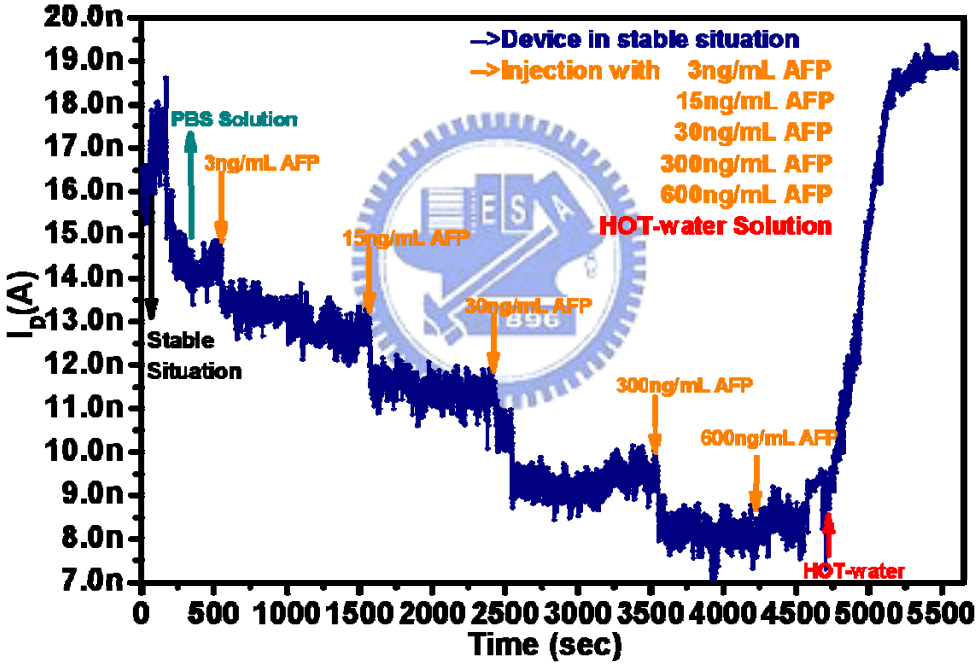

Figure 4.29 Real-time detection of AFP interaction with anti-AFP. (Plot of I_D versus time for modified SiNWs, where **region1**: stabilize device, **region2**: the buffer solution, **region3 to region7:** addition of different concentration from 3ng/mL to 600ng/mL AFP and region8: injection with hot-water flow out)

The shifting of I_D-V_G curve after AFP bound was also measured in this experiment, which is shown in figure 4.30. Obviously, the V_{th} shifted right because of an interaction between antibody and antigen. In this step, negative charge of AFP which was similar to the negative V_G, was applied to SiNW surface. It can be explained that the more negative charges are applied on the nanowire. The shift of V_{th} is about 0.56V. From the above results, the potential of applying nanowire to biomolecular sensing is possible. To control of the experiment, a denaturation process was also tested. Complex-antigen-antibody was washed at 100 °C with DI water, AFP will denature from antibody and be stripped by flow liquid washing out. The device recovered to near the original threshold voltage value once only antibody of AFP attachment after washing is displayed in **figure 4.30**. This test depicted the positively shift of V_{th} during interaction was totally contributed by the AFP. Therefore, detection of distinct marker proteins facilitating interaction analysis for diagnose, can be carried out with real-time, label-free, high sensitivity and selectivity with NW arrays modified with specific antibody receptors. Furthermore, control experiment with 1 mM of non-target bovine serum albumin (BSA) shows no change in the drain-current of the SiNW-FETs above the noise level, as shown in **figure 4.31**. No significant change in conductance even for exposing sensor to BSA of 10^9-fold higher concentration indicates the suppression of the nonspecific binding.

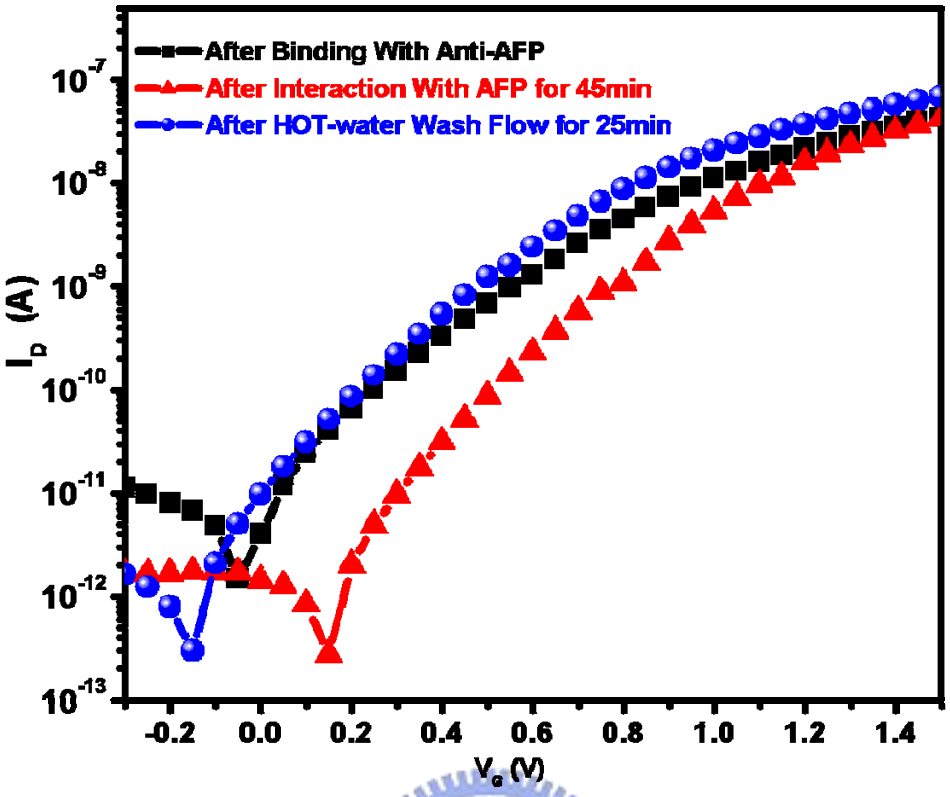

Figure 4.30 The I_D-V_G curve of detection for AFP interaction with antibody and denaturation assay

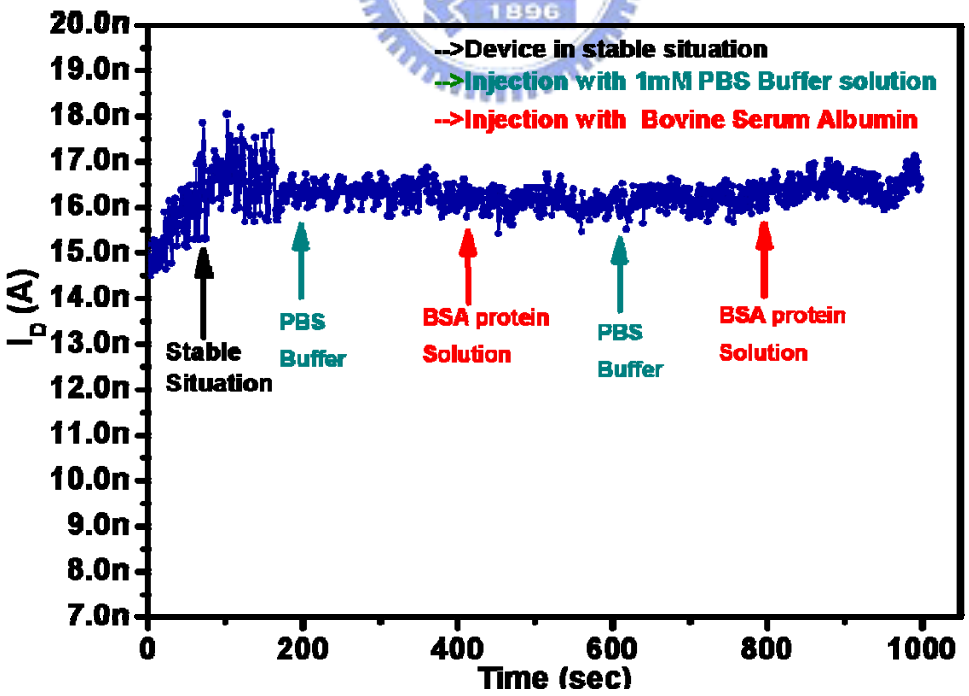

Figure 4.31 Real-time detection of BSA protein with anti-AFP.

4.3.3 Quantification of Detection Antigen-Alpha-Fetoprotein

After the electrical properties of the SiNW-FET had been confirmed, the AFP sensor was prepared by immobilizing anti-AFP onto the SiNW-FET. In the **figure 3.10**, we mentioned the mechanism of anti-AFP immobilization on the side-gate active oxide surface. The plot in **figure 4.29** shows the I_D characterizations versus time when the buffer solution without AFP was poured and with AFP was poured. According to the **figure 4.29**, the AFP solution with the concentration from 3~600ng/mL was introduced, the drain-current decreased with ΔI_D from 20nA to 7.5nA at V_G =+0.5 V. The charge of AFP, Qe, caused the threshold voltage shift ΔV_{th}, which is linearly proportional to Qe as

$$\mathbf{Q_e = C^* \Delta V_{th} = C^* \Delta I_D / gm} \text{----------(1)}$$

Where C is the detection area capacitance of the SiNW-FET biosensor. Therefore, the amount of the adsorbed α-AFP is proportional to ΔV_{th}. In our SiNW-FET AFP biosensor, the dependence of ΔI_D on the concentration of the AFP solution is shown in **figure 4.32. Figure4.32** is a kind of adsorption isotherm because ΔI_D is positive related to the amount of AFP adsorbed. The mechanism would be site-specific adsorption. The ΔI_D is linearly proportional to the logarithmic scale of AFP concentration below 600 ng/mL. As AFP concentration increased, the increase of ΔI_D became linearly and until saturated.

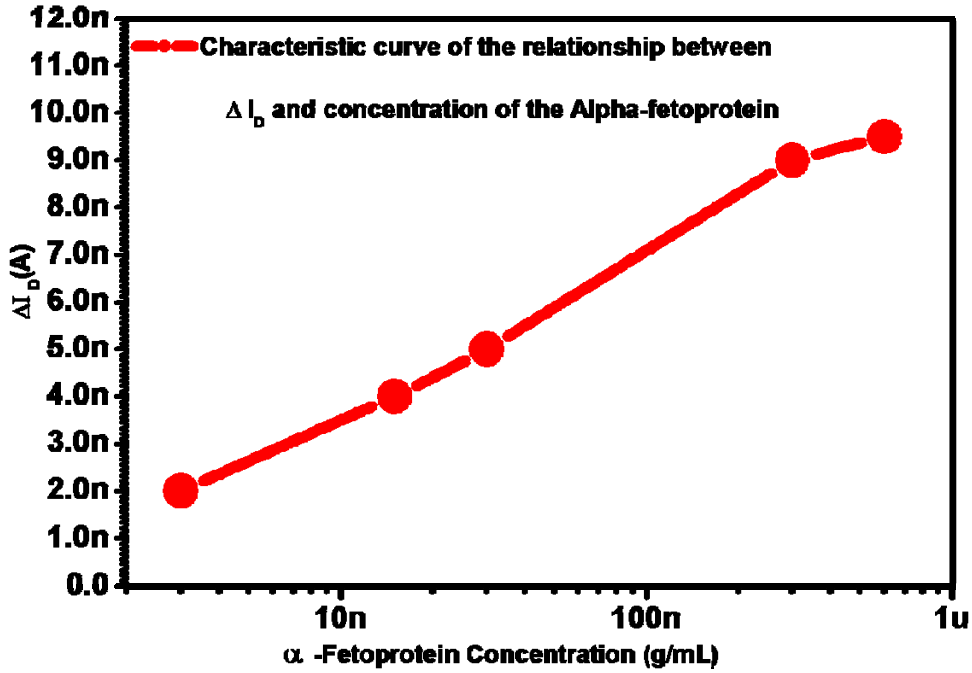

Figure 4.32 Characteristic curve of the AFP sensor measured in PBS buffer solution containing antigen-α-AFP. Drain voltage was set at +0.5V. It shows the ΔI_D positive related to logarithmic scale of AFP concentration.

Chapter 5: Conclusions

In conclusion, we have demonstrated a novel side-gate SiNW-FET for realizing integrated with SiNW-sensors for sensing $BRAF^{V599E}$ mutation gene and antigen-α-fetoprotein. The SiNW-FET was fabricated by integrating the top-down CMOS-SiNWFET technology, including the LOCOS isolation process, the shrank nanowires with higher surface-to-volume ratio, and individual side-gate for integration microfluidic system. Our side-gate devices which were fabricated using silicon-on-insulator wafers provide a good quality of gate dielectric. The device demonstrated lower leakage current and excellent field effect properties. The width of shrank nano-channel was 80 nm or thinner. The I_D-V_G characteristic of the SiNW-FET exhibited about five orders of magnitude on I_{on}/I_{off}, and the threshold voltage shifted right after hybridization of 100 fM concentrations of $BRAF^{V599E}$ mutation gene and 3 ng/mL concentrations of antigen-α-fetoprotein. The results showed that the nanowire-based device acted perfectly as an individual controlling-gate, real-time, label-free, highly sensitivity and selectivity biosensor for sensing mutation genes and antigen of cancer marker molecules. In addition, our approach offers the possibility of highly parallel detection of multiple chemical and biological species, as well as for monitoring real-time response and with individual side-gate elements in a single integrated chip in the future. An improvement in our study, in terms of sensitivity and reliability of the real-time recordings could be done well by using in-vitro biomolecule assays, where the DNA hybridization reaction and antibody interaction with antigen are achieved in a liquid environment by microfluidic system being used for real-time, label-free recording.

References

Chapter 1

1. Whitesides, G. M.; Love, J. C., The art of building small - Researchers are discovering cheap, efficient ways to make structures only a few billionths of a meter across. *Scientific American* **2001,** 285, (3), 38-47.

2. H. V. Jansen, N. R. Tas and J. W. Berenschot, *Encyclopedia of Nanoscience and Nanotechnology*, ed. H. S. Nalwa, **2004**, 5, 163.

3. *International Technology Roadmaps for Semiconductors ITRS*, **2005** Edition.

4. Harnett, C. K.; Coates, G. W.; Craighead, H. G., Heat-depolymerizable polycarbonates as electron beam patternable sacrificial layers for nanofluidics. *Journal of Vacuum Science & Technology B* **2001,** 19, (6), 2842-2845.

5. Tao, A.; Kim, F.; Hess, C.; Goldberger, J.; He, R. R.; Sun, Y. G.; Xia, Y. N.; Yang, P. D., Langmuir-Blodgett silver nanowire monolayers for molecular sensing using surface-enhanced Raman spectroscopy. *Nano Letters* **2003,** 3, (9), 1229-1233.

6. Kim, E.; Xia, Y. N.; Whitesides, G. M., Two- and three-dimensional crystallization of polymeric microspheres by micromolding in capillaries. *Advanced Materials* **1996,** 8, (3), 245-&.

7. Lithography. *International Technology Roadmaps for Semiconductors ITRS*, **2005** Edition.

8. Chou, S. Y.; Krauss, P. R.; Renstrom, P. J., Imprint lithography with 25-nanometer resolution. *Science* **1996,** 272, (5258), 85-87.

9. Chou, S. Y.; Krauss, P. R.; Renstrom, P. J., Imprint lithography for nanofabrication. *J. Vac. Sci. Technol. B* **1996**, 14, 4129.

10. Chou, S. Y., Nanoimprint lithography and lithographically induced self-assembly. *Mrs Bulletin* **2001,** 26, (7), 512-517.

11. Tsutsumi, T.; Suzuki, E.; Ishii, K.; Hiroshima, H.; Yamanaka, M.; Sakata, I.; Hazra, S.; Tomizawa, K., Properties of Si nanowire devices fabricated by using an inorganic EB resist process. *Superlattices and Microstructures* **2000,** 28, (5-6), 453-460.

12. Wilbur, J. L.; Kumar, A.; Kim, E.; Whitesides, G. M., Microfabrication by Microcontact Printing of Self-Assembled Monolayers. *Advanced Materials* **1994,** 6, (7-8), 600-604.

13. Johnson, S.; Burns, R.; Kim, E. K.; Schmid, G.; Dickey, M.; Meiring, J.; Burns, S.; Stacey, N.; Willson, C. G.; Convey, D.; Wei, Y.; Fejes, P.; Gehoski, K.; Mancini, D.; Nordquist, K.; Dauksher, W. J.; Resnick, D. J., Step and flash imprint lithography modeling and process development. *Journal of Photopolymer Science and Technology* **2004,** 17, (3), 417-419.

14. Colburn, M.; Grot, A.; Choi, B. J.; Amistoso, M.; Bailey, T.; Sreenivasan, S. V.; Ekerdt, J. G.; Willson, C. G., Patterning nonflat substrates with a low pressure, room temperature, imprint lithography process. *Journal of Vacuum Science & Technology B* **2001,** 19, (6), 2162-2172.

15. Chou, S. Y.; Krauss, P. R.; Renstrom, P. J., Imprint lithography with 25-nanometer resolution. *Science* **1996,** 272, (5258), 85-87.

16. Chou, S. Y.; Krauss, P. R.; Zhang, W.; Guo, L. J.; Zhuang, L., Sub-10 nm imprint lithography and applications. *Journal of Vacuum Science & Technology B* **1997,** 15, (6), 2897-2904.

17. Cheng, X.; Guo, L. J., One-step lithography for various size patterns with a hybrid mask-mold. *Microelectronic Engineering* **2004,** 71, (3-4), 288-293.

18. Teo, B. K.; Sun, X. H., From top-down to bottom-up to hybrid nanotechnologies: Road to nanodevices. Journal of Cluster Science 2006, 17, (4), 529-540.

19. Cooper, M. A., Label-free screening of bio-molecular interactions. Analytical and Bioanalytical Chemistry 2003, 377, (5), 834-842.

20. Hu, S. Q.; Xie, J. W.; Xu, Q. H.; Rong, K. T.; Shen, G. L.; Yu, R. Q., A label-free electrochemical immunosensor based on gold nanoparticles for detection of paraoxon. *Talanta* **2003,** 61, (6), 769-777.

21. Meadows, D., Recent developments with biosensing technology and applications in the pharmaceutical industry. *Advanced Drug Delivery Reviews* **1996,** 21, (3), 179-189.

22. Stefan, R. I.; van Staden, J. F.; Aboul-Enein, H. Y., Immunosensors in clinical analysis. *Fresenius Journal of Analytical Chemistry* **2000,** 366, (6-7), 659-668.

23. Guilbault, G. G.; Pravda, M.; Kreuzer, M.; O'Sullivan, C. K., Biosensors - 42 years and counting. *Analytical Letters* **2004,** 37, (8), 1481-1496.

24. Purvis, D.; Leonardova, O.; Farmakovsky, D.; Cherkasov, V., An ultrasensitive and stable potentiometric immunosensor. *Biosensors & Bioelectronics* **2003,** 18, (11), 1385-1390.

25. Susmel, S.; Guilbault, G. G.; O'Sullivan, C. K., Demonstration of labeless detection of food pathogens using electrochemical redox probe and screen printed gold electrodes. *Biosensors & Bioelectronics* **2003,** 18, (7), 881-889.

26. Canziani, G.; Zhang, W. T.; Cines, D.; Rux, A.; Willis, S.; Cohen, G.; Eisenberg, R.; Chaiken, I., Exploring biomolecular recognition using optical biosensors. *Methods* **1999,** 19, (2), 253-269.

27. Monk, D. J.; Walt, D. R., Optical fiber-based biosensors. *Analytical and Bioanalytical Chemistry* **2004,** 379, (7-8), 931-945.

28. Kukanskis, K.; Elkind, J.; Melendez, J.; Murphy, T.; Miller, G.; Garner, H., Detection of DNA hybridization using the TISPR-1 surface plasmon resonance biosensor. *Analytical Biochemistry* **1999,** 274, (1), 7-17.

29. Sapsford, K. E.; Shubin, Y. S.; Delehanty, J. B.; Golden, J. P.; Taitt, C. R.; Shriver-Lake, L. C.; Ligler, F. S., Fluorescence-based array biosensors for detection of biohazards. *Journal of Applied Microbiology* **2004,** 96, (1), 47-58.

30. Ivnitski, D.; Abdel-Hamid, I.; Atanasov, P.; Wilkins, E., Biosensors for detection of pathogenic bacteria. *Biosensors & Bioelectronics* **1999,** 14, (7), 599-624.

Chapter 2

1. Elibol, O. H.; Morisette, D.; Akin, D.; Denton, J. P.; Bashir, R., Integrated nanoscale silicon sensors using top-down fabrication. *Applied Physics Letters* **2003,** 83, (22), 4613-4615.

2. Schubert, P. J.; Neudeck, G. W., Confined lateral selective epitaxial growth of silicon for devicefabrication. *IEEE Electron Device Letters* **1990, 11, 181-183.**

3. Li, Z.; Chen, Y.; Li, X.; Kamins, T. I.; Nauka, K.; Williams, R. S., Sequence-specific label-free DNA sensors based on silicon nanowires. *Nano Letters* **2004,** 4, (2), 245-247.

4. Li, Z.; Rajendran, B.; Kamins, T. I.; Li, X.; Chen, Y.; Williams, R. S., Silicon nanowires for sequence-specific DNA sensing: device fabrication and simulation. *Applied Physics a-Materials Science & Processing* **2005,** 80, (6), 1257-1263.

5. Sheu, J. T.; Chen, C. C.; Huang, P. C.; Lee, Y. K.; Hsu, M. L., Selective deposition of gold nanoparticles on SiO2/Si nanowires for molecule detection. *Japanese Journal of Applied Physics Part 1-Regular Papers Brief Communications & Review Papers* **2005,** 44, (4B), 2864-2867.

6. Ko, F. H.; Yeh, Z. H.; Chen, C. C.; Liu, T. F., Self-aligned platinum-silicide nanowires for biomolecule sensing. *Journal of Vacuum Science & Technology B* **2005,** 23, (6), 3000-3005.

7. Stern, E.; Klemic, J. F.; Routenberg, D. A.; Wyrembak, P. N.; Turner-Evans, D. B.; Hamilton, A. D.; LaVan, D. A.; Fahmy, T. M.; Reed, M. A., Label-free immunodetection with CMOS-compatible semiconducting nanowires. *Nature* **2007,** 445, (7127), 519-522.

8. Lieber, C. M., Nanoscale science and technology: Building a big future from small things. *Mrs Bulletin* **2003,** 28, (7), 486-491.

9. Janata, J., 20 Years of Ion-Selective Field-Effect Transistors. *Analyst* **1994,** 119, (11), 2275-2278.

10. Cui, Y.; Lieber, C. M., Functional nanoscale electronic devices assembled using silicon nanowire building blocks. *Science* **2001,** 291, (5505), 851-853.

11. Chen, Y.; Wang, X. H.; Erramilli, S.; Mohanty, P.; Kalinowski, A., Silicon-based nanoelectronic field-effect pH sensor with local gate control.

Applied Physics Letters **2006,** 89, (22), -.

12. Cui, Y.; Zhong, Z. H.; Wang, D. L.; Wang, W. U.; Lieber, C. M., High performance silicon nanowire field effect transistors. *Nano Letters* **2003,** 3, (2), 149-152.

13. Jin, S.; Whang, D. M.; McAlpine, M. C.; Friedman, R. S.; Wu, Y.; Lieber, C. M., Scalable interconnection and integration of nanowire devices without registration. *Nano Letters* **2004,** 4, (5), 915-919.

14. Wu, Y.; Xiang, J.; Yang, C.; Lu, W.; Lieber, C. M., Single-crystal metallic nanowires and metal/semiconductor nanowire heterostructures (vol 430, pg 61, 2004). *Nature* **2004,** 430, (7000), 704-704.

15. Zheng, G. F.; Patolsky, F.; Cui, Y.; Wang, W. U.; Lieber, C. M., Multiplexed electrical detection of cancer markers with nanowire sensor arrays. *Nature Biotechnology* **2005,** 23, (10), 1294-1301.

16. Thevenot, D. R.; Toth, K.; Durst, R. A.; Wilson, G. S., Electrochemical biosensors: recommended definitions and classification. *Biosensors & Bioelectronics* **2001,** 16, (1-2), 121-131.

17. Wilson, G. S.; Gifford, R., Biosensors for real-time in vivo measurements. *Biosensors & Bioelectronics* **2005,** 20, (12), 2388-2403.

18. Peyssonnaux, C.; Eychene, A., The Raf/MEK/ERK pathway: new concepts of activation. *Biology of the Cell* **2001,** 93, (1-2), 53-62.

19. Kimura, E. T.; Nikiforova, M. N.; Zhu, Z. W.; Knauf, J. A.; Nikiforov, Y. E.; Fagin, J. A., High prevalence of BRAF mutations in thyroid cancer: Genetic evidence for constitutive activation of the RET/PTC-RAS-BRAF signaling pathway in papillary thyroid carcinoma. *Cancer Research* **2003,** 63, (7), 1454-1457.

20. Cohen, J.; Xing, M. Z.; Mambo, E.; Guo, Z. M.; Wu, G. G.; Trink, B.; Beller, U.; Westra, W. H.; Ladenson, P. W.; Sidransky, D., BRAF mutation in papillary thyroid carcinoma. *Journal of the National Cancer Institute* **2003,** 95, (8), 625-627.

21. Davies, H.; Bignell, G. R.; Cox, C.; Stephens, P.; Edkins, S.; Clegg, S.; Teague, J.; Woffendin, H.; Garnett, M. J.; Bottomley, W.; Davis, N.; Dicks, N.; Ewing, R.; Floyd, Y.; Gray, K.; Hall, S.; Hawes, R.; Hughes, J.; Kosmidou, V.; Menzies, A.; Mould, C.; Parker, A.; Stevens, C.; Watt, S.; Hooper, S.; Wilson,

R.; Jayatilake, H.; Gusterson, B. A.; Cooper, C.; Shipley, J.; Hargrave, D.; Pritchard-Jones, K.; Maitland, N.; Chenevix-Trench, G.; Riggins, G. J.; Bigner, D. D.; Palmieri, G.; Cossu, A.; Flanagan, A.; Nicholson, A.; Ho, J. W. C.; Leung, S. Y.; Yuen, S. T.; Weber, B. L.; Siegler, H. F.; Darrow, T. L.; Paterson, H.; Marais, R.; Marshall, C. J.; Wooster, R.; Stratton, M. R.; Futreal, P. A., Mutations of the BRAF gene in human cancer. *Nature* **2002,** 417, (6892), 949-954.

22. Rajagopalan, H.; Bardelli, A.; Lengauer, C.; Kinzler, K. W.; Vogelstein, B.; Velculescu, V. E., Tumorigenesis - RAF/RAS oncogenes and mismatch-repair status. *Nature* **2002,** 418, (6901), 934-934.

23. Schnater, J. M.; Kohler, S. E.; Lamers, W. H.; von Schweinitz, D.; Aronson, D. C., Where do we stand with hepatoblastoma? *Cancer* **2003,** 98, (4), 668-678.

24. Vonschweinitz, D.; Hecker, H.; Harms, D.; Bode, U.; Weinel, P.; Burger, D.; Erttmann, R.; Mildenberger, H., Complete Resection before Development of Drug-Resistance Is Essential for Survival from Advanced Hepatoblastoma - a Report from the German Cooperative Pediatric Liver-Tumor Study Hb-89. *Journal of Pediatric Surgery* **1995,** 30, (6), 845-852.

25. Pritchard, J.; Brown, J.; Shafford, E.; Perilongo, G.; Brock, P.; Dicks-Mireaux, C.; Keeling, J.; Phillips, A.; Vos, A.; Plaschkes, J., Cisplatin, doxorubicin, and delayed surgery for childhood hepatoblastoma: A successful approach - Results of the first prospective study of the international society of pediatric oncology. *Journal of Clinical Oncology* **2000,** 18, (22), 3819-3828.

26. Perilongo, G.; Brown, J.; Shafford, E.; Brock, P.; De Camargo, B.; Keeling, J. W.; Vos, A.; Philips, A.; Pritchard, J.; Plaschkes, J.; Pae, L. T. S. G. I. S.; , Hepatoblastoma presenting with lung metastases - Treatment results of the first cooperative, prospective study of the International Society of Paediatric Oncology on Childhood Liver Tumors. *Cancer* **2000,** 89, (8), 1845-1853.

27. Perilongo, G.; Shafford, E.; Maibach, R.; Aronson, D.; Brugieres, L.; Brock, P.; Childs, M.; Czauderna, P.; MacKinlay, G.; Otte, J. B.; Pritchard, J.; Rondelli, R.; Scopinaro, M.; Staalman, C.; Plaschkes, J., Risk-adapted treatment for childhood hepatoblastoma: final report of the second study of the International Society of Paediatric Oncology-SIOPEL 2. *European Journal of Cancer* **2004,** 40, (3), 411-421.

28. VonSchweinitz, D.; Byrd, D. J.; Hecker, H.; Weinel, P.; Bode, U.; Burger,

D.; Erttmann, R.; Harms, D.; Mildenberger, H., Efficiency and toxicity of ifosfamide, cisplatin and doxorubicin in the treatment of childhood hepatoblastoma. *European Journal of Cancer* **1997,** 33, (8), 1243-1249.

29. Brown, J.; Perilongo, G.; Shafford, E.; Keeling, J.; Pritchard, J.; Brock, P.; Dicks-Mireaux, C.; Phillips, A.; Vos, A.; Plaschkes, J., Pretreatment prognostic factors for children with hepatoblastoma results from the International Society of Paediatric Oncology (SIOP) Study SIOPEL 1. *European Journal of Cancer* **2000,** 36, (11), 1418-1425.

30. Oberg, K. A.; Uversky, V. N., Secondary structure of the homologous proteins, alpha-fetoprotein and serum albumin, from their circular dichroism and infrared spectra. *Protein and Peptide Letters* **2001,** 8, (4), 297-302.

31. Gillespie, J. R.; Uversky, V. N., Structure and function of alpha-fetoprotein: a biophysical overview. *Biochimica Et Biophysica Acta-Protein Structure and Molecular Enzymology* **2000,** 1480, (1-2), 41-56.

Chapter 3

1. National Nano Device Laboratories. http://www.ndl.gov.tw/

2. Anderson, J. R.; Chiu, D. T.; Jackman, R. J.; Cherniavskaya, O.; McDonald, J. C.; Wu, H. K.; Whitesides, S. H.; Whitesides, G. M., Fabrication of topologically complex three-dimensional microfluidic systems in PDMS by rapid prototyping. *Analytical Chemistry* **2000,** 72, (14), 3158-3164.

3. Yuan, H. D.; Mullett, W. M.; Pawliszyn, J., Biological sample analysis with immunoaffinity solid-phase microextraction. *Analyst* **2001,** 126, (8), 1456-1461.

4. Kim, A.; Ah, C. S.; Yu, H. Y.; Yang, J. H.; Baek, I. B.; Ahn, C. G.; Park, C. W.; Jun, M. S.; Lee, S., Ultrasensitive, label-free, and real-time immunodetection using silicon field-effect transistors. *Applied Physics Letters* **2007,** 91, (10), 103901.

Chapter 4

1. Terada, K.; Nishiyama, K.; Hatanaka, K., Comparison of MOSFET-threshold-voltage extraction methods. *Solid-State Electronics* **2001,** 45, (1), 35-40.

2. Sheehan, P. E.; Whitman, L. J., Detection limits for nanoscale biosensors. *Nano Letters* **2005,** 5, (4), 803-807.

3. Cui, Y.; Wei, Q. Q.; Park, H. K.; Lieber, C. M., Nanowire nanosensors for highly sensitive and selective detection of biological and chemical species. *Science* **2001,** 293, (5533), 1289-1292.

4. Laws, G. M.; Thornton, T. J.; Yang, J. M.; de la Garza, L.; Kozicki, M.; Gust, D., Molecular control of the drain current in a buried channel MOSFET. *Physica Status Solidi B-Basic Research* **2002,** 233, (1), 83-89.

5. Huang, Y.; Duan, X. F.; Wei, Q. Q.; Lieber, C. M., Directed assembly of one-dimensional nanostructures into functional networks. *Science* **2001,** 291, (5504), 630-633.

6. Duffy, D. C.; McDonald, J. C.; Schueller, O. J. A.; Whitesides, G. M., Rapid prototyping of microfluidic systems in poly(dimethylsiloxane). *Analytical Chemistry* **1998,** 70, (23), 4974-4984.

7. Iler, R. K., The Chemistry of Silica--Solubility, Polymerization, Colloid and Surface Properties, and Biochemistry. *Wiley: New York* **1979**.

8. Vezenov, D. V.; Noy, A.; Rozsnyai, L. F.; Lieber, C. M., Force titrations and ionization state sensitive imaging of functional groups in aqueous solutions by chemical force microscopy. *Journal of the American Chemical Society* **1997,** 119, (8), 2006-2015.

9. Bolt, G. H., Detemination of the charge density of silica sols. *J. Phys. Chem* **1957**, 61, 1166.

10. Nicollian, E. H.; Brews, J. R., MOS Physics and Technology, *Wiley, New York* **1982,** 11, 920.

11. Allen, L. H.; Matijevi, E., Stability of Colloidal Silica, II. Ion Exchange. *J. Colloid Interface Sci* **1970**, 33, 420

12. Stern, E.; Wagner, R.; Sigworth, F. J.; Breaker, R.; Fahmy, T. M.; Reed, M. A., Importance of the debye screening length on nanowire field effect transistor

sensors. *Nano Letters* **2007,** 7, (11), 3405-3409.

13. Elfstrom, N.; Juhasz, R.; Sychugov, I.; Engfeldt, T.; Karlstrom, A. E.; Linnros, J., Surface charge sensitivity of silicon nanowires: Size dependence. *Nano Letters* **2007,** 7, (9), 2608-2612.

14. Bunimovich, Y. L.; Shin, Y. S.; Yeo, W. S.; Amori, M.; Kwong, G.; Heath, J. R., Quantitative real-time measurements of DNA hybridization with alkylated nonoxidized silicon nanowires in electrolyte solution. *Journal of the American Chemical Society* **2006,** 128, (50), 16323-16331.

15. Poghossian, A.; Cherstvy, A.; Ingebrandt, S.; Offenhausser, A.; Schoning, M. J., Possibilities and limitations of label-free detection of DNA hybridization with field-effect-based devices. *Sensors and Actuators B-Chemical* **2005,** 111, 470-480.

16. Nielsen,; Egholm, P. E.; Berg M.; Buchardt R. H., Sequence-selective recognition of DNA by strand displacement with a thymine-substituted polyamide. *Science* **1991,** 254, (5037), 1497-1500.

17. Jensen, K. K.; Orum, H.; Nielsen, P. E.; Norden, B., Kinetics for hybridization of peptide nucleic acids (PNA) with DNA and RNA studied with the BIAcore technique. *Biochemistry* **1997,** 36, (16), 5072-5077.

18. Kopp, M. U.; de Mello, A. J.; Manz, A., Chemical amplification: Continuous-flow PCR on a chip. *Science* **1998,** 280, (5366), 1046-1048.

19. Hua, Q.; He, R. Q., Human neuronal tau promoting the melting temperature of DNA. *Chinese Science Bulletin* **2000,** 45, (11), 999-1002.

20. Krisch, K. S.; Bude, J. D.; Manchanda, L., Gate capacitance attenuation in MOS devices with thin gate dielectrics. *Ieee Electron Device Letters* **1996,** 17, (11), 521-524.

21. Etzioni, R.; Urban, N.; Ramsey, S.; McIntosh, M.; Schwartz, S.; Reid, B.; Radich, J.; Anderson, G.; Hartwell, L., The case for early detection. *Nature Reviews Cancer* **2003,** 3, (4), 243-252.

22. Wulfkuhle, J. D.; Liotta, L. A.; Petricoin, E. F., Proteomic applications for the early detection of cancer. *Nature Reviews Cancer* **2003,** 3, (4), 267-275.

23 Bellamy, L.L., The Infrared Spectra of Complex Molecules. *Chapman and Hall* **1975,** 1.

24 Barbucci, A.; Magnani, A.; Roncolini, C.; Silvestri, S., Antigen antibody recognition by Fourier transform IR spectroscopy/attenuated total reflection studies/biotin-avidin complex as an example. *Biopolymers* **1991,** 31, 827.

25 Ockman, N.,The antibody-antigen interaction at an aqueous-solid interface: a study by means of polarized infrared ATR spectroscopy, *Biopolymers* **1978,** 17, 1273.

26. Mizejewski, G. J., Alpha-fetoprotein structure and function: Relevance to isoforms, epitopes, and conformational variants. *Experimental Biology and Medicine* **2001,** 226, (5), 377-408.